

POLITECNICO DI TORINO

Collegio di Ingegneria per l'Ambiente e il Territorio

Master of Science Course in Georesources and Geoenergy Engineering

Master of Science Thesis

Experimental Evaluation of Sandstone Permeability to Hydrogen and Nitrogen under Variable Saturation Conditions: Implications for Underground Hydrogen Storage

Tutors

Prof. Francesca Verga Dr. Costanzo Peter

Candidate

Diego Alejandro Millan Chavez

November 2025

Abstract

This thesis investigates the permeability of sandstones to hydrogen and nitrogen under dry and irreducible-water conditions, with implications for underground hydrogen storage (UHS). Three sandstone samples: a tight rock, a moderate-permeability rock, and a high-permeability rock were analysed using two systems, both operating under steady-state conditions: a low-pressure PoroPerm and a high-pressure Hydrogen Permeameter. The combined results reveal how gas properties, pressure regime, and saturation history govern gas flow in reservoir-type formations.

Low-pressure PoroPerm measurements at ambient conditions showed a strong dependence on mean pressure due to gas slippage. Applying the Klinkenberg correction reduced the overestimation of absolute permeability, up to 40%. In contrast, the Hydrogen Permeameter, operated under controlled backpressure, confining stress, and temperature, suppressed most of the slippage. Under these conditions, apparent and corrected permeabilities differed by less than 10%, indicating that backpressured testing yields values close to intrinsic permeability. The comparison demonstrates that discrepancies between both systems arise primarily from experimental configuration and flow stability rather than from the rocks themselves.

Knudsen-number analysis showed that the tight rock remained in the slip-flow regime across the entire measured pressure range, whereas the high- and moderate-permeability rocks transitioned toward continuum flow above 25 bar and 5 bar, respectively. When irreducible water was present, the Knudsen number decreased for all samples, as the water narrowed the gas pathways and reduced the effective characteristic pore size.

Under dry conditions, hydrogen and nitrogen showed nearly identical permeability once the mean pressure in the plug was stabilized, confirming that molecular-scale differences become negligible at reservoir pressures. As expected, when irreducible water was present, permeability declined markedly in all samples. These results confirm the sensitivity of gas flow to irreducible or residual water saturation.

A key finding of this work is the strong sequence-dependent behaviour observed during gas-flow experiments. When hydrogen was injected before nitrogen, the measured permeability was lower than when hydrogen was injected after nitrogen, likely due to transient adsorption, wettability alterations, or capillary condensation that narrowed effective flow paths. This "pore-memory" effect demonstrates that effective permeability is path-dependent and influenced by the order according to which rock is exposed to different gases. Recognizing and standardizing such history effects is essential for reproducible laboratory testing and for predicting performance in cyclic hydrogen storage operations.

In addition, further observations provided relevant complementary insights. The high-permeability rock displayed a pronounced non-linear decrease in permeability with increasing pressure, attributed to pore heterogeneity and selective activation of flow channels rather than inertial effects. Minor declines in hydrogen permeability for the moderate-permeability rock were associated with small hydrogen leaks during the experiments.

Together, these findings define the conditions required for reliable hydrogen testing: rigorous leak control, backpressure regulation, and clear accounting of saturation history.

Outline

| 1. | Obje | ctives | 8 |
|----|--------------|--|----|
| 2. | Gene | ral context | 9 |
| 2 | 2.1. | Geological Reservoirs for Hydrogen Storage | 9 |
| í | 2.2. | Critical Parameters in UHS | 11 |
| 2 | 2.3. | Hydrogen Trapping in Porous Media | 11 |
| 2 | 2.4. | Permeability in UHS: Characteristics and Challenges | 13 |
| 3. | State | of the art | 14 |
| (| 3.1. | Definitions | 14 |
| | 3.2. | Darcy's Law | 15 |
| (| 3.3. | Permeability | 17 |
| (| 3.4. | Laboratory Measurement of Permeability | 18 |
| (| 3.5. | Measuring Permeability to Gases | 18 |
| í | 3.6. | Effect of Flow Velocity on Pressure Gradient in Porous Media | 20 |
| | 3.7. | Slippage Effect | 22 |
| | 3.8. | Klinkenberg Equation | 23 |
| | 3.9. | Effect of Backpressure on Apparent Permeability | 26 |
| (| 3.10. | Knudsen Number | 27 |
| (| 3.11. | Effect of Gas Non-Ideality on Apparent Permeability | 30 |
| í | 3.12. | Effect of Temperature on Apparent Permeability | 32 |
| (| 3.13. | Effect of Water Saturation on Permeability Behaviour | 36 |
| | 3.14. | Gas Diffusion in Porous Media: Application of Graham-Fick Law and Pressure | |
| | • | lence | |
| • | 3.15. | Effect of Confining Pressure on Permeability | |
| • | 3.16. | The Importance of Absolute Permeability in UHS | |
| 4. | Mate | rials and methods | |
| 4 | 4.1. | Samples | |
| 4 | 4.2. | Experimental Equipment | 43 |
| | 4.2.1 | Permeameters: Axial, Steady-State Flow of Gases | 44 |
| | 4.2.2 | Saturators | 47 |
| 4 | 4.3. | Experimental Procedure | 48 |
| 4 | 4.4 . | Experimental Conditions. | 49 |

| 4.6. | Corrections |
|---------------|---|
| 5. Res | sults |
| 5.1. | PoroPerm Measurements |
| 5.2. Cond | Hydrogen Permeameter Measurements: H ₂ vs. N ₂ Permeability Under Dry itions |
| 5.3. | Irreducible Water Saturation (Swi) |
| 5.4. Irred | Hydrogen Permeameter Measurements: H ₂ vs. N ₂ Effective Permeability Under ucible Water Saturation |
| 5.5. | Knudsen Number (Kn): Continuum Flow vs. Slip Flow |
| 6. Dis | cussion |
| 6.1. | PoroPerm: Nitrogen Permeability to Absolute Permeability Under Dry Conditions |
| 6.2. Cond | Hydrogen Permeameter: Nitrogen Permeability to Absolute Permeability Under Dry itions |
| 6.3. | PoroPerm vs. Hydrogen Permeameter |
| 6.4. | Permeability Under Dry Conditions: H ₂ vs. N ₂ |
| 6.5. | Effective Permeability at Irreducible Water Saturation: Role of Irreducible Water |
| 6.6. | Permeability Under Irreducible Water Saturation Conditions: H2 vs. N2 |
| 6.7. | The Non-Linearity: Apparent Permeability vs. Mean Reciprocal Pressure |
| 6.8. | Critical Considerations in Measuring Hydrogen Permeability |
| | nclusions |

Figures

| Figure 1. Types of geological reservoirs for hydrogen storage (Sadkhan et al., 2024) | 10 |
|--|------|
| Figure 2. Critical parameters in UHS (Zeng et al., 2024). | . 12 |
| Figure 3. Experimental configuration of Darcy's experiment in 1856 (Modified from Hubert, 1956) | . 15 |
| Figure 4. Friction factor vs. Reynolds number for all simple fluids through porous materials (Fanche | r & |
| Lewis, 1933) | . 20 |
| Figure 5. Correlation of velocity coefficient (β) and intrinsic permeability (k) | . 21 |
| Figure 6. Graphical representation of Equation 18, where M is the molecular weight, gc is a conversi | ion |
| factor, and G the gas gravity (Firoozabadi & Katz, 1979) | . 23 |
| Figure 7. Permeability correction to hydrogen, nitrogen and carbon dioxide of a core sample | |
| (Klinkenberg, 1941) | . 25 |
| Figure 8. Variation of mean apparent gas permeability with backpressure for a core sample (Li et al., | |
| 2009) | . 26 |
| Figure 9. Plot of apparent gas permeability vs. reciprocal mean pressure of a low-permeability sample | le |
| (Li et al., 2009) | . 27 |
| Figure 10. Variation of the Knudsen number with pressure for different gases, of a permeable medium | |
| Sakhaee-Pour & Alessa, 2022). | . 29 |
| Figure 11. Flow regimes based on the Knudsen number (Sakhaee-Pour & Alessa, 2022) | . 30 |
| Figure 12. Temperature-dependent variation of modified second and third virial coefficients for diffe | rent |
| gases (Guria, 2023) | . 31 |
| Figure 13. The variation of apparent permeability of a core sample with temperature using H_2 at | |
| lifferent pressures (Guria, 2023). | . 33 |
| Figure 14. The variation of apparent permeability of a core sample with temperature using N_2 at | |
| different pressures (Guria, 2023). | . 34 |
| Figure 15. The variation of apparent permeability of a core sample with temperature using CH ₄ at | |
| different pressures (Guria, 2023). | . 35 |
| Figure 16. Experimental (Exp) and simulated (Sim) hydrogen-water relative permeabilities (Kr) on | |
| semilogarithmic scale for (a) primary drainage (PD), (b) imbibition (IMB), and (c) secondary drainage | - |
| (SD) Lysyy et al. (2022) | . 37 |
| Figure 17. Effect of confining pressure on permeability in a) limestones and b) sandstones | |
| (Kozhevnikov et al., 2024) | |
| Figure 18. PoroPerm components diagram. | |
| Figure 19. Hydrogen Permeameter components diagram. | |
| Figure 20. Generalized experimental procedure. | |
| Figure 21. Nitrogen viscosity experimental data at 25°C from Mason & Sputling (1969) and empirical | |
| equations calculated regarding those experiments. | |
| Figure 22. Hydrogen viscosity experimental data at 25°C from Mason & Sputling (1969) and empirical | |
| equations calculated regarding those experiments. | |
| Figure 23. Mean free path behavior with pressure for hydrogen and nitrogen gases | |
| Figure 24. Klinkenberg correction graph for PoroPerm results of sample DM1 | |
| Figure 25. Klinkenberg correction graph for PoroPerm results of sample DM2. | |
| Figure 26. Klinkenberg correction graph for PoroPerm results of sample DM3. | . 57 |

| Figure 27. Klinkenberg correction graph for Hydrogen Permeameter results of sample DM1 under dry | |
|--|----|
| conditions. | |
| Figure 28. Klinkenberg correction graph for Hydrogen Permeameter results of sample DM2 under dry conditions. | |
| Figure 29. Klinkenberg correction graph for Hydrogen Permeameter results of sample DM3 under dry | |
| conditions. | |
| Figure 30. Klinkenberg correction graph for Hydrogen Permeameter results of sample DM1 under | 02 |
| irreducible water saturation conditions. | 63 |
| Figure 31. Klinkenberg correction graph for Hydrogen Permeameter results of sample DM2 under | - |
| irreducible water saturation conditions. | 64 |
| Figure 32. Klinkenberg correction graph for Hydrogen Permeameter results of sample DM3 under | |
| irreducible water saturation conditions. | 64 |
| Figure 33. Knudsen number vs. Pressure under dry and irreducible water saturation conditions for | |
| sample DM1 (Blue=Continuum flow, Green=Slip flow). | 70 |
| Figure 34. Knudsen number vs. Pressure under dry and irreducible water saturation conditions for | |
| sample DM2 (Blue=Continuum flow, Green=Slip flow). | 70 |
| Figure 35. Knudsen number vs. Pressure under dry and irreducible water saturation conditions for | |
| sample DM3 (Blue=Continuum flow, Green=Slip flow). | 71 |
| Figure 36. Klinkenberg correction graph for Hydrogen Permeameter vs PoroPerm results of sample | |
| DM1 under dry conditions. | 75 |
| Figure 37. Klinkenberg correction graph for Hydrogen Permeameter vs PoroPerm results of sample | |
| DM2 under dry conditions. | 75 |
| Figure 38. Klinkenberg correction graph for Hydrogen Permeameter vs PoroPerm results of sample | |
| DM3 under dry conditions. | |
| Figure 39. Klinkenberg correction graph for Hydrogen Permeameter results of sample DM1 under dry | |
| conditions vs. irreducible water saturation conditions. | |
| Figure 40. Klinkenberg correction graph for Hydrogen Permeameter results of sample DM2 under dry | |
| conditions vs. irreducible water saturation conditions. | |
| Figure 41. Klinkenberg correction graph for Hydrogen Permeameter results of sample DM3 under dry | |
| conditions vs. irreducible water saturation conditions. | 79 |

Tables

| Table 1. Characteristics of sample DM1 | 43 |
|---|----|
| Table 2. Characteristics of sample DM2. | 43 |
| Table 3. Characteristics of sample DM3. | 43 |
| Table 4. Experimental conditions for permeability measurements with PoroPerm equipment. | 49 |
| Table 5. Experimental conditions for permeability measurement with Hydrogen Permeameter | |
| equipment | 49 |
| Table 6. Experimental conditions for permeability measurement with Hydrogen Permeameter | |
| equipment | 49 |
| Table 7. Nitrogen properties for viscosity calculations. | 50 |
| Table 8. Viscosity and compressibility factor data for hydrogen and nitrogen at different pressures | 52 |
| Table 9. Mean free path data for hydrogen and nitrogen at different pressures. | 53 |
| Table 10. DM1 PoroPerm permeability results. | 55 |
| Table 11. DM2 PoroPerm permeability results. | 55 |
| Table 12. DM3 PoroPerm permeability results. | 55 |
| Table 13. DM1 Hydrogen Permeameter permeability results under dry conditions. | 58 |
| Table 14. DM2 Hydrogen Permeameter permeability results under dry conditions. | 59 |
| Table 15. DM3 Hydrogen Permeameter permeability results under dry conditions. | 60 |
| Table 16. Irreducible water saturation results. | 62 |
| Table 17. DM1 Hydrogen Permeameter permeability results under irreducible saturation conditions | 65 |
| Table 18. DM2 Hydrogen Permeameter permeability results under irreducible saturation conditions | 66 |
| Table 19. DM3 Hydrogen Permeameter permeability results under irreducible saturation conditions | 67 |
| Table 20. Knudsen number calculation for all samples (Blue=continuum flow, Green=slip flow) | 68 |
| Table 21. Apparent permeability to nitrogen vs. Absolute permeability for PoroPerm results | 72 |
| Table 22. Apparent permeability to nitrogen vs. Absolute permeability for Hydrogen Permeameter | |
| results | 73 |

1. Objectives

Research Objective

The research objective was to experimentally evaluate the permeability behaviour of sandstones to hydrogen and nitrogen under both dry and irreducible water saturation conditions, with particular emphasis on the implications for underground hydrogen storage.

Specific objectives were the following:

- Determine the absolute permeability of dry sandstone plugs with different permeability levels using nitrogen and hydrogen under steady-state and isothermal conditions.
- Saturate the rock samples to irreducible water saturation and re-evaluate their permeability, thereby obtaining the effective permeability to both nitrogen and hydrogen.
- Examine the key factors affecting permeability measurements when using non-ideal gases such as hydrogen and nitrogen at reservoir conditions, and apply the appropriate corrections required for accurate data interpretation.
- Assess the influence of gas type and water saturation on measured permeability.
- Identify and explain the underlying mechanisms governing gas flow under dry and irreducible water saturation conditions, respectively.
- Discuss the broader relevance of permeability variations in relation to the efficiency and deliverability of underground hydrogen storage operations.

2. General context

The global shift toward renewable energy has shown that one of the biggest challenges isn't just producing clean energy but finding reliable ways to store it. Because solar and wind energy depend on weather and time of day, the supply doesn't always match the demand. This mismatch has pushed researchers to explore large-scale storage options that can stabilize the grid. One of the most promising ideas in that direction is underground hydrogen storage (UHS), which makes it possible to convert surplus renewable electricity into hydrogen, store it underground, and later reuse it when energy demand rises (Müller *et al.*, 2023).

UHS offers several benefits. Besides allowing massive and long-term storage, it helps balance power systems and supports decarbonization in sectors that are still hard to electrify, such as heavy transport, aviation, and some industrial processes (Sadkhan *et al.*, 2024). It also enhances energy security, acting as a buffer for fluctuations in renewable generation and reducing dependency on fossil fuels (Yan *et al.*, 2023).

However, the feasibility of UHS depends heavily on how well we understand the geological system. The interactions between hydrogen, rock, and formation fluids are key for assessing storage potential and risks. Parameters such as storage capacity, injectivity, retention, and the potential for microbial or geochemical reactions must be properly evaluated before selecting a storage site (Zeng *et al.*, 2024).

2.1. Geological Reservoirs for Hydrogen Storage

Salt Caverns

Salt caverns are currently the most developed and proven technology for hydrogen storage (Figure 1). They have extremely low permeability and a natural ability to "self-heal," meaning they can withstand repeated pressurization cycles without leakage. These characteristics make them ideal for short-term and high-turnover storage. The main challenges, however, are issues like hydrogen embrittlement in metallic components and the possible growth of microorganisms that can affect gas purity (Yan *et al.*, 2023).

<u>Depleted Gas Reservoirs</u>

Another strong candidate for UHS are depleted gas fields (Figure 1). They already have existing infrastructure, such as wells and pipelines, and offer significant pore space for gas injection. These formations can work well for seasonal storage, although certain risks remain such us hydrogen—rock interactions, microbial hydrogen consumption, or leakage through old wellbores or faults (Sadkhan *et al.*, 2024).

Saline Aquifers

Saline aquifers are widely distributed and could be a practical alternative in areas where salt formations are absent (Figure 1). They are typically located deeper than one kilometre, and their suitability depends on porosity, permeability, and the integrity of the caprock. The chemical composition of the brine, along with local temperature and pressure, can influence hydrogen behaviour. Over long storage periods, geochemical reactions might even alter the petrophysical properties of the reservoir (Dehury *et al.*, 2024).

Lined Rock Caverns

In places that lack suitable geological formations, it's possible to build lined rock caverns: artificial underground chambers excavated in hard rock and sealed with impermeable linings (Figure 1). Their design must consider rock heterogeneity, potential fracture zones, and mechanical stability during repeated pressurization and depressurization cycles (Yan *et al.*, 2023).

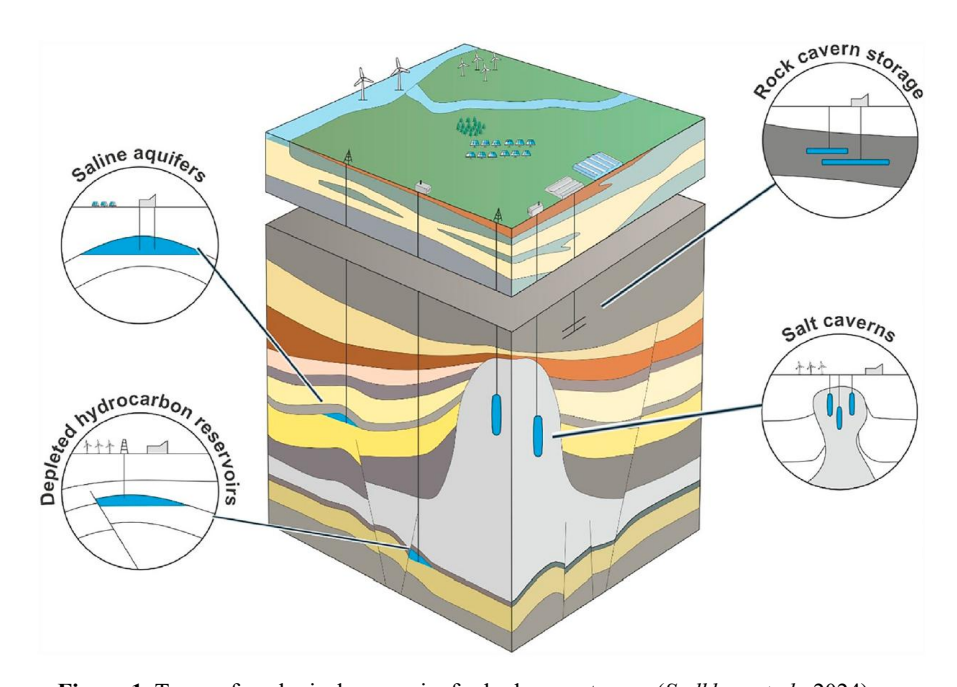


Figure 1. Types of geological reservoirs for hydrogen storage (Sadkhan et al., 2024).

Working and Cushion Gas in Underground Hydrogen Storage

The operation of subsurface reservoirs for hydrogen storage is defined by two primary parameters: the Working Gas Capacity (WGC) and the Cushion Gas Requirement (CGR). The WGC represents the volume of hydrogen that can be cyclically injected and withdrawn

to meet market demand, while the CGR corresponds to the volume of gas that must remain permanently in the reservoir to maintain the necessary pressure levels for deliverability and to avoid extensive recompression costs (Amid *et al.*, 2016). Together, these two components define the Total Gas Capacity (TGC = WGC + CGR) of the reservoir. From an economic perspective, a high WGC/TGC ratio is desirable, as it maximizes the usable storage volume while minimizing the capital tied up in non-recoverable cushion gas (Amid *et al.*, 2016).

2.2. Critical Parameters in UHS

The success and safety of UHS depend on the combined behaviour of the rock, the fluids, and their interactions parameters (Sadkhan *et al.*, 2024, Zeng *et al.*, 2024):

Rock properties: Porosity determines how much hydrogen can be stored, while permeability controls how easily it can flow during injection and withdrawal. Capillary pressure and wettability influence displacement efficiency, and mechanical strength ensures structural stability.

Rock—fluid interactions: Hydrogen's solubility, diffusion rate, and chemical reactivity with minerals can affect both capacity and recoverability. Microbial activity can also consume hydrogen or generate unwanted byproducts (Yan *et al.*, 2023).

Fluid characteristics: Since hydrogen has low density and high diffusivity, its flow behavior differs from that of other gases. The chemistry of the formation water and the type of cushion gas also play roles in determining recovery efficiency and purity (Zeng et al., 2024).

2.3. Hydrogen Trapping in Porous Media

A major challenge in underground hydrogen storage (UHS) within depleted gas fields lies in how hydrogen becomes trapped inside the rock's pore network after injection. As discussed by Zeng *et al.* (2024), several physical and chemical factors influence this phenomenon, including the mechanisms of gas entrapment and the specific interactions between hydrogen, formation fluids, and rock surfaces (Figure 2). Together, these parameters determine how mobile hydrogen remains in the reservoir, its recovery, and how efficient the storage process is overall.

Capillary and Residual Trapping: In porous rocks, the main control on hydrogen entrapment comes from capillary forces and the wettability characteristics of the rock—fluid system. Under most subsurface conditions, hydrogen behaves as a non-wetting phase, particularly in water-wet environments typical of sandstones, carbonates, and shales. Once injected, the hydrogen displaces the brine occupying the pores, but a portion becomes immobilized in disconnected clusters because of capillary effects, a process referred to as residual trapping (Zeng et al., 2024). According to laboratory experiments summarized by Zeng et al. (2024), the contact angles between hydrogen, brine, and mineral surfaces usually range from 20° to

60°, indicating a dominantly water-wet nature. Consequently, a notable fraction of the injected gas can remain locked within isolated pore spaces, forming small "pockets" that lead to permanent storage losses and lower recovery efficiency.

Capillary Entry Pressure and Interfacial Tension: Hydrogen has a comparatively low interfacial tension with brine when contrasted with gases such as methane or carbon dioxide. This means that, theoretically, hydrogen should be able to penetrate the pore network more easily since it requires less capillary pressure to displace the brine. In practice, however, the extent of its migration depends strongly on the geometry of the pore throats and on the local water saturation. In fine-grained or highly water-saturated formations, capillary trapping may still dominate, even with the advantage of low interfacial tension (Zeng *et al.*, 2024).

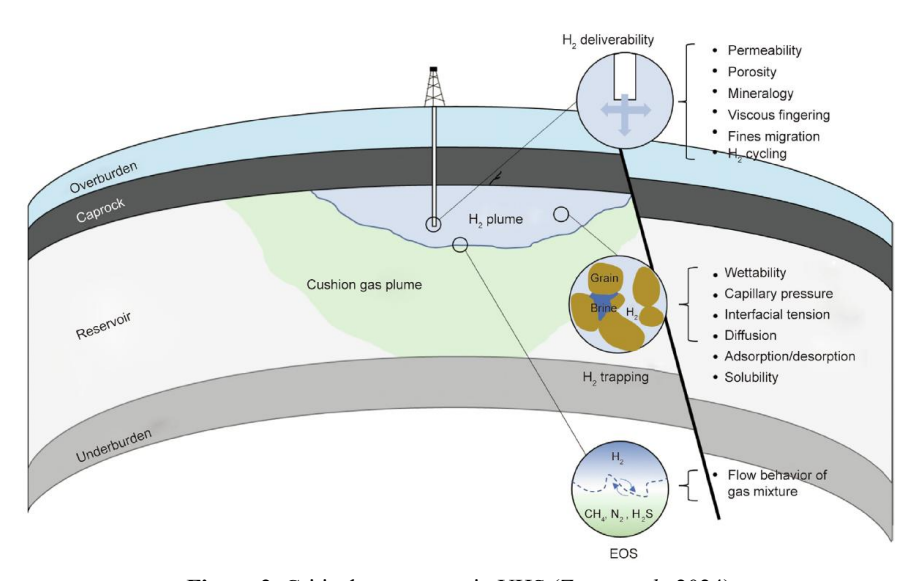


Figure 2. Critical parameters in UHS (Zeng et al., 2024).

Dissolution in Brine: Another mechanism is the dissolution of hydrogen into the formation water, although this process is relatively minor. At 25 °C and atmospheric pressure, hydrogen's solubility in water is around 7.9×10^{-4} mol/kg. It increases slightly with pressure but decreases as temperature or salinity rises (Zeng *et al.*, 2024). This means that only a small proportion of hydrogen is lost to dissolution, and most of it remains in the gaseous state under typical reservoir conditions.

Diffusion into Water-Saturated Zones: Due to its very low molecular weight, hydrogen has a high diffusion coefficient, raising the possibility of it spreading into surrounding zones that are water-saturated or of low permeability. Even so, simulation studies indicate that these diffusive losses are minimal, normally below 1% of the total amount injected throughout a storage cycle (Zeng et al., 2024). Thus, while molecular diffusion does occur, it is considered a secondary trapping process compared to capillary retention.

Adsorption and Geochemical Processes: Hydrogen may also be retained through adsorption on mineral surfaces or through microbial reactions such as methanogenesis (Zeng et al., 2024). Minerals like clays, which possess large surface areas, can adsorb gases to some degree, but their capacity to hold hydrogen is quite low under normal reservoir conditions. Similarly, microorganisms can potentially convert hydrogen to methane when carbon dioxide is present, though the rate and scale of these reactions under in situ conditions are still uncertain. For this reason, adsorption and microbial conversion are recognized as possible but minor risks compared to other trapping mechanisms.

2.4. Permeability in UHS: Characteristics and Challenges

Permeability plays a decisive role in underground hydrogen storage, as it controls how efficiently the gas can be injected and later withdrawn from the reservoir. In general, suitable storage formations display permeabilities ranging from about 0.5 mD to several hundred mD, depending on the lithology and depositional environment. While salt caverns depend on the nearly impermeable nature of halite to safely confine hydrogen, porous rock reservoirs must achieve a balance between adequate permeability for gas flow and sufficient sealing capacity to prevent leakage. Laboratory and field investigations have revealed that hydrogen behaves differently from other gases in its flow characteristics, largely due to variations in relative permeability, capillary pressure, and residual trapping. Moreover, the coexistence of formation water introduces additional complexity because hysteresis effects in relative permeability and potential geochemical interactions with minerals can alter the flow regime (Zeng *et al.*, 2024).

Formations with higher permeability enable hydrogen to move more freely, which lowers the pressure gradient necessary for injection and enhances production rates during withdrawal. In contrast, reservoirs with low permeability impose greater resistance to gas flow, leading to a decrease in working gas capacity (WGC) and an increase in operational costs due to the need for higher compression pressures (Amid *et al.*, 2016). Empirically, depleted gas fields with permeabilities on the order of tens to hundreds of millidarcies are considered most favorable, as these systems provide sufficient injectivity and deliverability while maintaining containment integrity (Amid *et al.*, 2016).

Another operational parameter affected by permeability is the emptying period, which is the time required to withdraw the full WGC at the rated deliverability. Reservoirs with high permeability can achieve short emptying periods and high output rates, making them suitable for applications that demand rapid gas delivery, such as peak-load storage. Conversely, formations with lower permeability generally operate on longer withdrawal cycles and are therefore better suited for seasonal or base-load hydrogen storage (Amid *et al.*, 2016).

3. State of the art

3.1. Definitions

The theoretical foundations and definitions discussed in this study, which are aligned to established industry standards, are mainly based on *Practical Petrophysics* (Kennedy, 2024) and the *Recommended Practice for Core Analysis* published by the American Petroleum Institute (API, 1998). Both references serve as essential frameworks for understanding and interpreting petrophysical parameters, offering detailed guidance on core analysis and permeability evaluation under reservoir conditions. The following section outlines the most relevant definitions drawn from these two key references:

Porosity (ϕ) is defined as a ratio of the void space volume or pore volume (PV) to the bulk volume (BV) of a porous medium.

$$\phi = \frac{PV}{BV} \tag{1}$$

Saturation (S_f) is the portion of the pore volume occupied by any fluid in a porous medium. It is defined as the ratio of the pore fluid volume (FV) to the total pore volume (PV) of the material.

$$S_f = \frac{FV}{PV} \tag{2}$$

Irreducible water saturation (S_{wi}) represents the lower limit of water saturation in a rock, resulting from the strong affinity of commonly occurring minerals, such as clays and silicates, for water. At this saturation level, water is held tightly in the pore spaces by capillary and surface tension forces and cannot be displaced by any fluid under reservoir conditions.

Absolute permeability (k) is a property of a porous medium, defined when only a single fluid is present and does not chemically interact with the rock matrix, that quantifies the capacity of the medium to transmit fluid.

Effective permeability (k_{eff}) is a measure of the permeability of a porous medium to a specific fluid phase within a multiphase system, under a given distribution of saturations. Saturation defines the fraction of pore volume occupied by each phase and therefore governs the partitioning of effective permeabilities.

Relative permeability (k_r) provides a normalized measure. It is defined as the ratio of the effective permeability of a fluid phase at a given saturation to a reference permeability. The reference permeability corresponds to the absolute permeability of a porous medium.

$$k_r = \frac{k_{eff}}{k} \tag{3}$$

3.2. Darcy's Law

Darcy's Law is a fundamental principle widely used in reservoir engineering to describe fluid flow through porous media. It was first formulated by Henry Darcy in 1856, based on careful experimental investigations. In his study, Darcy conducted experiments in which water flowed vertically through a vessel packed with sand until the medium reached steady-state conditions (Muskat, 1937; Hubert, 1956), allowing for systematic observation and analysis of the fluid's behaviour under controlled conditions (Figure 3).

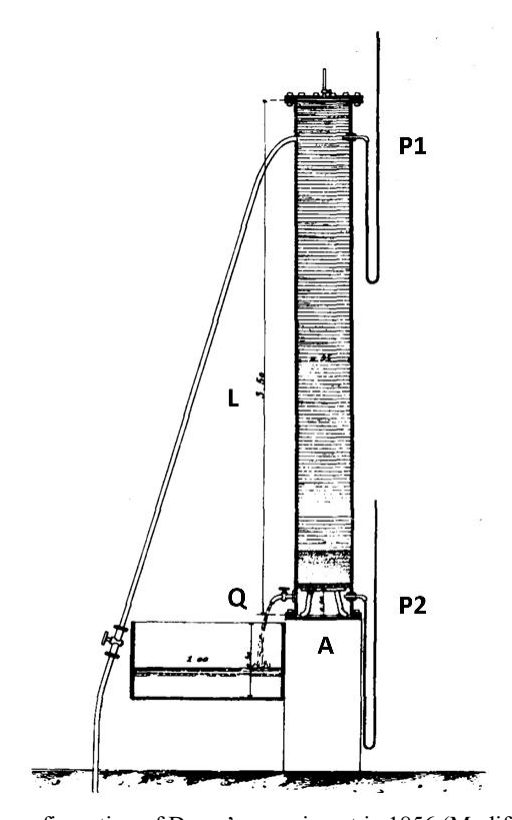


Figure 3. Experimental configuration of Darcy's experiment in 1856 (Modified from Hubert, 1956).

From these experiments, he deduced that, for vertical flow through a sand column, the volumetric flow rate (Q) per unit time can be expressed as:

$$Q = KA \frac{P_1 - P_2}{L} \tag{4}$$

Where K is a proportionality constant, A represents the cross-sectional area, L is the thickness of the sand, and P_1 and P_2 are the pressures measured at the top and bottom of the sand using piezometric manometers.

Based on this, Darcy was able to conclude that the macroscopic velocity (v) of a fluid in a porous medium is directly proportional to the pressure gradient (Muskat, 1937; Hubert, 1956, which can be written in differential form as:

$$v = \frac{Q}{A} = -K \frac{dP}{dL} \tag{5}$$

The negative sign in this equation arises because, when pressure is measured in the direction of flow, it decreases as the length (l) increases. This decrease produces a negative value for dP/dL. Therefore, the negative sign must be included to ensure that the velocity remains positive.

According to Muscat (1937), the macroscopic flow velocity is directly related to the square of the effective pore diameter (d^2) and inversely related to the fluid viscosity (μ) . This relationship leads to the definition of a new proportionality constant K' that incorporates the dimensionless characteristics of the flow system. Such characteristics naturally reflect the geometric properties of the porous medium, including porosity, grain shape, and the degree of cementation. The variability in pore sizes is captured through the effective pore diameter term.

$$v = \frac{Q}{A} = -K' \frac{d^2}{\mu} \frac{dP}{dL} \tag{6}$$

Subsequently, the constant K' was denoted as N known as the shape factor (Hubert, 1956), which specifically characterizes the geometry of the flow passages. Since shape is expressed through angular measurements, which are dimensionless, this factor is therefore a dimensionless parameter that remains constant for systems that are either geometrically identical or statistically similar.

$$v = \frac{Q}{A} = -\frac{Nd^2}{\mu} \frac{dP}{dL} \tag{7}$$

Hubert (1956) also demonstrated that Darcy's law remains valid regardless of the flow direction relative to gravity. For a given potential difference, the volumetric flow rate (Q) is the same whether the fluid moves downward, upward, or in any other spatial direction. This result highlights that flow in porous media is governed solely by the total potential difference, comprising both pressure and gravitational effects rather than by the orientation of the system in the gravitational field. In this regard, Hubert (1956) provided a complete physical statement of Darcy's law, expressed in vector form as:

$$\boldsymbol{v} = -\frac{Nd^2}{\mu} (\nabla P - \rho \boldsymbol{g}) \tag{8}$$

Where ρ represents the density of the flowing fluid and $(\nabla P - \rho g)$ corresponds to the total energy gradient driving the flow. The term ρg is zero for horizontal flow, but in other directions it is comparable in magnitude to dP/dL and therefore cannot be neglected.

3.3. Permeability

The concept of permeability arises from lumping together the previously introduced factor N with the square of the effective pore diameter (d^2) , resulting in a single constant that fully characterizes the porous medium uniquely with respect to the flow passing through it. This constant, denoted k, represents permeability, which was defined as "the volume of a unit-viscosity fluid flowing through a unit cross-sectional area of the medium per unit time under a unit pressure gradient, determined exclusively by the medium's structure and independent of the fluid's nature" (Muscat, 1937).

With the definition of permeability established, the complete form of Darcy's law can be expressed as:

$$\boldsymbol{v} = -\frac{k}{\mu}(\nabla P - \rho \boldsymbol{g}) \tag{9}$$

For flow in a horizontal direction:

$$v = -\frac{k}{\mu} \frac{dP}{dL} \tag{10}$$

Through this formulation, permeability (k) can be determined analytically by using the following equation, when the vector quantities are resolved into their components along the horizontal flow direction (L):

$$k = -\frac{v\mu}{dP/dL} \tag{11}$$

Permeability has units of L^2 and is expressed in Darcys. 1 Darcy corresponds to values for v=1 [$(cm^3/cm^2)/s$], $\mu=1$ [cP] and dP/dl=1 [atm/cm] and is equivalent to 0.987x10⁻⁸ cm^2 (Hubert, 1956).

In general, several conditions are required for the law to remain valid:

- 1) Flow must occur under steady-state conditions.
- 2) The fluid should be incompressible.
- 3) Isothermal conditions must be maintained.
- 4) The flow must be single-phase.
- 5) There should be no interactions between the fluid and the rock.

3.4. Laboratory Measurement of Permeability

The determination of permeability in a porous medium requires the experimental measurement of the volumetric flow rate per unit cross-sectional area of a fluid with known viscosity through a linear core sample. During the experiment, the fluid velocity must remain uniform across the sample, which implies that the pressure gradient (dP/dl) also maintains a constant value along the flow column (Muscat, 1937). Under steady-state conditions, the gradient can therefore be expressed as: $\frac{dP}{dl} = \frac{P_u - P_d}{L}$.

From these measurements, permeability can be calculated using an expression derived from Equation 11:

$$k = \frac{\mu QL}{A(P_u - P_d)} \tag{12}$$

Where Q is the total volumetric flow through the sample, A is the cross-sectional area, L is the sample length, and P_u and P_d are the inlet and outlet pressures, respectively.

It is further assumed that the permeability is spatially uniform within the sample. For liquidphase measurements, compressibility effects can be neglected, as the density of the fluid does not significantly vary with pressure under typical laboratory conditions.

3.5. Measuring Permeability to Gases

When studying gas flow through porous media, the classical form of Darcy's law requires modification to account for gas compressibility. Unlike liquids, whose density can often be approximated as constant, gases exhibit densities that vary continuously with both pressure and temperature. This variation directly affects both the velocity distribution and the pressure gradient along the porous medium. Consequently, to measure gas permeability, it is essential to recognize that the mass flow rate must remain constant along the flow path (Muscat, 1937). This is expressed through the one-dimensional continuity condition:

$$m = \rho v \tag{13}$$

Where ρ is the gas density and v is the velocity (volumetric flow per unit area). This relationship ensures conservation of mass: although the gas may expand or compress along the sample, the mass passing through any cross-section per unit time remains constant.

By combining Darcy's law in one-dimensional horizontal form (Equation 11) with this continuity condition, the mass flux becomes proportional to the product of pressure and the pressure gradient, $P\frac{dP}{dL}$, once the gas density is expressed via the real-gas equation of state:

$$m = \rho v = \frac{P}{zT} \left(-\frac{k}{\mu} \frac{dP}{dL} \right) = -\frac{k}{\mu Z R_s T} P \frac{dP}{dL}$$
 (14)

Where z is the compressibility factor, R_s is the specific gas constant, and T is the absolute temperature. This substitution explicitly introduces the variation of density with pressure into the flow equation (Muscat, 1937).

Integrating along the length of the porous sample from the inlet P_u to the outlet P_d gives the pressure-squared form:

$$m = \frac{k}{2\mu Z R_S T L} (P_u^2 - P_d^2)$$
 (15)

Where L is the sample length, where P_u and P_d are the pressures at the upstream and downstream ends of the porous medium.

This shows that permeability to gas can be determined from the difference in squared pressures, rather than from a simple linear pressure drop as in incompressible liquids (Muscat, 1937):

$$k = \frac{2\mu z R_S T L m}{(P_u^2 - P_d^2)} = \frac{2\mu z R_S T L \rho v}{(P_u^2 - P_d^2)} = \frac{2\mu L}{A} \frac{P_d Q_d}{(P_u^2 - P_d^2)}$$
(16)

Where Q_d is the volumetric flow rate measured at downstream conditions at pressure P_d .

This derivation highlights several important points:

- 1. The *m* remains constant, even though both velocity and density change along the flow path.
- 2. The permeability (k) is an intrinsic property of the porous medium, independent of the gas type.
- 3. The formulation is valid under isothermal conditions and linear low-velocity flow. Corrections for non-ideal behavior can be incorporated using the compressibility factor z or through pseudo-pressure approaches, especially at high pressures.

3.6. Effect of Flow Velocity on Pressure Gradient in Porous Media

Forchheimer (1901) and later researchers such as Fancher & Lewis (1933) and Muscat (1937), concluded that the pressure gradient in a porous medium ceases to be directly proportional to the flow velocity and increases more rapidly, especially under high-velocity conditions. The conditions under which this deviation occurs also depend on several parameters, including the effective pore diameter, fluid density and viscosity (Fancher & Lewis, 1933), and permeability (Firoozabadi & Katz, 1979), all of which are encompassed in the Reynolds number, defined as:

$$Re = \frac{vd\rho}{\mu} \tag{17}$$

Where v is the velocity, ρ is the fluid density, μ is the fluid viscosity, and d is the effective grain diameter of the porous medium.

The Reynolds number provides an indication of when the transition from linear to non-linear flow behaviour occurs (Figure 4). Flow is considered Darcian (or linear, or – with a less accurate definition - laminar) when the pressure gradient varies linearly with velocity, corresponding to Re < 1 and low velocities, whereas it becomes inertia-dominated or high-velocity when the pressure gradient increases faster than velocity, generally for Re > 10, under high-velocity conditions (Fancher & Lewis, 1933; Muscat, 1937, Firoozabadi & Katz, 1979).

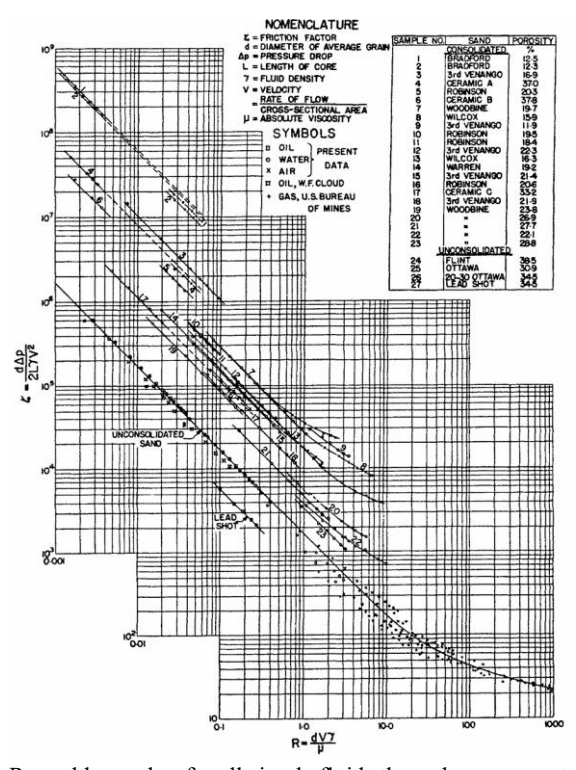


Figure 4. Friction factor vs. Reynolds number for all simple fluids through porous materials (Fancher & Lewis, 1933).

Under Darcian flow conditions, Darcy's law accurately describes the relationship between velocity and pressure gradient, with permeability being one of the primary parameters governing flow resistance. However, at high velocity, the linear assumption of Darcy's law becomes inadequate due to additional pressure losses as "the flow lines with increased velocity are no longer constant in length and are believed to increase the shear and tension areas with increased velocity" (Firoozabadi & Katz, 1979).

To account for this deviation, Forchheimer (1901) introduced an additional quadratic term to Darcy's law, which later became the fundamental component of the Darcy–Forchheimer equation, formalized by Green & Duwez (1951):

$$-\frac{\Delta P}{\Delta l} = \frac{\mu}{k} v + \beta \rho v^2 \tag{18}$$

Where $\frac{\mu}{k}v$ represents the viscous contribution, $\beta\rho v^2$ accounts for the dominance of inertial effects or Forchheimer effect, and β is the velocity coefficient, characteristic of the porous medium, that has a good correlation with permeability and porosity (Figure 5) (Firoozabadi & Katz, 1979).

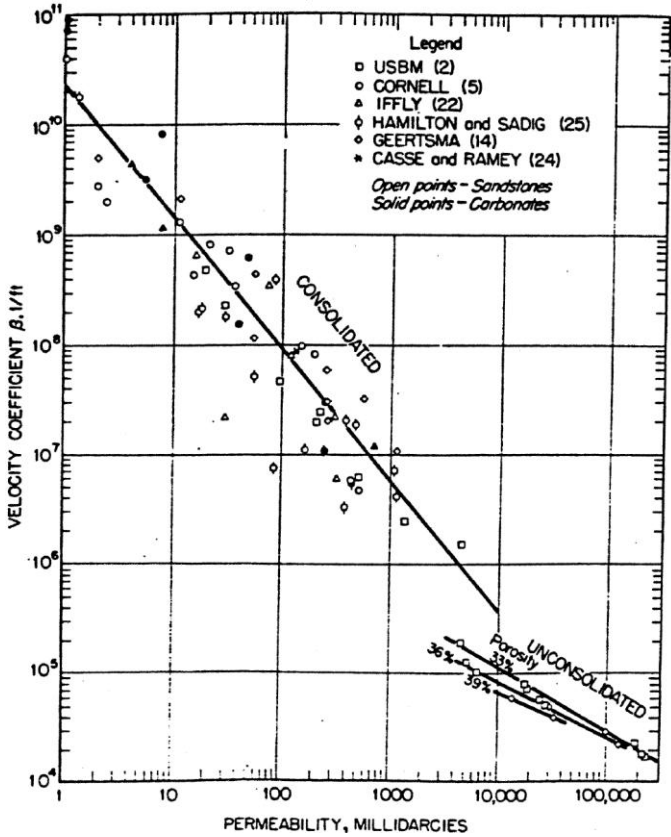


Figure 5. Correlation of velocity coefficient (β) and intrinsic permeability (k).

In the case of gases, the corrected permeability, accounting for high-velocity effects, and the velocity coefficient can be graphically determined from Equation 18. By multiplying by the cross-sectional area A and substituting $v = \frac{m}{\rho A}$, the following expression is obtained:

$$\frac{A(P_u^2 - P_d^2)}{2\mu Z R_s T L m} = \frac{1}{k} + \beta \frac{m}{A\mu}$$
 (19)

A plot of $\frac{A(P_u^2-P_d^2)}{2\mu ZR_STLm}$ versus $\frac{m}{A\mu}$ yields a straight line, where the slope corresponds to the velocity coefficient β and the intercept represents the inverse of the corrected permeability to gas (Firoozabadi & Katz, 1979). The first term on the right-hand side, $\frac{1}{k}$, reflects the linear Darcy resistance, while the second term, $\beta \frac{m}{A\mu}$, represents the additional non-linear resistance associated with the Forchheimer effect.

Considering the above, the permeability under high-velocity flow effects, steady-state conditions, horizontal linear flow, and isothermal conditions, is calculated using the following expression:

$$k = \frac{2\mu L \overline{P}Q}{A(P_u^2 - P_d^2) - \frac{2L\beta \overline{P}^2 Q^2}{AZR_S T}}$$
(20)

This formulation is commonly applied in laboratory gas flow experiments, as it allows for the correction of both high-velocity effects and gas compressibility.

3.7. Slippage Effect

In many instances, the results obtained using the Equation 19 approach do not follow a perfectly linear trend, particularly in the lower section of the graph (Figure 6). This nonlinearity is mainly linked to the slippage phenomenon described by Firoozabadi and Katz (1979), which affects the movement of gases through porous media.

The slippage effect takes place when the mean free path of gas molecules becomes comparable in scale to the pore diameter (Klinkenberg, 1941; Firoozabadi & Katz, 1979; Guria, 2023). Under these conditions, gas molecules tend to collide more often with the pore walls than with one another, generating a slipping motion along the boundaries. Unlike liquids, which typically adhere to pore surfaces, gas molecules can rebound upon impact, effectively increasing the apparent permeability measured with gases.

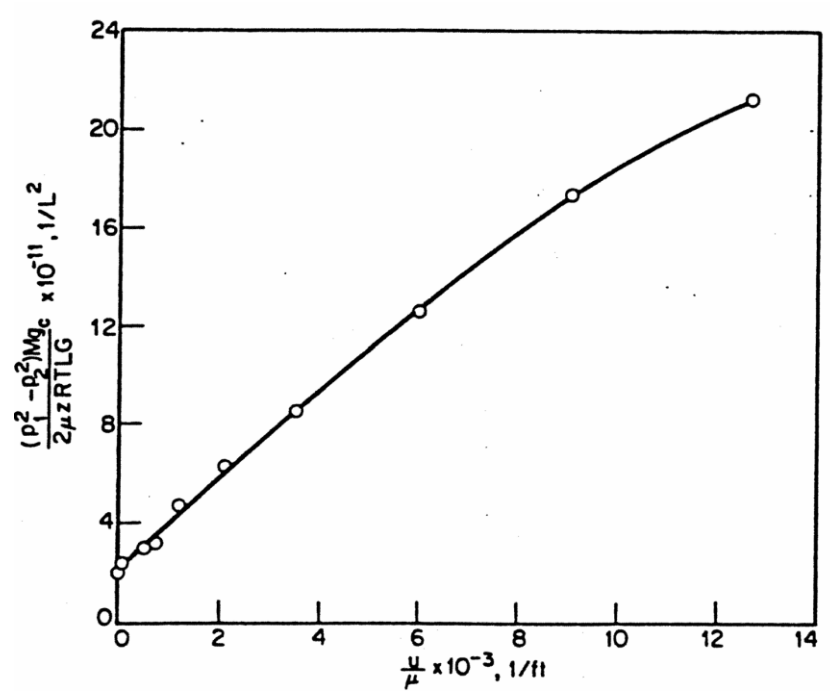


Figure 6. Graphical representation of Equation 18, where *M* is the molecular weight, *gc* is a conversion factor, and *G* the gas gravity (Firoozabadi & Katz, 1979).

This phenomenon is most pronounced at low pressures, while at higher pressures, the mean free path decreases, intermolecular collisions dominate, and the influence of wall slippage diminishes. Similarly, it is more significant in gases with lower molecular weights like hydrogen (H₂) than in heavier gases such as nitrogen (N₂). Therefore, "the permeability of a sample to a gas usually depends upon the molecular weight of the gas and the applied mean pressure, resulting in gas slippage at the wall of the porous media" (Guria, 2023).

According to Guria (2023), the mean free path parameter (λ) can be analytically defined in terms of the pressure and various gas properties using the following expression:

$$\lambda = \frac{\mu Z}{\overline{P}} \sqrt{\frac{\pi RT}{2M}} \tag{21}$$

Where μ is the viscosity, Z is the compressibility factor, R is the gas constant, T is the temperature, and M is the molecular weight of the gas at mean pressure \overline{P} .

3.8. Klinkenberg Equation

By considering gas flow through an idealized porous medium, modelled as a 1 cm³ cube with capillaries of equal radius, Klinkenberg (1941) demonstrated that the slippage effect can be incorporated into Darcy's law by relating the intrinsic or absolute permeability of the porous

medium to the apparent gas permeability (kg) measured under slippage conditions. This relationship is expressed as:

$$kg = k\left(1 + \frac{4c\lambda}{r}\right) \tag{22}$$

Where kg is the apparent gas permeability of the porous medium, k is the intrinsic or absolute permeability included in Darcy's law, r is the radius of the capillaries in the 1 cm cube, λ is the mean free path of the gas molecules, and c is a proportionality factor slightly less than 1.

Considering that the mean free path is inversely proportional to pressure, Equation 22 can be rewritten as:

$$kg = k\left(1 + \frac{b}{\overline{p}}\right) \tag{23}$$

Where \overline{P} in the mean pressure $(\frac{P_u+P_d}{2})$ y b the Klinkenberg coefficient. This equation is known as Klinkenberg equation.

The parameter *b*, expressed in units of pressure, depends on the mean free path of the gas molecules and the capillary diameter of the porous medium. Since permeability is a function of the capillary aperture, *b* is therefore dependent on permeability. This coefficient tends to be small for highly permeable samples with large pores and larger for less permeable samples with smaller pores.

The values of b and k can be determined graphically by rearranging the Equation 23 into the form of a straight-line equation plotted against the reciprocal of the mean pressure, $\frac{1}{p}$. This can be rewritten as:

$$kg = k + k\frac{b}{\overline{p}} = k + \alpha\frac{1}{\overline{p}}$$
 (24)

Where $\alpha = kb$ represents the slope of the line and the intrinsic or absolute permeability (k) is the intercept on the vertical axis (Figure 7) (Klinkenberg, 1941).

Jones (1972) reports that the Klinkenberg coefficient decreases as the rock permeability increases, following an empirical relationship of the form: $b/k \approx 0.36$.

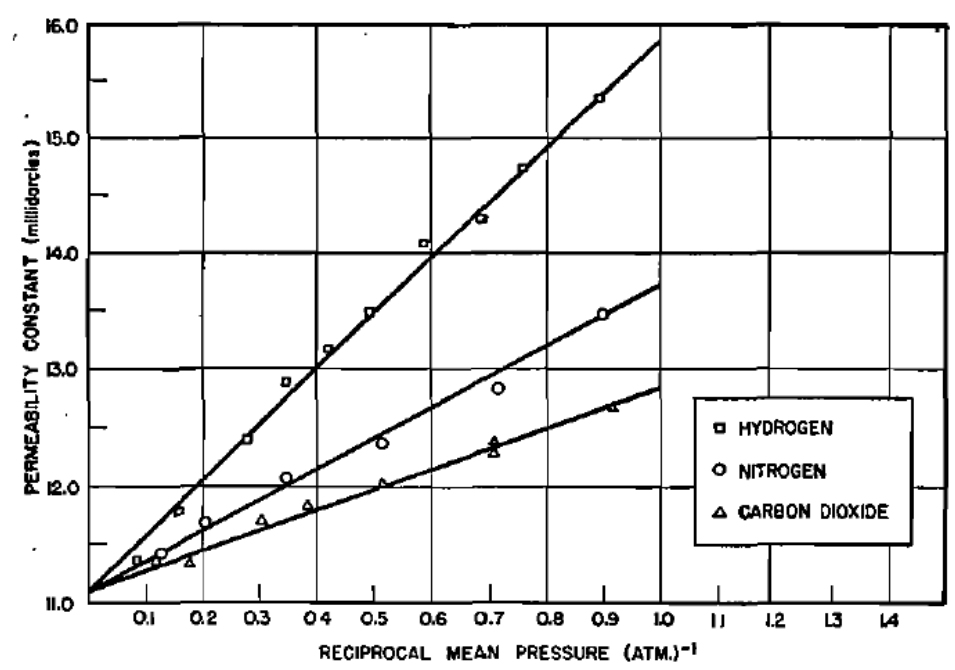


Figure 7. Permeability correction to hydrogen, nitrogen and carbon dioxide of a core sample (Klinkenberg, 1941).

The validity of this expression is based on the following considerations (Klinkenberg, 1941):

- 1) Gas permeability is a linear function of the reciprocal of the mean pressure.
- 2) Gas permeability does not depend on the applied pressure difference as long as the mean pressure remains constant.
- 3) The Klinkenberg coefficient is inversely proportional to the effective pore radius.
- 4) At the same mean pressure, permeability varies for different gases.
- 5) The apparent permeability extrapolated to infinite pressure corresponds to the true permeability; at sufficiently high pressures, the slippage effect vanishes, yielding the intrinsic or absolute, liquid-equivalent permeability of the porous medium.

Considering the slippage effect in the gas flow equation and applying the assumption that P = P + b (Collins & Crawford, 1953), Equation 14 can be reformulated as follows:

$$m = \rho v = -\frac{k}{\mu z R_s T} (P + b) \frac{dP}{dL}$$
 (25)

Integrating along the length of the porous sample from the inlet P_u to the outlet P_d gives:

$$m = \rho v = -\frac{k}{2\mu z R_s T L} [(P_u + b)^2 - (P_d + b)^2]$$
 (26)

This expression indicates that permeability can be determined from the difference in squared pressures, corrected for the Klinkenberg coefficient when the slippage effect is present, rather

than solely from the difference in squared pressures (Equation 16 and associated assumptions). This approach is particularly applicable at low pressures and for low-permeability rocks, especially when using low-molecular-weight gases such as hydrogen, according to:

$$k = \frac{2\mu L \overline{P}Q}{(P_u + b)^2 - (P_d + b)^2}$$
 (27)

3.9. Effect of Backpressure on Apparent Permeability

Li et al. (2009) presented an improved experimental approach for determining apparent gas permeability in which a controlled backpressure was applied at the outlet of the core sample, effectively eliminating the Klinkenberg effect in the gas. By gradually increasing the backpressure, the gas slippage effect is progressively reduced and ultimately removed once a critical threshold, referred to as the minimum backpressure, is reached (Figure 8) (Li et al., 2009). At this stage, the mean free path of gas molecules becomes significantly smaller than the pore diameter, intermolecular collisions dominate over wall collisions, and the slippage effect ceases due to the restricted expansion of the gas. This procedure allows for the direct measurement of the intrinsic, non-slip permeability of the porous medium, in contrast to the traditional Klinkenberg correction, which relies on extrapolating apparent permeability to infinite pressure.

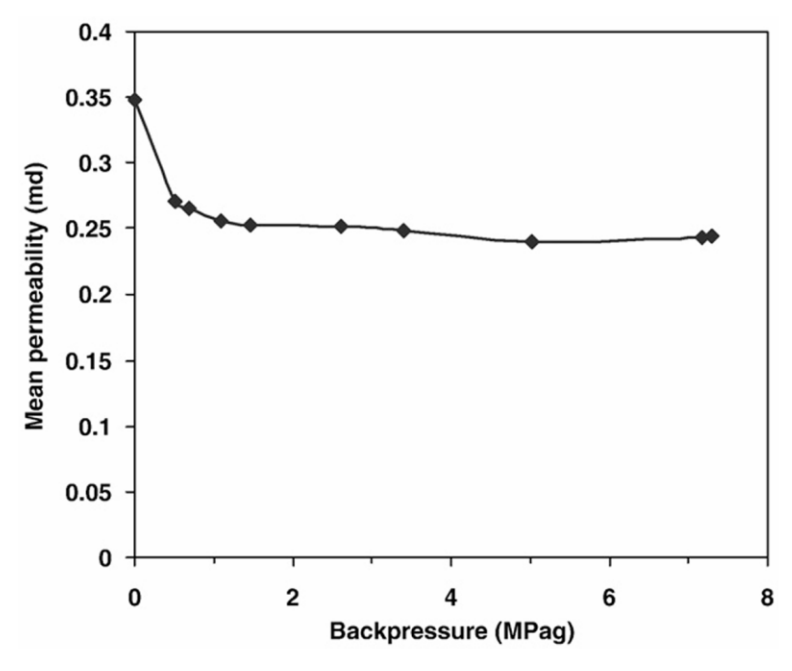


Figure 8. Variation of mean apparent gas permeability with backpressure for a core sample (Li et al., 2009).

Li *et al.* (2009) pointed out that, in the case of non-ideal gases such as hydrogen and nitrogen, the relationship between the mean free path (λ) and pressure (\bar{P}) does not follow a simple inverse proportionality. Consequently, the Klinkenberg coefficient (b) cannot be assumed to remain fixed at elevated pressures, where non-ideal effects become more pronounced. This deviation limits the precision of traditional slip-flow corrections typically used in gas permeability evaluations.

Furthermore, experimental evidence demonstrated that, particularly in very low-permeability cores, permeabilities obtained using the Klinkenberg correction often differ from those measured under backpressure conditions as the reciprocal of the mean pressure approaches zero (Figure 9). In these cores, the assumption of a linear relationship between apparent permeability and the reciprocal of mean pressure is no longer valid because the gas mean free path becomes comparable to the pore dimensions. Consequently, extrapolation to infinite pressure frequently overestimates the true permeability (Li *et al.*, 2009).

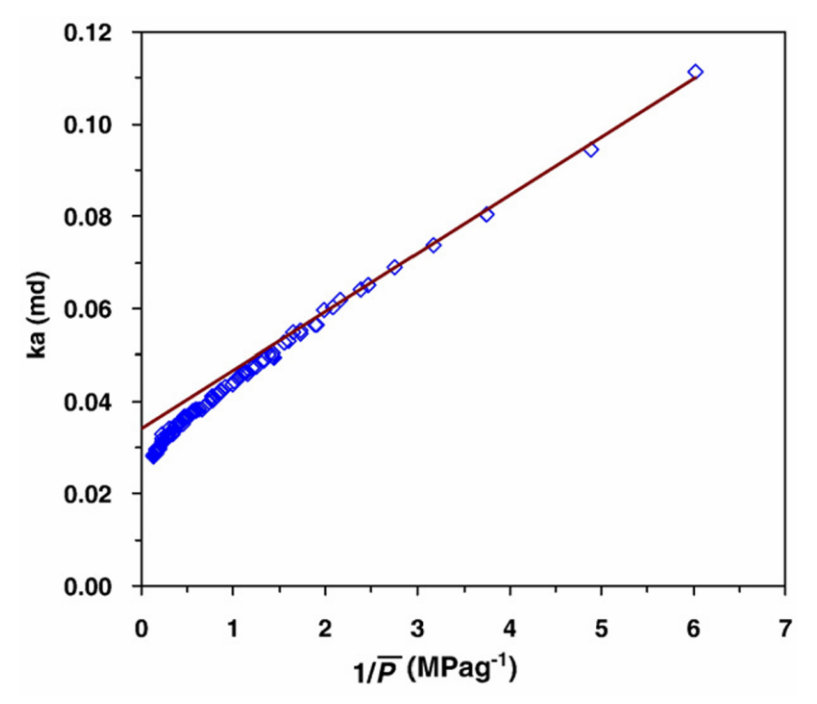


Figure 9. Plot of apparent gas permeability vs. reciprocal mean pressure of a low-permeability sample (Li et al., 2009).

3.10. Knudsen Number

Several authors refer to the Knudsen number as a dimensionless parameter that indicates the presence of slip flow in gas flow through porous media (Sakhaee-Pour & Alessa, 2022; Garia, 2023). It allows for the comparison of different gas types under varying conditions, as it is defined by the following expression (Kandlikar *et al.*, 2014):

$$Kn = \frac{\mu}{\rho d} \sqrt{\frac{\pi}{2RT}} \tag{28}$$

Where μ is the viscosity, ρ is density, d the characteristic size of the pores, R is the gas constant and T is the absolute temperature.

The characteristic size of the pore refers to a representative pore or pore-throat dimension in the rock formation that controls the flow regime, particularly when the flow shifts from continuum (Darcy) to slip or Knudsen regimes. According to Sakhaee-Pour & Alessa (2022) the characteristic pore size of the rock is calculated based on the Hagene-Poiseuille relation:

$$d = \sqrt{\frac{32k}{\phi}} \tag{29}$$

Where d is the characteristic size in micrometres (μ m), k represents the permeability in square micrometres (μ m²), and ϕ denotes the porosity as a fraction. This equation provides a first-order approximation of pore structure based on the simplifying assumption that the rock is homogeneous and composed of uniform, parallel cylindrical capillaries. It is important to note, however, that this idealized representation does not accurately reflect the complex and heterogeneous nature of real porous media.

The Knudsen number represents the ratio between the mean free path (λ) (Equation 21) of gas molecules and the characteristic dimension of the pores (d). This dimensionless parameter decreases when intermolecular collisions occur more frequently than collisions with the channel walls. Consequently, gas flow can be more accurately modelled as a Darcian flow by considering only molecular interactions when the Knudsen number is small. Conversely, as the Knudsen number increases, interactions between gas molecules and the confining walls become increasingly significant (Sakhaee-Pour & Alessa, 2022; Guria, 2023). Overall, "the Knudsen number depends on pressure, conduit size, and temperature, and the continuum assumptions are inapplicable when it is larger than 0.001" (Sakhaee-Pour & Alessa, 2022).

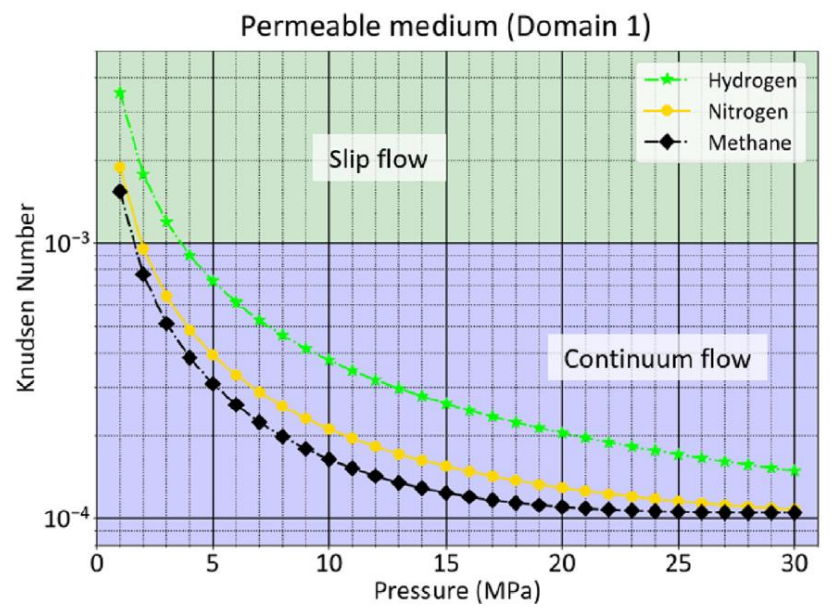


Figure 10. Variation of the Knudsen number with pressure for different gases, of a permeable medium (Sakhaee-Pour & Alessa, 2022).

Figure 10 shows how different non-ideal gases behave when flowing through a porous medium with a uniform pore characteristic size (d) of 3.55 μ m at various pressures, as represented by the Knudsen number. The results demonstrate that the slippage effect becomes more significant at lower pressures, and that gases with smaller molecular weights tend to experience stronger slippage behaviour (Sakhaee-Pour & Alessa, 2022).

When the Knudsen number lies between 0.01 and 0.1 (Figure 11), the system enters what is known as the Slip-flow regime. In this range, gas molecules interact less frequently with the solid rock surface, leading to both velocity slip and temperature jumps at the pore boundaries. Although the overall flow can still be described using continuum-based models, traditional relations such as Darcy's law require adjustments, like the Klinkenberg correction, to better represent gas flow under these non-ideal conditions (Ziarani & Aguilera, 2012).

As the Knudsen number increases to between 0.1 and 10 (Figure 11), the behaviour transitions to the so-called Transition flow regime. Here, neither continuum flow nor pure molecular diffusion dominates completely. In this intermediate state, classical fluid mechanics equations lose reliability; even though modified versions of Darcy's law may still be applied, their predictive accuracy becomes uncertain. For this reason, models incorporating Knudsen-based diffusion become more suitable as Kn approaches the higher end of this interval.

Once the Knudsen number exceeds 10 (Figure 11), the system reaches the Free molecular or Knudsen flow regime, where gas molecules move almost independently, with very few intermolecular collisions. At this point, continuum assumptions are no longer valid, and

diffusion-based models must be used to accurately represent gas flow. This type of flow typically occurs at very low pressures or within ultra-tight porous media, such as shale gas and coalbed methane formations (Ziarani & Aguilera, 2012).

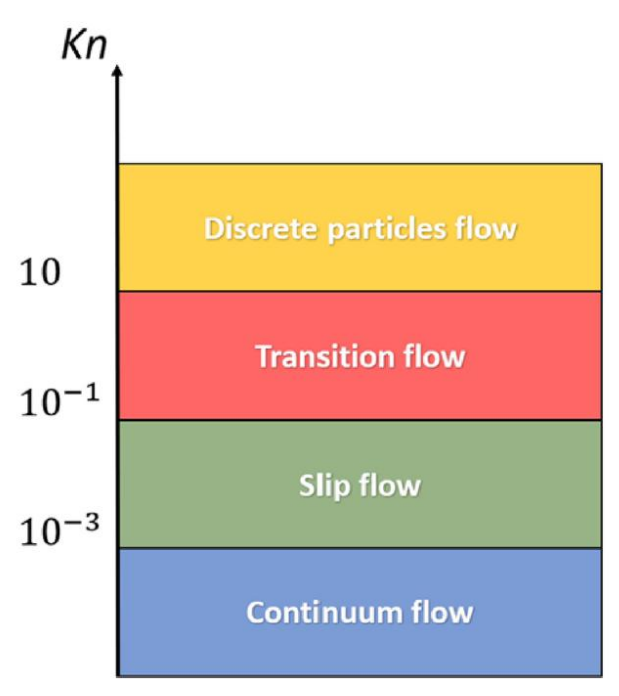


Figure 11. Flow regimes based on the Knudsen number (Sakhaee-Pour & Alessa, 2022).

3.11. Effect of Gas Non-Ideality on Apparent Permeability

Guria (2023) extended the classical Klinkenberg model to account for non-ideal gas behaviour in porous media by incorporating cubic equations of state (either van der Waals, or Soave–Redlich–Kwong, or Peng–Robinson), with apparent permeability as a function of pressure and temperature $(k(T, \overline{P}))$. These formulations include virial coefficients (B' and C') to capture two-body and three-body molecular interactions. The values of the virial coefficients were calculated for several gases including H_2 , air, N_2 , CH_4 , C_2H_6 , C_3H_8 , and CO_2 .

Formulation of apparent permeability with only B' coefficient:

$$k(T, \overline{P}) = k(1 + B') \left(1 - bB' + \frac{b}{\overline{P}}\right) \tag{30}$$

Formulation of apparent permeability with both B' and C' coefficients, where $\Delta = 4C' + B'^2$:

$$k(T, \overline{P}) = k(1 + B' + C') \left[\left\{ \left(1 - \frac{B'^2}{2C'} \right) - \frac{16B'C'^2}{\Delta^2} \left(1 - \frac{2B'^2}{\Delta} + \frac{3B'^4}{\Delta^2} - \frac{4B'^6}{\Delta^3} + \cdots \right) \left(b - \frac{B'}{2C'} \right) \right\} + \frac{\frac{2B'^2}{\Delta} + \frac{3B'^4}{\Delta^2} \left(1 - \frac{2B'^2}{\Delta} + \frac{3B'^4}{\Delta^2} - \frac{4B'^6}{\Delta^3} + \cdots \right) \left(b - \frac{B'}{2C'} \right)}{\overline{P}} \right]$$

$$\Delta < 0$$

$$k(T, \overline{P}) = k(1 + B' + C')(1 - bB' + \frac{b}{\overline{P}})$$
 (32)

The application of these models demonstrated that light gases such as hydrogen and nitrogen exhibit B' and C' values close to zero, behaving nearly ideally under temperatures from 273 K to 523K (Figure 12). Their low molecular weight, simple molecular structure, and proximity to the Boyle temperature explain why deviations from ideality are negligible (Guria, 2023). Accordingly, the predicted intrinsic permeability values (k) obtained using non-ideal corrections closely matched those from the classical Klinkenberg approach. In contrast, heavier gases such as ethane, propane, and carbon dioxide displayed large negative B' and C' values, reflecting stronger long-range attractive forces and multi-body interactions (Guria, 2023). These non-idealities significantly influenced permeability predictions, confirming the necessity of extended models for accurate characterization.

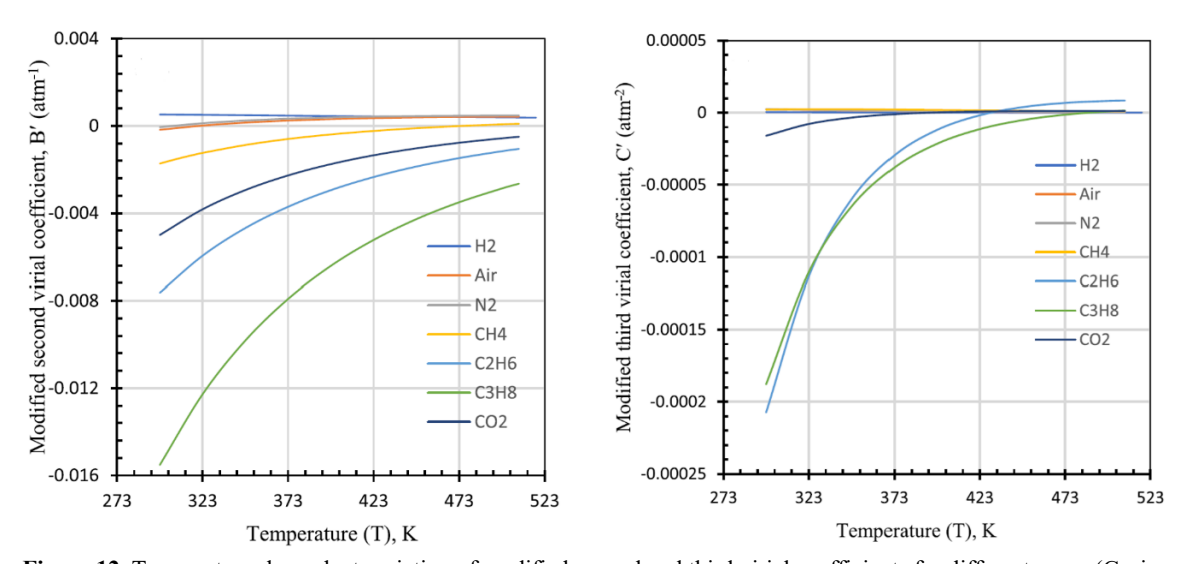


Figure 12. Temperature-dependent variation of modified second and third virial coefficients for different gases (Guria, 2023)

3.12. Effect of Temperature on Apparent Permeability

Since the mean free path depends not only on pressure and gas type but also on temperature (Guria, 2023), it is essential to understand how temperature affects apparent permeability in non-ideal gases.

In terms of temperature-dependent apparent permeability $(k(T, \overline{P}))$, Guria (2023) highlighted clear distinctions between gases. For nearly ideal gases such as H₂ (Figure 13), N₂ (Figure 14), and air, variations in temperature produced minimal changes in permeability across the studied pressure ranges (1.2 atm; 2 atm; 5 atm; 10 atm; 15 atm; 20 atm). For H₂, apparent permeability predictions become unstable at low to moderate temperatures due to near-zero C' values when using Equation 31 (Figure 12), but this instability can be mitigated by using Equation 32 (Guria, 2023). Overall, for those gases, the apparent permeability exhibits a slight non-linear increase with temperature at a given mean pressure, while remaining nearly constant at elevated temperatures. The observed maximum increase in $k(T, \overline{P})$ is less than 0.1%.

On the other hand, gases that display stronger non-ideal behaviour, such as CH₄ (Figure 15), C₂H₆, C₃H₈, and CO₂, exhibit a marked sensitivity to temperature, especially under low mean pressure conditions where gas slippage effects are dominant (Guria, 2023). In these situations, the permeability function $k(T, \overline{P})$ tends to decrease slightly as temperature increases at a constant pressure, before reaching a stable value at higher temperatures. The maximum reduction observed in $k(T, \overline{P})$ remains relatively small, not exceeding about 0.25%.

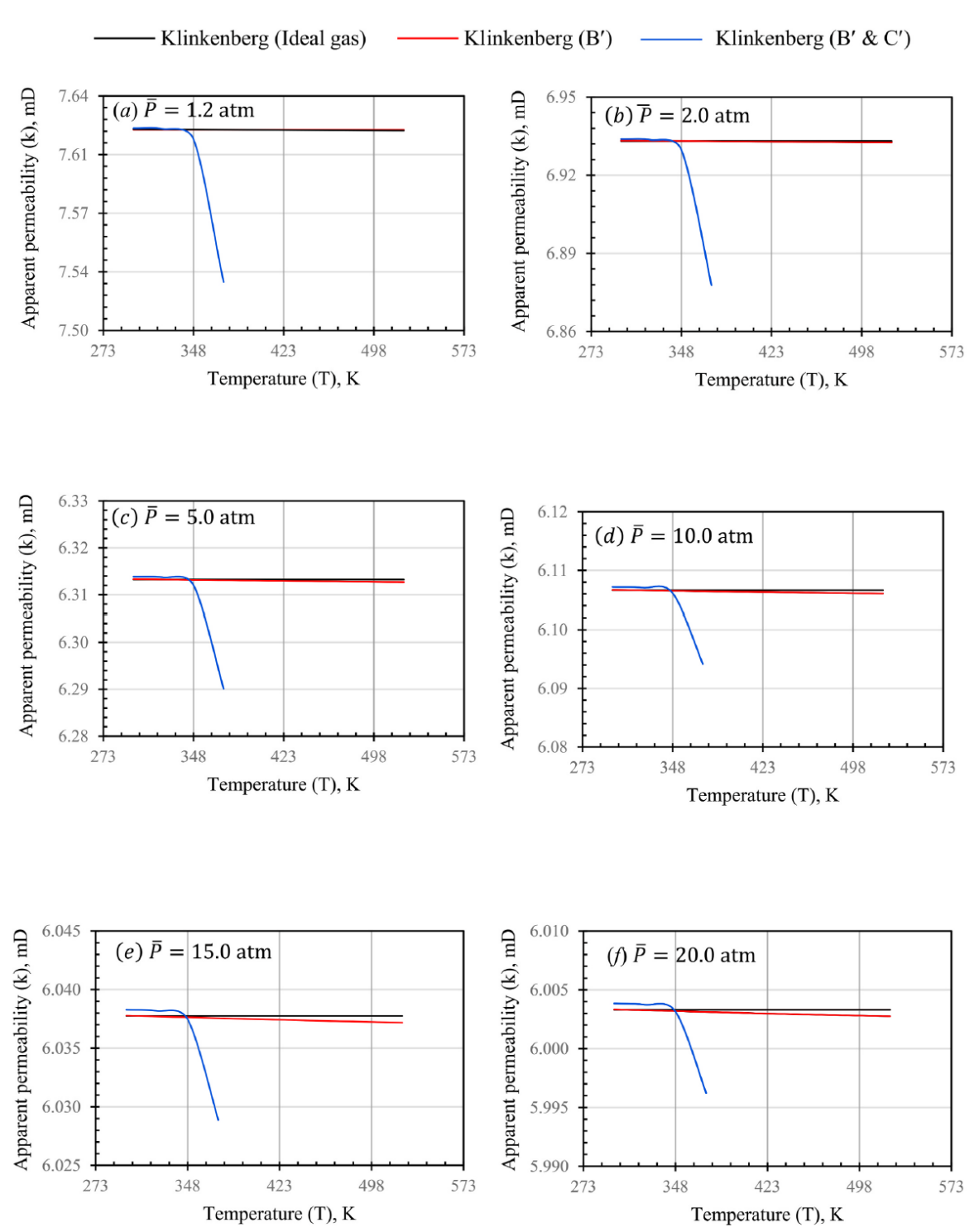


Figure 13. The variation of apparent permeability of a core sample with temperature using H_2 at different pressures (Guria, 2023).

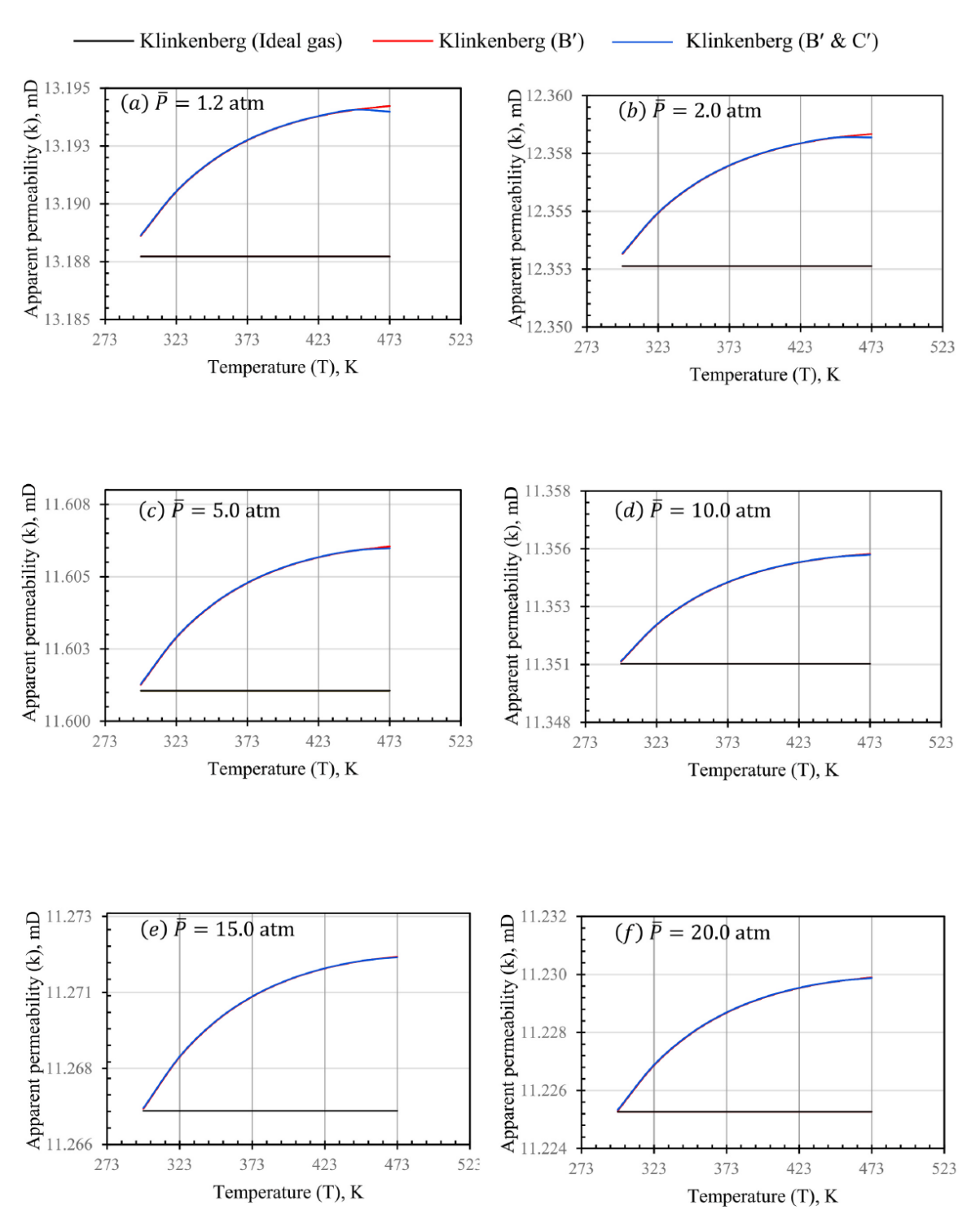


Figure 14. The variation of apparent permeability of a core sample with temperature using N₂ at different pressures (Guria, 2023).

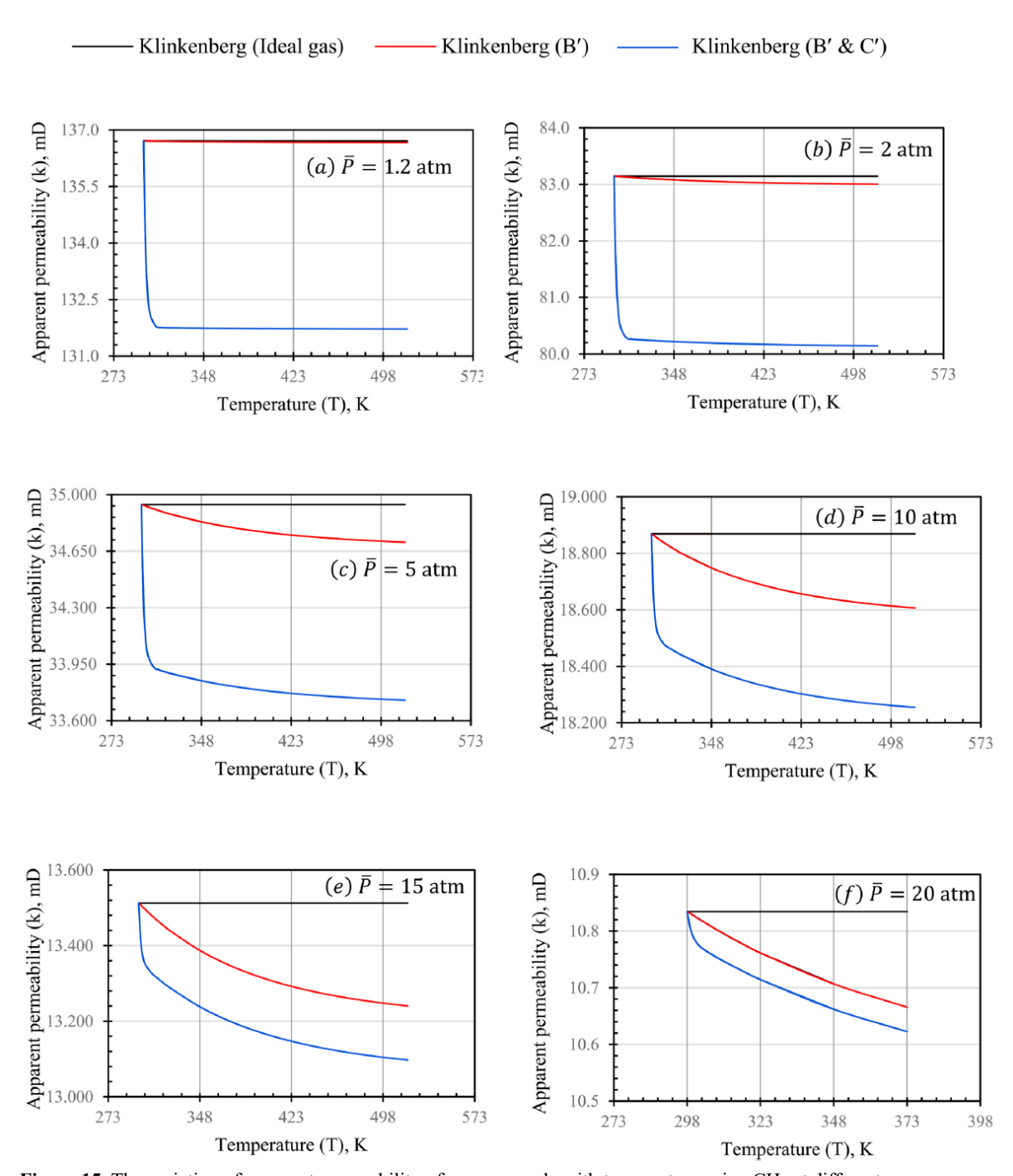


Figure 15. The variation of apparent permeability of a core sample with temperature using CH₄ at different pressures (Guria, 2023).

3.13. Effect of Water Saturation on Permeability Behaviour

At irreducible water saturation, the pore space of a rock sample contains immobile water retained by capillary forces, which does not contribute to fluid flow. Under these conditions, permeability measurements reflect the effective permeability to the non-wetting phase as the water phase remains stationary and occupies pore spaces that reduce the effective flow pathways for the gas phase (Bear, 1972).

The presence of irreducible water has a notable effect on permeability, as it limits the effective cross-sectional area through which gas can move. As a result, the effective permeability becomes lower than the absolute permeability obtained under single-phase, fully saturated conditions. The degree of this reduction is influenced by several parameters, including the rock's wettability, the distribution of pore sizes, and its capillary pressure behaviour (Leverett, 1941). At irreducible saturation levels, water typically occupies the smallest pore throats and forms thin films along pore walls, which increases flow tortuosity and resistance for the gas phase (Tiab & Donaldson, 2015).

Experimental studies of gas permeability under different water saturation conditions (Jones & Roszelle, 1978) show that permeability values are lower than those measured with gas under dry conditions, especially in tight formations or rocks with high clay content. Furthermore, gas slippage effects (Klinkenberg, 1941) become more evident at low confining pressures and in low-permeability systems, leading to apparent increases in permeability that require correction for accurate interpretation.

On the other hand, Lysyy *et al.* (2022) performed one of the first systematic experimental studies on hydrogen—water relative permeability and hysteresis under conditions relevant to underground hydrogen storage (UHS). Using steady-state core-flood experiments on sandstone samples, they quantified how hydrogen moves through partially water-saturated porous media during successive drainage and imbibition cycles.

Their results revealed a clear hysteresis between the drainage and imbibition processes. Following imbibition, a considerable portion of hydrogen remained trapped within the pore network, resulting in a residual gas saturation (S_{gr}) significantly higher than that estimated by models that neglect hysteresis. The endpoint values of gas relative permeability (k_{rg}) for hydrogen were much lower than those commonly applied in numerical simulations, suggesting that hydrogen exhibits limited mobility even when it constitutes the dominant phase (Figure 16).

Moreover, Lysyy et al. (2022) observed that hydrogen displays a behaviour distinct from that of nitrogen under comparable experimental conditions. Both the shape and magnitude of the

relative permeability curves, along with the degree of hysteresis, differed between the two gases. As a consequence, empirical correlations or proxy datasets developed for nitrogen or air cannot reliably represent hydrogen flow in UHS scenarios. These discrepancies stem from hydrogen's low viscosity and density, together with capillary and pore-scale phenomena that govern gas distribution and trapping within water-saturated pores. Such mechanisms enhance gas entrapment and reduce effective permeability throughout both the injection and withdrawal stages.

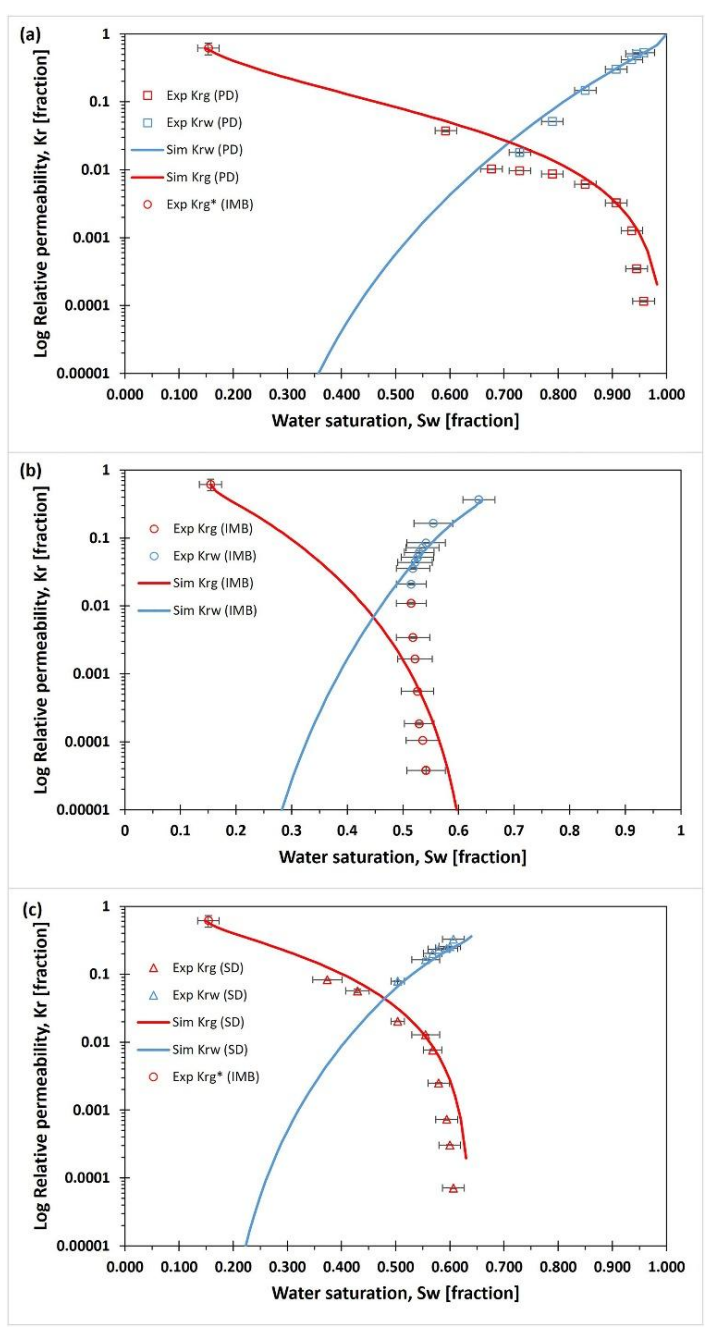


Figure 16. Experimental (Exp) and simulated (Sim) hydrogen-water relative permeabilities (Kr) on semilogarithmic scale for (a) primary drainage (PD), (b) imbibition (IMB), and (c) secondary drainage (SD) Lysyy *et al.* (2022).

Modelling based on their experimental data revealed that ignoring hysteresis or using non-hydrogen-specific curves can significantly overestimate the recoverable gas fraction and withdrawal performance in storage reservoirs. Consequently, Lysyy *et al.* (2022) emphasized the need to incorporate hydrogen-specific, hysteretic relative permeability functions into reservoir simulations to realistically predict storage efficiency and cyclic behaviour.

3.14. Gas Diffusion in Porous Media: Application of Graham-Fick Law and Pressure Dependence

In porous systems, diffusion refers to the molecular-scale flow of gas species due to gradients in concentration or chemical potential (Bear, 1972; Cussler, 2009). In contrast, convection (or advective flow) refers to the bulk movement of fluids through the pore space driven by pressure gradients. This is formally described by Darcy's Law.

Gas flow through porous media by diffusion occurs independently of any bulk fluid motion and becomes the prevailing mechanism when pressure differences are negligible or absent. This phenomenon is generally characterized by using Fick's and Graham's laws. Fick's Law describes the mass flux that arises from concentration gradients (Cussler, 2009), whereas Graham's Law relates diffusion velocity to the inverse square root of the gas's molar mass (Graham, 1833). These two formulations are known as the Graham–Fick framework.

Fick's First Law is expressed as:

$$J = -D\frac{dC}{dx} \tag{33}$$

Where J is the molar flux, D is the diffusion coefficient (m²/s), and $\frac{dC}{dx}$ is the concentration gradient.

Graham's Law states:

$$\frac{v_{\rm H_2}}{v_{\rm N_2}} = \sqrt{\frac{M_{\rm N_2}}{M_{\rm H_2}}} \approx 3.73\tag{34}$$

Indicating that hydrogen, with its low molar mass (2.016 g/mol), diffuses significantly faster than nitrogen (28.014 g/mol) under identical conditions.

Importantly, the diffusion coefficient *D* for gases is not constant since it varies inversely with pressure. This relationship can be described by kinetic gas theory (Cussler, 2009):

$$D = \frac{AT^{3/2}}{P\sqrt{M}} \tag{35}$$

where T is absolute temperature, P is absolute pressure, M is molar mass, and A is a proportionality constant dependent on gas properties. Consequently, increasing pressure leads to reduced diffusivity due to enhanced molecular interactions and reduced mean free paths.

In porous media with irreducible water saturation (S_{wi}), the effective diffusivity D_{eff} is further diminished due to restricted gas-filled pore volume and increased tortuosity. This is captured in this expression (Ruth & Ma, 1992):

$$D_{\text{eff}} = \phi \cdot S_g \cdot \frac{\tau}{\delta} \cdot D \tag{36}$$

Where ϕ is porosity, S_g is gas saturation, τ is tortuosity, and δ is the constrictivity factor.

Xu (2022) highlighted that the relative importance of advective and diffusive gas flow in unconventional reservoirs depends primarily on pore-scale characteristics and the prevailing pressure regime. The research indicated that advective mechanisms overwhelmingly control flow behaviour in most shale and coal formations, whereas diffusion only becomes relevant in the smallest pore structures. Specifically, the diffusive contribution to the total mass flux exceeds roughly 10% only within micropores smaller than 2 nm and narrow mesopores below 10 nm. In larger pore networks, advective flow dominates by several orders of magnitude, implying that molecular diffusion can typically be disregarded when evaluating flow capacity in these kinds of reservoirs.

Furthermore, this research showed that elevated reservoir pressure strengthens advective flow while simultaneously diminishing the role of diffusion, as the mean free path of gas molecules shortens under compression. In contrast, increasing temperature slightly enhances diffusive motion due to higher molecular energy, although this influence remains secondary. Consequently, under representative reservoir conditions (pressures between 10 and 50 MPa and temperatures between 300 and 400 K) the movement of supercritical fluids is predominantly governed by advection rather than diffusion.

Xu (2022) also emphasized the influence of pore geometry on apparent flow capacity. Models dominated by spherical pores systematically overestimated permeability, while those with slit or cylindrical pore structures produced more realistic values. The comparison between different rock types showed consistent trends: both are characterized by advection-dominated flow, indicating that the differences in lithology play a lesser role than pore-scale characteristics. Overall, the findings confirmed that pore structure heterogeneity, particularly

pore size and shape, dictates the transition between diffusive and advective regimes, and that advection remains the principal mechanism under most reservoir conditions.

These conclusions underscore that diffusion-driven flow is relevant only in systems rich in nanopores or under depleted pressure conditions, while for conventional reservoirs as well as for the majority of unconventional gas reservoirs, flow capacity can be accurately captured by advective models alone. Xu's analysis provides a clear physical basis for simplifying permeability estimation and reservoir simulation by excluding bulk diffusion effects in formations with average pore sizes above 10 nm.

3.15. Effect of Confining Pressure on Permeability

When studying rock permeability under varying confining pressures, it is common to observe a decrease in permeability as pressure increases. This behaviour occurs because the applied pressure partially closes pores and microfractures. The most used empirical relationship to describe this behaviour is the power law (Kozhevnikov *et al.*, 2024):

$$\frac{k}{k_0} = A \cdot (\Delta P)^{-n} \tag{37}$$

Where k and k_o represent the current and initial permeability, respectively, ΔP is the pressure change, A is an empirical coefficient, and n is an exponent characterizing the sensitivity of permeability to pressure variations. When n is large, permeability is highly sensitive to pressure, indicating the presence of microfractures that close easily. Conversely, when n is small, permeability is less sensitive, suggesting that flow is dominated by pores, which are less affected by increasing pressure.

According to Kozhevnikov *et al.* (2024), based on the analysis of laboratory data, the relationship between permeability and confining stress in sandstones undergoing purely elastic deformation can be accurately described using a power law. This mathematical formulation effectively reproduces the experimental trends, achieving a very high correlation ($R \approx 0.98-0.99$) (Figure 17).

The outcomes obtained from fitting the data to the power law reveal that rocks with higher initial permeability tend to exhibit the greatest decreases under stress. Sandstone samples, in particular, show pronounced sensitivity due to their coarse-grained framework. When compared to finer-grained limestones, sandstones display a sharper drop in permeability, sometimes approaching 20%, as reflected by their n values. These observations suggest that the power law formulation not only captures the elastic response of the material effectively but also emphasizes the fundamental contrasts among lithologies in how they accommodate

mechanical stress through variations in pore geometry and fluid flow capacity (Kozhevnikov *et al.*, 2024).

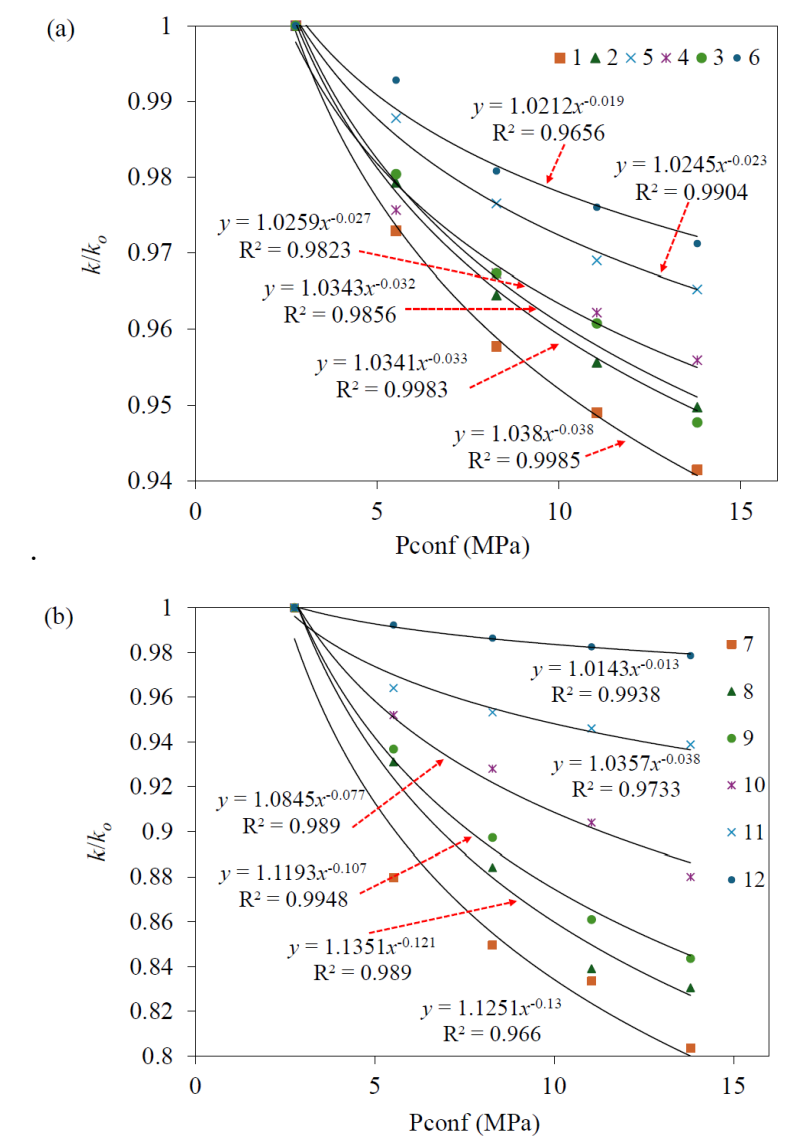


Figure 17. Effect of confining pressure on permeability in a) limestones and b) sandstones (Kozhevnikov et al., 2024).

3.16. The Importance of Absolute Permeability in UHS

Permeability is a critical parameter for hydrogen storage, directly controlling the efficiency of both injection and withdrawal operations. The well deliverability of hydrogen can be described by the relation:

$$P_{si}^2 - P_f^2 = aD_w + bD_w^2 (38)$$

where D_w is the well deliverability at surface pressures P_{si} (shut-in) and P_f (flowing), a is the coefficient associated with Darcy flow in the reservoir, and b is the coefficient representing non-Darcy flow near the wellbore. For injection operations, the sign of one side of the equation is adjusted accordingly.

The coefficient a depends explicitly on absolute permeability (k) and other reservoir and fluid properties:

$$a = 1.2927 \cdot 10^6 \frac{\mu z T}{kH} \left[1.15 \log \left(\frac{10.06 A_W}{C_A r_W^2} \right) - \frac{3}{4} + s \right]$$
 (39)

where μ is fluid viscosity, z the compressibility factor, T the reservoir temperature, H the thickness, A_w the well drainage area, C_A the drainage area shape factor, r_w the well radius, and s the skin factor. This expression highlights that higher permeability reduces flow resistance, increasing deliverability and operational flexibility (Zeng *et al.*, 2024; Amid *et al.*, 2016)

The coefficient *b* accounts for non-Darcy effects close to the wellbore, where turbulence and inertial losses can occur:

$$b = F\mu z \tag{40}$$

Although *b* depends on fluid and reservoir properties, its impact is secondary to the effect of permeability in most practical scenarios.

The time to fully withdraw the working gas capacity (WGC) is another operational metric influenced by permeability:

$$t_e = \frac{WGC}{D_R} \tag{41}$$

where D_R is the sum of deliverabilities from all wells. High-permeability reservoirs allow for shorter emptying periods, supporting peak-load hydrogen supply, whereas low-permeability reservoirs are better suited for seasonal or base-load storage (Amid *et al.*, 2016).

4. Materials and methods

4.1. Samples

The experiments were conducted on three sandstone plug samples, whose characteristics are described in detail below in Table 1, Table 2, and Table 3:

Table 1. Characteristics of sample DM1.



| * | |
|---------------|-------------------------|
| Sample name | DM1 |
| Weight (dry) | 98.487 g |
| Length | 40.9 mm |
| Diameter | 37.2 mm |
| Porosity | 0.2192 |
| Grain density | 2.837 g/ml |
| Lithology | Heterogeneous Sandstone |
| | |

Table 2. Characteristics of sample DM2.



| Sample name | DM2 |
|---------------|------------|
| Weight (dry) | 190.604 g |
| Length | 72.8 mm |
| Diameter | 37.5 mm |
| Porosity | 0.1454 |
| Grain density | 2.774 g/ml |
| Lithology | Sandstone |
| | |

Table 3. Characteristics of sample DM3.



| Sample name | DM3 |
|---------------|------------|
| Weight (dry) | 164.652 g |
| Length | 67.8 mm |
| Diameter | 37.6 mm |
| Porosity | 0.1774 |
| Grain density | 2.659 g/ml |
| Lithology | Sandstone |
| | |

4.2. Experimental Equipment

To achieve the objectives of this research, different pieces of laboratory equipment were employed. In the following section, each device is briefly described, highlighting its operating principle and the type of data it provides.

4.2.1. Permeameters: Axial, Steady-State Flow of Gases

In laboratory permeability measurements, gases are directed axially through a cylindrical rock plug that has been cleaned and dried prior to testing. The sample is mounted inside a core holder equipped with a flexible sleeve, which provides a gas-tight seal along the cylindrical surface while enabling the application of radial confining stress. At relatively low gas pressures (up to several hundred psig), gravitational effects are negligible, and the apparatus may be oriented either horizontally or vertically.

Gas injection and withdrawal are carried out through two end plugs equipped with axial ports, which promote even gas distribution across the inlet surface and efficient recovery from the outlet side. Pressure measurements are obtained using transducers that continuously record the upstream and downstream pressures (P_1 and P_2), allowing the differential pressure ($\Delta P = P_1 - P_2$) to be calculated. To reduce the influence of transient or dynamic pressure effects, the transducers are connected to branch lines on tubing tees positioned close to the sample faces.

The outlet flow can either be released to the atmosphere, routed through a flowmeter, or controlled with a backpressure regulator to sustain elevated average pore pressures. Flow rate measurements may be taken on either side of the sample and are generally reported as a volumetric flow rate (Q_r) referenced to an absolute pressure (P_r) under thermal equilibrium conditions.

PoroPerm (Vinci Technologies)

The Vinci Technologies PoroPerm (Figure 18) is a precision steady-state gas permeameter and porosimeter renowned for its ability to deliver fast, accurate permeability measurements This system was employed to determine the absolute permeability of dry sandstone plugs under steady-state conditions using nitrogen at low pressure and room temperature.

In this operating mode, nitrogen is injected at a controlled and constant flow rate through the plug, which is confined within a low-pressure Hassler-type core holder positioned vertically. The system accommodates samples with diameters of 1.5 inches and lengths between 1 and 3 inches.

In the standard configuration, the confining pressure is equal to the inlet pore pressure, with maximum values (400 psi) limited by the regulator. The outlet stream is vented directly to the atmosphere, as the system is not equipped with a backpressure regulator. Flow rates are controlled via a precision mass flow controller, and once equilibrium is reached, when inlet and outlet flow rates remain constant, the permeability is calculated.

These are the main components of the PoroPerm system (Figure 18):

- Gas Inlet / Regulator Reduces and stabilizes gas supply pressure.
- HV01–HV07 (Manual Valves) Direct and isolate gas flow paths.
- FQT (Flow Controller) Measures and controls gas flow rate.
- Tank (Buffer) Maintains pressure stability in the circuit.
- Core Holder Holds the rock sample for testing.
- Matrix Cup Contains the confining fluid around the sample.
- Confining Pressure Line Applies external pressure on the core holder.
- PT01 / PT02 (Pressure Transducers) Measure inlet and outlet pressures.
- TE01 (Temperature Sensor) Monitors gas or core temperature.
- PI01 (Pressure Indicator) Displays confining pressure value.
- HV06 (Metering Valve) Fine control of outlet pressure drop.
- Flow Direction Selector (Forward / Backward) Allows permeability testing in both flow directions.

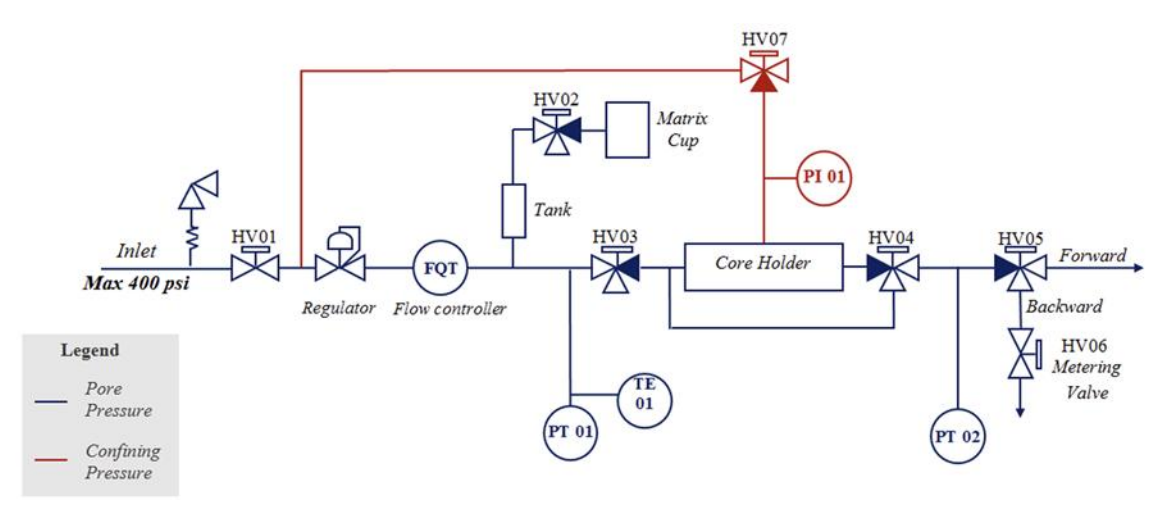


Figure 18. PoroPerm components diagram.

Hydrogen Permeameter (Vinci Technologies)

The Vinci Technologies Hydrogen Permeameter (Figure 19) is a high-precision instrument specifically designed to evaluate rock permeability to hydrogen gas under controlled laboratory conditions. This system was employed in the present study to determine both the absolute permeability of dry sandstone plugs and the effective permeability of samples saturated to irreducible water saturation, under steady-state flow. Measurements were conducted with both nitrogen and hydrogen as test fluids, across defined temperature and pressure conditions. The experimental setup incorporates a high-pressure Hassler-type core holder designed to house core plugs with diameters ranging from 1 to 1.5 inches and lengths

between 0.5 and 3 inches. This device can withstand confining pressures up to 10,000 psi, enabling tests to be conducted under conditions that closely replicate those found in subsurface reservoirs.

Gas injection can be regulated by two hydrogen-calibrated mass flow controllers, which provide precise control of flow rates. Pressure difference across the sample can be measured with two differential pressure transducers, the DPT offering the highest accuracy. Since the apparatus is calibrated to measure hydrogen flow rates, when nitrogen is used as the test gas the recorded values must be corrected by dividing the measured flow rate by a correction factor of 1.008. This data is used to calculate the permeability of the sample to hydrogen and nitrogen.

A dome-loaded backpressure regulator is used to maintain a stable downstream pressure, allowing experiments to be performed at elevated mean pore pressures. The setup also includes a thermostatically controlled heating mantle capable of regulating temperatures up to 100 °C. This component ensures thermal stability during testing, which is crucial given that both gas viscosity and rock permeability are highly sensitive to temperature variations.

These are the components of the Hydrogen Permeameter (Figure 19):

- Gas Inlet / Regulator Controls hydrogen supply pressure.
- MFC-01 (Mass Flow Controller Inlet) Sets precise inlet gas flow.
- MFC-02 (Mass Flow Controller Outlet) Measures outlet gas flow.
- PT01–PT04 (Pressure Transducers) Monitor pressures at multiple points along the system.
- DPT (Differential Pressure Transducer) Measures pressure drop across the core.
- Core Holder Contains the rock plug under confining pressure.
- Heating Mantle / Temperature Control Maintains test temperature.
- Confining Pressure Circuit Applies radial stress to the sample.
- BPR (Back Pressure Regulator) Controls and stabilizes outlet pressure.
- N₂ Buffer Line Dampens downstream pressure fluctuations.
- Exhaust / Vent Line Safely releases used gas.
- Data Acquisition Unit Records flow, pressure, and temperature signals.

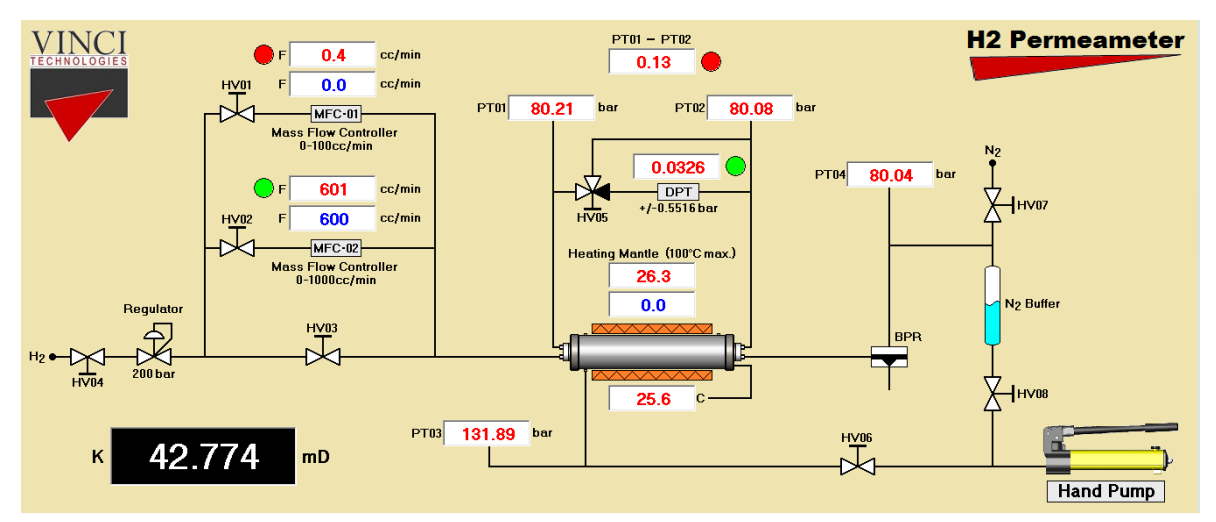


Figure 19. Hydrogen Permeameter components diagram.

4.2.2. Saturators

Manual Humidifier (Vinci Technologies)

The manual saturator provided by Vinci Technologies was employed to achieve full saturation of the core plugs through a combination of vacuum application and controlled fluid injection. Each dried sample was first placed in the saturation chamber, where a vacuum was drawn to remove air from the pore system. After a stable vacuum was reached, deionized water was introduced, allowing the liquid to infiltrate the sample gradually by capillary action. For low-permeability cores, additional pressure could be applied manually with a hand pump or regulator to enhance saturation efficiency.

During the process, the escape of air bubbles served as a qualitative indication that trapped air was being displaced from the pores. A noticeable reduction or disappearance of bubbles suggested that most of the air had been removed. However, this observation alone was not considered sufficient proof of complete saturation. To confirm full saturation, a mass balance check was performed: each sample was weighed before and after saturation, and 100% saturation was assumed when the mass increase matched the theoretical pore volume calculated from the porosity and grain volume.

Threshold Pressure System (CoreLab)

To obtain the irreducible water saturation (S_{wi}) in core samples, the Threshold Pressure System from Core Laboratories was used to displace mobile water through capillary pressure. This procedure involves applying a fluid pressure gradient across the core that exceeds the capillary threshold pressure, allowing only the non-bound (mobile) water to be expelled from the pore system.

The test starts with a fully saturated core sample, at 100% water saturation, placed inside the core holder and subjected to confining pressure. Nitrogen gas, acting as the non-wetting phase, is then injected through the sample at a differential pressure ($\Delta P > 50$ psi) higher than that used for the standard permeability test. This ensures that the gas has enough driving force to overcome the capillary forces holding the movable water inside the pores. The injection is performed at low flow rates to prevent any damage or disturbance to the rock structure. As the gas moves through the core, the displaced water is collected and its volume is recorded over time. The process continues until no more water is produced, which indicates that only the irreducible, or bound, water remains within the pore system.

4.3. Experimental Procedure

The following graph (Figure 20) illustrates the step-by-step experimental procedure for each of the analysed samples. First, permeability was measured in the PoroPerm Permeameter in the dry state using nitrogen, after weighing the samples and calculating their porosity. Subsequently, each sample's permeability was measured with both hydrogen and nitrogen using the Hydrogen Permeameter. After these initial measurements, the samples were fully saturated with distilled water using the Manual Humidifier, and the samples were weighed to confirm 100% water saturation. Once saturation was achieved, the Threshold Pressure System was used to remove the mobile water by applying a differential pressure higher than the typical values observed in the permeameters ($\Delta P > 50$ psig). After this step, the samples were weighed again to determine the irreducible water saturation (S_{wi}). Finally, the samples were measured again with hydrogen and nitrogen in the Hydrogen permeameter. For sample DM3, measurements were taken first with nitrogen and then with hydrogen, whereas samples DM1 and DM2 were measured first with hydrogen and immediately afterward with nitrogen.

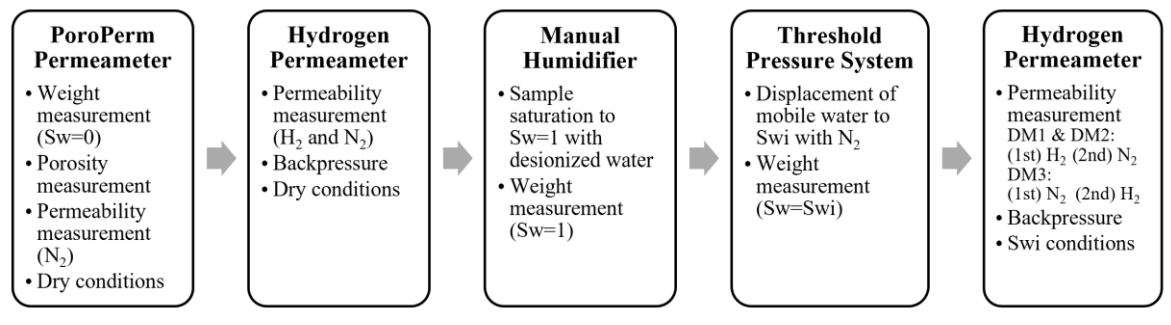


Figure 20. Generalized experimental procedure.

4.4. Experimental Conditions

Experiments were carried out using three main systems: the PoroPerm Permeameter, the Hydrogen Permeameter, and the Threshold Pressure System, provided by Vinci Technologies and CoreLab. The following tables (Table 4, 5 and 6) describe the main setup conditions that were used for the measurements performed with these instruments:

PoroPerm (Vinci Technologies)

Table 4. Experimental conditions for permeability measurements with PoroPerm equipment.

| Gas type | Nitrogen |
|------------------------|--|
| Confining pressure | 400 psi / 27.58 bar |
| Backpressure | Absent, P ₂ to atmospheric pressure |
| Temperature | Room temperature |
| Flow rate | 5 runs |
| Stabilization criteria | 0.01 psi/2min / 0.000689 bar/2min |

Hydrogen Permeameter (Vinci Technologies)

Table 5. Experimental conditions for permeability measurement with Hydrogen Permeameter equipment.

| Gas type | Hydrogen, Nitrogen |
|------------------------|---|
| Confining pressure | 130 bar |
| Mean pressure | 5, 25, 40, 60, 80 bar |
| Backpressure | Present |
| Temperature | 25.6 °C / 298.75 K |
| Flow rate | 3 to 4 runs (Hydrogen); 4 runs (Nitrogen), Correction factor: 1/1.008 |
| Stabilization criteria | 0.005 bar/3min |

Threshold Pressure System (CoreLab)

Table 6. Experimental conditions for permeability measurement with Hydrogen Permeameter equipment.

| Gas type | Nitrogen |
|-----------------------|--|
| Confining pressure | 100 bar |
| Differential pressure | \geq 50 psi \geq 3.45 bar |
| Backpressure | Absent, P ₂ to atmospheric pressure |
| Temperature | Room temperature |
| Flow rate | 60 ml/min |

4.5. Calculations

The following section presents the main data and formulations used to determine the apparent permeability values for each gas under dry conditions and at irreducible water saturation:

PoroPerm (Vinci Technologies)

Viscosity: Viscosity for nitrogen μ is calculated from Sutherland's formula (Sutherland, 1893) depending on temperature during the test:

$$\mu = \lambda_s \frac{T^{\frac{3}{2}}}{T + C} \tag{42}$$

with:

$$\lambda_s = \mu_o \frac{T_o + C}{T_o^{\frac{3}{2}}} \tag{43}$$

Where μ is the gas viscosity at temperature T, μ_o is the reference viscosity, T is the mean temperature of flowing gas, T_o is the reference temperature, and C is the Sutherland's constant (Table 7).

Table 7. Nitrogen properties for viscosity calculations.

| Gas | <i>C</i> [K] | μ_o [cp] | T_o [K] | λ_s [μ Pa.s.K ^(-1/2)] |
|----------|--------------|--------------|-----------|--|
| Nitrogen | 111 | 0.01781 | 300.55 | 1.407 |

Permeability: Apparent permeability to nitrogen k_g is calculated using the following expression, modified from Equation 18:

$$k_{g(N_2)} = \frac{\mu L}{4} \frac{P_2 Q_2}{\Lambda P \overline{P}}$$
 (44)

Where μ is the nitrogen viscosity at room temperature, A is the cross-sectional area, L is the sample length, Q_2 is the outlet flow rate, and P_2 is the outlet pressure (atmospheric pressure), considering plug pressure drop ($\Delta P = P_1 - P_2$) and plug mean pressure ($\overline{P} = \frac{(P_1 + P_2)}{2}$), where P_1 is the inlet pressure.

This is valid when the room temperature equals the mean temperature of the flowing gas and gas compressibility factor is taken as 1, which is approximately true for nitrogen under ambient conditions.

Hydrogen Ppermeameter (Vinci Technologies)

Viscosity: The viscosity of nitrogen and hydrogen was calculated at different pressures based on the experimental data at 25 °C reported by Mason & Spurling (1969). The values used are presented in Table 8, and shown in Figures 21 and 22.

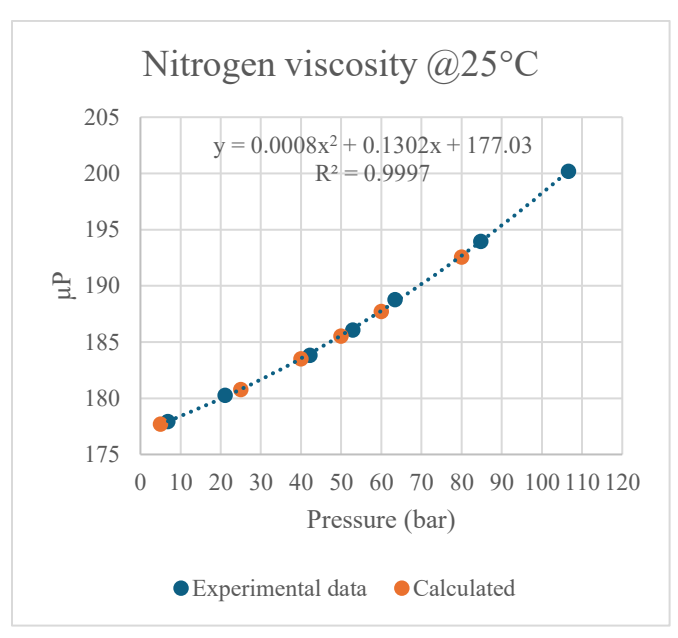


Figure 21. Nitrogen viscosity experimental data at 25°C from Mason & Sputling (1969) and empirical equations calculated regarding those experiments.

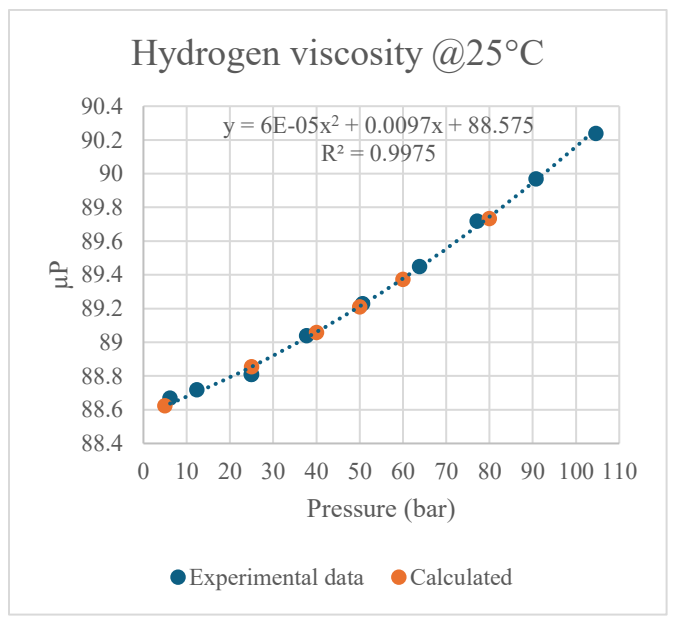


Figure 22. Hydrogen viscosity experimental data at 25°C from Mason & Sputling (1969) and empirical equations calculated regarding those experiments.

Compressibility factor: Although both nitrogen and hydrogen behave almost ideally under the ambient temperature and pressure conditions used in this study, their compressibility factors (z) at 25 °C and different pressures were calculated using the Peng–Robinson equation of state (Peng & Robinson, 1976) (Table 8). For nitrogen, the z factor remains very close to 1, showing only a slight decrease below unity at low to moderate pressures (up to around 70 bar) before rising marginally above 1 at higher pressures. This trend confirms that nitrogen exhibits nearly ideal gas behaviour across the examined pressure range. Hydrogen, on the

other hand, consistently shows z values greater than 1, indicating a mild positive deviation from ideality. This deviation is mainly attributed to its higher compressibility and the dominance of repulsive molecular interactions under the tested conditions.

Permeability: Apparent permeability to nitrogen or hydrogen k_g is calculated using the following expression, modified from Equation 18:

$$k_g = \frac{\mu(T, \overline{P})z(T, \overline{P})TL}{AT_{atm}} \frac{Q}{(P_1^2 - P_2^2)}$$
 (45)

Where $\mu(T, \overline{P})$ is the gas viscosity at certain temperature and pressure conditions, $z(T, \overline{P})$ is the mean compressibility factor at certain temperature and pressure conditions, A is the cross-sectional area, L is the sample length, T is the gas mean temperature, T_{atm} is the room temperature, Q_2 is the outlet flow rate, P_1 is the inlet pressure and P_2 is the outlet pressure.

Effective permeability is determined using the same equations applied for absolute permeability but with the core sample at irreducible water saturation.

| Pressure (bar) Viscosity (cP) Compressibility factor z - PR | | | | | |
|---|----------------------|----------|--|--|--|
| 1 ressure (Dar) | • ` ' | | | | |
| | H | 2 | | | |
| 5 0.008863 1.001428 | | | | | |
| 25 | 0.008886 | 1.007562 | | | |
| 40 | 0.008906 | 1.012579 | | | |
| 50 | 0.008921 | 1.016108 | | | |
| 60 | 0.008937 | 1.019778 | | | |
| 80 | 0.008974 | 1.027511 | | | |
| | N ₂ | 2 | | | |
| 5 | 0.017770 | 0.997845 | | | |
| 25 | 0.018079 | 0.99095 | | | |
| 40 | 40 0.018352 0.987549 | | | | |
| 50 | 0.018554 | 0.986097 | | | |
| 60 | 60 0.018772 0.985276 | | | | |
| 80 | 0.019257 | 0.985442 | | | |

Table 8. Viscosity and compressibility factor data for hydrogen and nitrogen at different pressures.

Knudsen number: The Knudsen number is calculated as the ratio between the mean free path and the average pore diameter or characteristic pore size for each sample (Equation 28). The mean free path values for each gas (hydrogen and nitrogen) is determined by using Equation 21 at a temperature of 25°C, across the range of pressures considered (Table 9). The characteristic pore size of each sample was determined at different apparent permeability values under a given pressure using Equation 29.

| Table 9. Mean free path data for hydrogen and nitrogen at different press | ires. |
|--|-------|
|--|-------|

| Pressure (bar) | H ₂ Mean free path (μm) | N ₂ Mean free path (μm) |
|----------------|------------------------------------|------------------------------------|
| 5 | 5 0.022186 0.013986 | |
| 25 | 0.004437 | 0.002797 |
| 40 | 0.0027733 | 0.0017482 |
| 60 | 0.001849 | 0.0011655 |
| 80 | 0.0013867 | 0.0008741 |

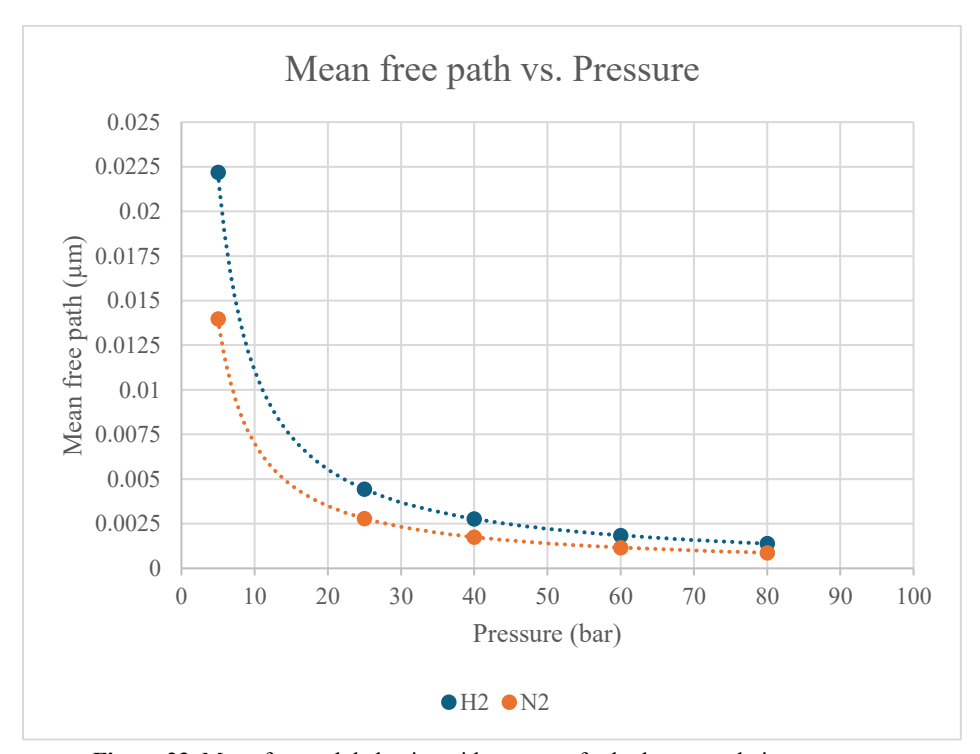


Figure 23. Mean free path behavior with pressure for hydrogen and nitrogen gases.

Threshold pressure system (CoreLab)

Irreducible water saturation: The irreducible water saturation (S_{wi}) is determined using the gravimetric method, which compares the mass of a core sample at different saturation stages. First, the dry weight of the sample (W_{dry}) is recorded after it has been completely dried $(S_w = 0)$. Then, the fully saturated weight (W_{sat}) is measured once the sample reaches full water saturation $(S_w = 1)$. The irreducible state corresponds to the sample's weight when no additional movable water can be expelled, referred to as W_i . The value of S_{wi} is then calculated using the following expression:

$$S_{wi} = \frac{W_i - W_{\text{dry}}}{W_{\text{sat}} - W_{\text{dry}}} \tag{46}$$

4.6. Corrections

Klinkenberg effect

The corrections accounting for the Klinkenberg effect, aimed at determining absolute permeability whenever possible, were carried out graphically according to Equation 24.

5. Results

5.1. PoroPerm Measurements

The PoroPerm tests using nitrogen were conducted under a relatively low confining pressure of approximately 27 bar, without backpressure and at different flow rates, resulting in various mean pressure values.

The apparent nitrogen permeabilities for sample DM1 ranged from 199 to 194 mD at mean pressures between 1.097 and 1.181 bar, respectively. For sample DM2, apparent nitrogen permeabilities varied from 5 to 4 mD, corresponding to mean pressures between 1.1 and 1.7 bar. For sample DM3, the apparent permeability to nitrogen ranged from 49 to 45 mD, with mean pressures between 1.6 and 4.6 bar. In all samples, a consistent decrease in permeability with increasing pressure was observed (Tables 10, 11, and 12).

Table 10. DM1 PoroPerm permeability results.

| | | | DM3-N ₂ -Dry | | | |
|-------------|---------------------|------------|-------------------------|----------------|----------------------|------------|
| P_{Inlet} | P _{Outlet} | T_{Room} | Q | $\mathbf{k_g}$ | $1/P_{mean}$ | ΔP |
| (bar) | (bar) | (°C) | (ncc/min) | (mD) | (bar ⁻¹) | (bar) |
| 1.050 | 1.016 | 23.2 | 49.99 | 178 | 0.968 | 0.034 |
| 1.082 | 1.016 | 23.2 | 100 | 182 | 0.954 | 0.066 |
| 1.185 | 1.010 | 23.9 | 300 | 199 | 0.911 | 0.174 |
| 1.244 | 1.016 | 23.2 | 400.01 | 196 | 0.885 | 0.228 |
| 1.297 | 1.016 | 23.2 | 499.99 | 194 | 0.865 | 0.281 |
| 1.347 | 1.016 | 23.3 | 599.97 | 194 | 0.847 | 0.331 |

Table 11. DM2 PoroPerm permeability results.

| | DM2-N ₂ -Dry | | | | | |
|-------------|-------------------------|------------|-----------|---------------------------|----------------------|-------|
| P_{Inlet} | P_{Outlet} | T_{Room} | Q | $\mathbf{k}_{\mathbf{g}}$ | 1/P _{mean} | ΔΡ |
| (bar) | (bar) | (°C) | (ncc/min) | (mD) | (bar ⁻¹) | (bar) |
| 2.276 | 1.002 | 26.9 | 49.99 | 5.3 | 0.610 | 1.273 |
| 3.196 | 1.003 | 26.7 | 100 | 4.8 | 0.476 | 2.193 |
| 5.643 | 1.003 | 26.6 | 300.04 | 4.3 | 0.301 | 4.640 |
| 6.548 | 1.002 | 26.8 | 400.02 | 4.2 | 0.265 | 5.545 |
| 7.427 | 1.003 | 26.7 | 500.04 | 4.1 | 0.237 | 6.424 |
| 8.206 | 1.002 | 26.7 | 599.98 | 4.0 | 0.217 | 7.204 |

Table 12. DM3 PoroPerm permeability results.

| | DM3-N ₂ -Dry | | | | | | | | | |
|--------------------|-------------------------|------------|-----------|----------------|----------------------|-------|--|--|--|--|
| P _{Inlet} | Poutlet | T_{Room} | Q | $\mathbf{k_g}$ | 1/P _{mean} | ΔΡ | | | | |
| (bar) | (bar) | (°C) | (ncc/min) | (mD) | (bar ⁻¹) | (bar) | | | | |
| 1.193 | 1.008 | 21.5 | 49.95 | 49.2 | 0.908 | 0.185 | | | | |
| 1.355 | 1.008 | 21.5 | 99.99 | 49.0 | 0.846 | 0.347 | | | | |
| 1.886 | 1.009 | 21.5 | 300.16 | 47.4 | 0.691 | 0.877 | | | | |
| 2.107 | 1.009 | 21.4 | 400.03 | 46.8 | 0.642 | 1.098 | | | | |
| 2.319 | 1.009 | 21.3 | 499.98 | 45.8 | 0.601 | 1.311 | | | | |
| 2.511 | 1.009 | 21.3 | 599.84 | 45.3 | 0.568 | 1.502 | | | | |

Klinkenberg correction

After applying the Klinkenberg correction, the plot of apparent permeability versus the reciprocal of mean pressure for sample DM1 displayed a characteristic linear trend, with the y-intercept representing the absolute permeability according to Klinkenberg's method, yielding a value of 123 mD (Figure 24) and lower pressure points considered as outliers. In the case of sample DM2, the linear relationship was nearly perfect, resulting in an absolute permeability of 3.3 mD after correction (Figure 25). In contrast, sample DM3 showed a more dispersed data distribution, with a linear trend and an intercept value of 39 mD (when all data points were considered) (Figure 26).

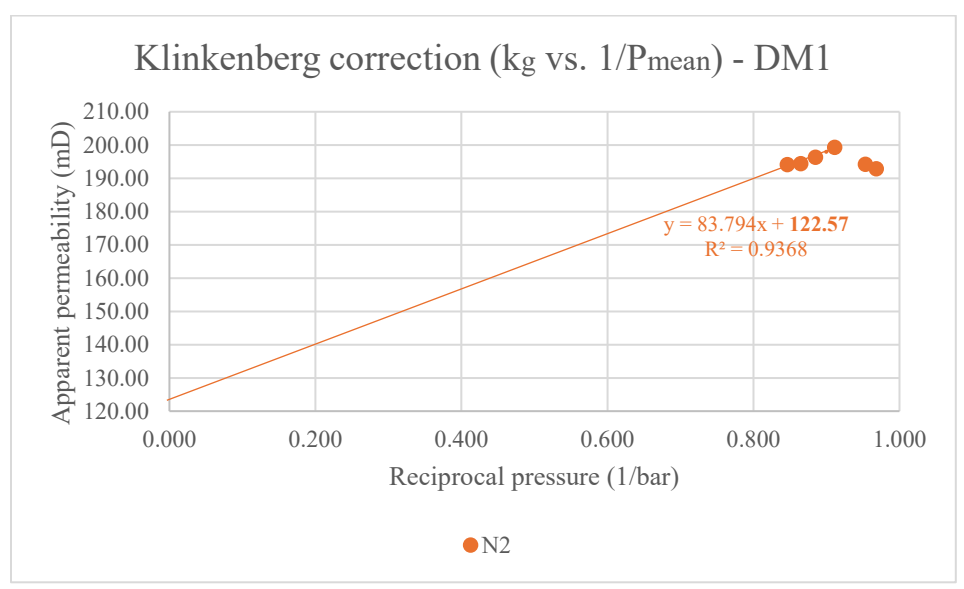


Figure 24. Klinkenberg correction graph for PoroPerm results of sample DM1.

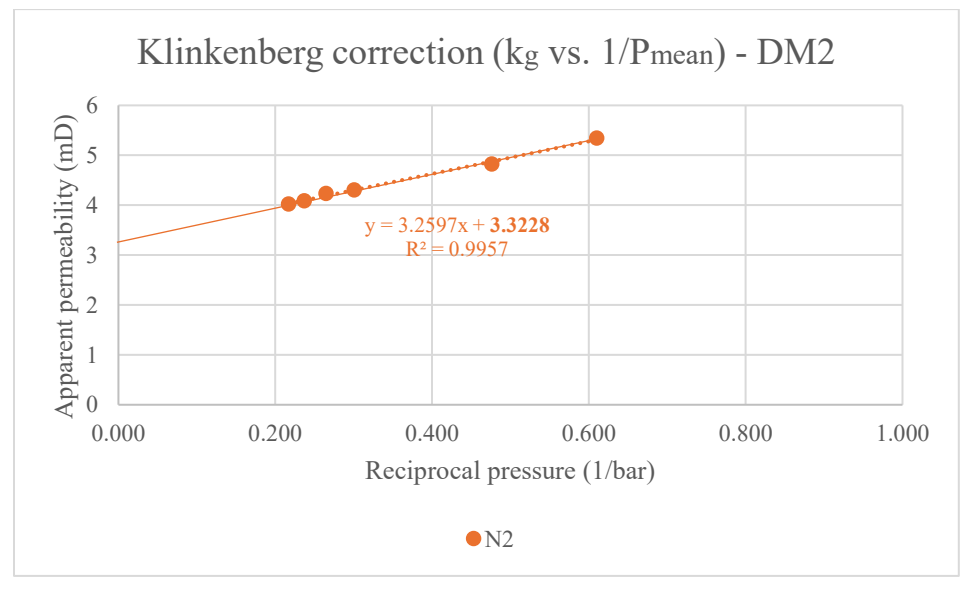


Figure 25. Klinkenberg correction graph for PoroPerm results of sample DM2.

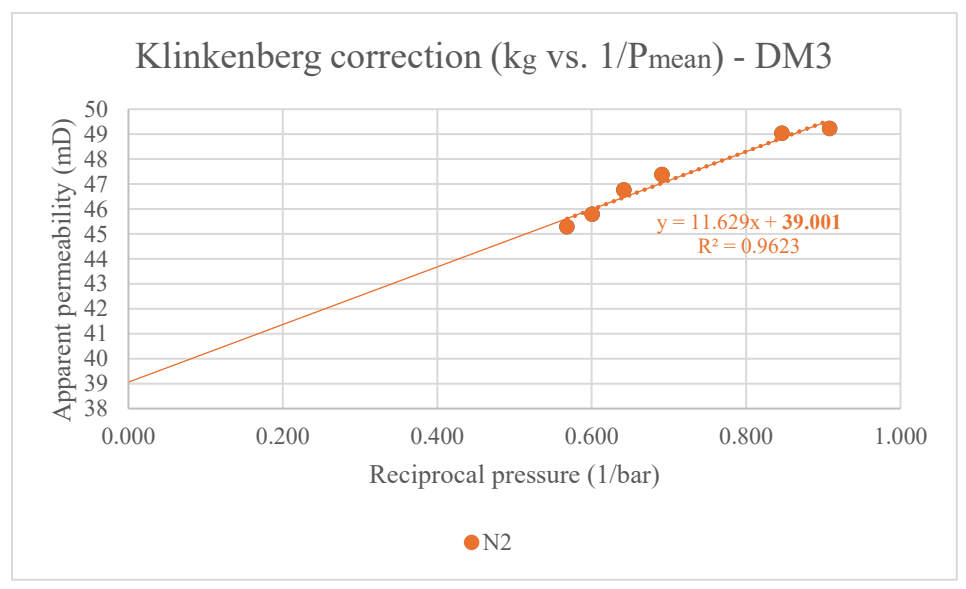


Figure 26. Klinkenberg correction graph for PoroPerm results of sample DM3.

5.2. Hydrogen Permeameter Measurements: H₂ vs. N₂ Permeability Under Dry Conditions

Permeability measurements were conducted at a confining pressure of 130 bar and a controlled temperature of 25°C, using nitrogen and hydrogen as test gases at different pressures (5, 25, 40, 60, and 80 bar) and backpressure.

In the case of sample DM1 (Table 13), a clear non-linear decrease in permeability with increasing pressure is observed for both nitrogen and hydrogen measurements. For hydrogen, the permeability values range from 158 mD at 5 bar to 29 mD at 80 bar, while for nitrogen they range from 191 mD at 5 bar to 50 mD at 80 bar. Overall, permeability to nitrogen is higher than to hydrogen, with the difference between them gradually decreasing as pressure increases, from approximately 40 mD at 5 bar to about 20 mD at 80 bar. For sample DM2 (Table 14), permeability values ranged from 2.50 to 1.95 mD, showing no clear trend of permeability reduction with pressure and no significant difference between nitrogen and hydrogen measurements. Finally, for sample DM3 (Table 15), permeability ranged from 46.6 to 41.7 mD, decreasing with pressure. Nitrogen data shows a clear linear trend while hydrogen data depicts a minor nonlinear trend showing a reduction in permeability at high pressures. However, there was no relevant distinction between hydrogen and nitrogen results. The permeability value of 35 mD to hydrogen at 80 bar is regarded as an outlier.

 Table 13. DM1 Hydrogen Permeameter permeability results under dry conditions.

| $_{ m H_2}$ | 0.041 0.031 0.022 0.014 0.012 0.010 0.008 0.012 0.010 0.008 0.012 | 6.234 6.225 6.215 6.197 25.978 25.975 25.973 25.951 41.405 41.384 41.382 | 6.193 6.193 6.193 6.183 25.963 25.963 25.963 25.943 41.393 41.373 | 6.204 | 25.8 25.8 25.8 25.8 25.8 25.8 25.8 25.8 | 25.3 25.3 25.3 25.3 25.6 25.6 25.6 25.6 | 801.00 601.00 400.00 200.00 801.00 601.00 400.00 | 181.511 176.788 166.768 134.818 122.636 108.613 88.195 | 158.153 77.293 | 0.161 |
|-------------|---|--|--|-------------------|--|--|--|--|-------------------|-------|
| $_{ m H_2}$ | 0.022 0.014 0.014 0.012 0.010 0.008 0.012 0.010 0.009 | 6.215 6.197 25.978 25.975 25.973 25.951 41.405 41.384 41.382 | 6.193 6.183 25.963 25.963 25.963 25.943 41.393 41.373 | | 25.8 25.8 25.8 25.8 25.8 25.8 25.8 | 25.3 25.3 25.6 25.6 25.6 | 400.00 200.00 801.00 601.00 | 166.768 134.818 122.636 108.613 | | |
| $_{ m H_2}$ | 0.014 0.014 0.012 0.010 0.008 0.012 0.010 0.009 | 6.197 25.978 25.975 25.973 25.951 41.405 41.384 41.382 | 6.183 25.963 25.963 25.963 25.943 41.393 41.373 | | 25.8 25.8 25.8 25.8 25.8 | 25.3 25.6 25.6 25.6 | 200.00 801.00 601.00 | 134.818 122.636 108.613 | | |
| H_2 | 0.014 0.012 0.010 0.008 0.012 0.010 0.009 | 25.978 25.975 25.973 25.951 41.405 41.384 41.382 | 25.963 25.963 25.963 25.943 41.393 41.373 | 25.964 | 25.8 25.8 25.8 25.8 | 25.6 25.6 25.6 | 801.00 601.00 | 122.636 108.613 | 77.293 | 0 039 |
| H_2 | 0.012 0.010 0.008 0.012 0.010 0.009 | 25.975 25.973 25.951 41.405 41.384 41.382 | 25.963 25.963 25.943 41.393 41.373 | 25.964 | 25.8 25.8 25.8 | 25.6 25.6 | 601.00 | 108.613 | 77.293 | 0.039 |
| H_2 | 0.010 0.008 0.012 0.010 0.009 | 25.973 25.951 41.405 41.384 41.382 | 25.963 25.943 41.393 41.373 | 25.964 | 25.8 25.8 | 25.6 | | | 77.293 | 0.039 |
| H_2 | 0.008 0.012 0.010 0.009 | 25.951 41.405 41.384 41.382 | 25.943 41.393 41.373 | 23.904 | 25.8 | | 400.00 | 88.195 | 11.293 | 0.019 |
| $ m H_2$ | 0.012 0.010 0.009 | 41.405 41.384 41.382 | 41.393 41.373 | | | 25.6 | | | | 0.057 |
| H_2 | 0.010 0.009 | 41.384 41.382 | 41.373 | | 25.8 | | 200.00 | 57.316 | | |
| H_2 | 0.009 | 41.382 | | | | 25.5 | 801.00 | 93.334 | | |
| | | | 41 272 | 41 201 | 25.8 | 25.5 | 601.00 | 80.171 | 51 041 | 0.024 |
| | 0.008 | | 41.373 | 41.381 | 25.8 | 25.5 | 400.00 | 61.659 | 51.841 | 0.024 |
| | | 41.371 | 41.363 | | 25.8 | 25.5 | 200.00 | 36.518 | | |
| | 0.011 | 61.214 | 61.203 | | 25.8 | 25.3 | 801.00 | 69.206 | | |
| | 0.010 | 61.213 | 61.203 | (1 100 | 25.8 | 25.3 | 601.00 | 56.600 | 24 220 | 0.016 |
| | 0.009 | 61.182 | 61.173 | 61.188 | 25.8 | 25.3 | 400.00 | 41.416 | 34.320 | 0.016 |
| | 0.008 | 61.161 | 61.153 | | 25.8 | 25.3 | 200.00 | 23.564 | | |
| | 0.011 | 81.544 | 81.533 | 01.510 | 25.8 | 25.5 | 801.00 | 51.657 | | |
| | 0.010 | 81.524 | 81.513 | 81.512 | 25.8 | 25.5 | 601.00 | 41.403 | 29.370 | 0.012 |
| Dry | 0.009 | 81.482 | 81.473 | | 25.8 | 25.5 | 200.00 | 15.953 | | |
| DM1 - Dry | 0.063 | 7.226 | 7.163 | | 25.8 | 25.5 | 794.64 | 202.416 | 190.738 | 0.140 |
| DM | 0.048 | 7.181 | 7.133 | 7 1 4 0 | 25.8 | 25.5 | 596.23 | 200.883 | | |
| | 0.033 | 7.146 | 7.113 | 7.148 | 25.8 | 25.5 | 396.83 | 194.362 | | |
| | 0.018 | 7.121 | 7.103 | | 25.8 | 25.5 | 198.41 | 178.511 | | |
| | 0.020 | 26.073 | 26.053 | | 25.8 | 25.5 | 794.64 | 176.761 | | |
| | 0.016 | 26.059 | 26.043 | 26.050 | 25.8 | 25.5 | 596.23 | 165.653 | 120 246 | 0.020 |
| | 0.013 | 26.056 | 26.043 | 26.050 | 25.8 | 25.5 | 396.83 | 139.777 | 128.246 | 0.038 |
| | 0.008 | 26.042 | 26.033 | | 25.8 | 25.5 | 198.41 | 105.714 | | |
| | 0.016 | 40.869 | 40.853 | | 25.8 | 25.5 | 794.64 | 146.525 | | |
| NI | 0.013 | 40.846 | 40.833 | 40.942 | 25.8 | 25.5 | 596.23 | 133.872 | 07 122 | 0.024 |
| N_2 | 0.010 | 40.844 | 40.833 | 40.842 | 25.8 | 25.5 | 396.83 | 111.594 | 97.133 | 0.024 |
| | 0.008 | 40.831 | 40.823 | | 25.8 | 25.5 | 198.41 | 74.658 | | |
| | 0.013 | 61.247 | 61.233 | | 25.8 | 25.5 | 794.64 | 117.168 | | |
| | 0.011 | 61.215 | 61.203 | 61.194 | 25.8 | 25.5 | 596.23 | 103.388 | (0.500 | 0.016 |
| | 0.010 | 61.183 | 61.173 | | 25.8 | 25.5 | 396.83 | 82.615 | 68.599 | 0.016 |
| | 0.008 | 61.151 | 61.143 | | 25.8 | 25.5 | 198.41 | 50.336 | | |
| | 0.013 | 81.466 | 81.453 | | 25.8 | 25.5 | 794.64 | 95.341 | | |
| | 0.011 | 81.434 | 81.423 | 01 410 | 25.8 | 25.5 | 596.23 | 81.147 | 40.003 | 0.012 |
| | 0.010 | 81.403 | 81.393 | ⊣ 81.419 ⊢ | 25.8 | 25.5 | 396.83 | 61.123 | | |
| | 0.008 | 81.392 | 81.383 | | 25.8 | 25.5 | 198.41 | 36.024 | | |

 Table 14. DM2 Hydrogen Permeameter permeability results under dry conditions.

| | | ΔΡ | P _{Inlet} | Poutlet | P _{Mean} | | T _{Sample} | Q | k | kg | 1/P _{mean} |
|-----------|-------|-------|--------------------|---------|-------------------|------|---------------------|---------|-------|-------|----------------------|
| | | (bar) | (bar) | (bar) | (bar) | (°C) | (°C) | Ncc/min | (mD) | (mD) | (bar ⁻¹) |
| | | 0.318 | 6.771 | 6.453 | | 25.8 | 25.6 | 50.00 | 2.379 | | |
| | | 0.256 | 6.709 | 6.453 | 6.576 | 25.8 | 25.6 | 40.00 | 2.380 | 2.376 | 0.152 |
| | | 0.164 | 6.617 | 6.453 | | 25.8 | 25.6 | 25.00 | 2.330 | | |
| | | 0.098 | 26.581 | 26.483 | | 25.8 | 25.7 | 50.00 | 1.936 | | |
| | | 0.078 | 26.561 | 26.483 | 26.521 | 25.8 | 25.7 | 40.00 | 1.934 | 1.949 | 0.038 |
| | | 0.049 | 26.532 | 26.483 | | 25.8 | 25.7 | 25.00 | 1.930 | | |
| | | 0.059 | 41.242 | 41.183 | | 25.8 | 25.8 | 50.00 | 2.102 | | |
| | H_2 | 0.046 | 41.229 | 41.183 | 41.205 | 25.8 | 25.8 | 40.00 | 2.124 | 2.130 | 0.024 |
| | | 0.028 | 41.211 | 41.183 | | 25.8 | 25.8 | 25.00 | 2.169 | | |
| | | 0.034 | 62.497 | 62.463 | | 25.8 | 25.6 | 50.00 | 2.360 | | |
| | | 0.028 | 62.471 | 62.443 | 62.457 | 25.8 | 25.6 | 40.00 | 2.299 | 2.378 | 0.016 |
| | | 0.018 | 62.441 | 62.423 | | 25.8 | 25.6 | 25.00 | 2.308 | | |
| | | 0.026 | 83.169 | 83.143 | | 25.8 | 25.5 | 50.00 | 2.426 | | |
| 5 | | 0.021 | 83.145 | 83.123 | 83.137 | 25.8 | 25.5 | 40.00 | 2.352 | 2.367 | 0.012 |
| DM2 - Dry | | 0.014 | 83.127 | 83.113 | | 25.8 | 25.5 | 25.00 | 2.205 | | |
| M2 | | 0.444 | 7.057 | 6.613 | | 25.8 | 25.3 | 34.72 | 2.291 | | |
| D | | 0.325 | 6.938 | 6.613 | 6.775 | 25.8 | 25.3 | 24.80 | 2.258 | 2.272 | 0.148 |
| | | 0.201 | 6.814 | 6.613 | | 25.8 | 25.3 | 14.88 | 2.215 | | |
| | | 0.125 | 26.478 | 26.353 | | 25.8 | 25.3 | 34.72 | 2.144 | | |
| | | 0.089 | 26.432 | 26.343 | 26.394 | 25.8 | 25.3 | 24.80 | 2.162 | 2.141 | 0.038 |
| | | 0.051 | 26.404 | 26.353 | | 25.8 | 25.3 | 14.88 | 2.250 | | |
| | | 0.070 | 41.273 | 41.203 | | 25.8 | 25.1 | 34.72 | 2.503 | | |
| | N_2 | 0.051 | 41.244 | 41.193 | 41.218 | 25.8 | 25.1 | 24.80 | 2.462 | 2.462 | 0.024 |
| | | 0.030 | 41.213 | 41.183 | | 25.8 | 25.1 | 14.88 | 2.532 | | |
| | | 0.046 | 63.049 | 63.003 | | 25.8 | 25.5 | 34.72 | 2.549 | | |
| | | 0.033 | 63.016 | 62.983 | 62.986 | 25.8 | 25.5 | 24.80 | 2.513 | 2.504 | 0.016 |
| | | 0.019 | 62.973 | 62.953 | | 25.8 | 25.5 | 14.88 | 2.582 | | |
| | | 0.039 | 83.192 | 83.153 | | 25.8 | 25.3 | 34.72 | 2.353 | | |
| | | 0.028 | 83.171 | 83.143 | 83.147 | 25.8 | 25.3 | 24.80 | 2.317 | 2.301 | 0.012 |
| | | 0.017 | 83.120 | 83.103 | | 25.8 | 25.3 | 14.88 | 2.291 | | |

 Table 15. DM3 Hydrogen Permeameter permeability results under dry conditions.

| | | ΔP (bar) | P _{Inlet} (bar) | P _{Outlet} (bar) | P _{Mean} (bar) | T _{Room} (°C) | T _{Sample} (°C) | Q Ncc/min | k (mD) | kg (mD) | 1/P _{mean} (bar ⁻¹) |
|-----------|----------------|-------------|--------------------------|---------------------------|-------------------------|------------------------|--------------------------|--------------|-----------|---------------|--|
| | | 0.064 | 26.407 | 26.343 | | 25.8 | 25.3 | 801.00 | 44.338 | | |
| | | 0.047 | 26.390 | 26.343 | 26 250 | 25.8 | 25.3 | 601.00 | 45.490 | 45 271 | 0.028 |
| | | 0.030 | 26.373 | 26.343 | 26.358 | 25.8 | 25.3 | 400.00 | 47.044 | 45.371 | 0.038 |
| | | 0.014 | 26.338 | 26.323 | | 25.8 | 25.3 | 200.00 | 49.399 | | |
| | | 0.041 | 41.185 | 41.143 | | 25.8 | 25.3 | 801.00 | 43.916 | | |
| | | 0.030 | 41.163 | 41.133 | 41.141 | 25.8 | 25.3 | 601.00 | 45.079 | 45 210 | 0.024 |
| | | 0.019 | 41.153 | 41.133 | 41.141 | 25.8 | 25.3 | 400.00 | 46.953 | 45.210 | 0.024 |
| | тт | 0.010 | 41.113 | 41.103 | | 25.8 | 25.3 | 200.00 | 46.751 | | |
| | H_2 | 0.030 | 61.513 | 61.483 | | 25.8 | 25.4 | 801.00 | 41.005 | | |
| | | 0.022 | 61.485 | 61.463 | 61.460 | 25.8 | 25.4 | 601.00 | 41.176 | 42.020 | 0.016 |
| | | 0.014 | 61.458 | 61.443 | 61.460 | 25.8 | 25.4 | 400.00 | 42.266 | 42.039 | 0.016 |
| | | 0.008 | 61.422 | 61.413 | | 25.8 | 25.4 | 200.00 | 36.248 | | |
| | | 0.026 | 81.039 | 81.013 | | 25.8 | 25.5 | 801.00 | 35.550 | | |
| | | 0.020 | 81.024 | 81.003 | 01.002 | 25.8 | 25.5 | 601.00 | 34.132 | 24.007 | 0.013 |
| | | 0.016 | 81.009 | 80.993 | 81.002 | 25.8 | 25.5 | 400.00 | 29.711 | 34.987 | 0.012 |
| | | 0.010 | 80.973 | 80.963 | | 25.8 | 25.5 | 200.00 | 23.657 | | |
| 5 | | 0.263 | 6.166 | 5.903 | 5.047 | 25.8 | 25.6 | 396.83 | 46.525 | 46.629 | 0.168 |
| DM3 - Dry | | 0.131 | 6.014 | 5.883 | | 25.8 | 25.6 | 198.41 | 47.304 | | |
| M3 | | 0.065 | 5.948 | 5.883 | 5.947 | 25.8 | 25.6 | 99.21 | 47.860 | | |
| ū | | 0.032 | 5.905 | 5.873 | | 25.8 | 25.6 | 49.60 | 49.055 | | |
| | | 0.122 | 27.095 | 26.973 | | 25.8 | 25.6 | 794.64 | 45.654 | | |
| | | 0.089 | 27.082 | 26.993 | 27.025 | 25.8 | 25.6 | 596.23 | 46.729 | 45 001 | 0.027 |
| | | 0.058 | 27.051 | 26.993 | 27.025 | 25.8 | 25.6 | 397.82 | 48.145 | 45.881 | 0.037 |
| | | 0.028 | 27.021 | 26.993 | | 25.8 | 25.6 | 198.41 | 50.133 | | |
| | | 0.084 | 41.317 | 41.233 | | 25.8 | 25.1 | 794.64 | 44.209 | | |
| | N.T | 0.062 | 41.265 | 41.203 | 41.224 | 25.8 | 25.1 | 596.23 | 44.824 | 42 072 | 0.024 |
| | N ₂ | 0.041 | 41.224 | 41.183 | 41.224 | 25.8 | 25.1 | 396.83 | 45.704 | 43.873 | 0.024 |
| | | 0.020 | 41.193 | 41.173 | | 25.8 | 25.1 | 198.41 | 47.004 | | |
| | | 0.058 | 61.741 | 61.683 | | 25.8 | 25.0 | 794.64 | 43.812 | | |
| | | 0.043 | 61.706 | 61.663 | | 25.8 | 25.0 | 595.17 | 44.231 | 42 452 | 0.016 |
| | | 0.028 | 61.681 | 61.653 | 61.674 | 25.8 | 25.0 | 396.83 | 45.036 | 43.453 | 0.016 |
| | | 0.015 | 61.638 | 61.623 | | 25.8 | 25.0 | 198.41 | 43.664 | | |
| | | 0.044 | 81.087 | 81.043 | | 25.8 | 25.6 | 794.64 | 45.060 | | |
| | | 0.033 | 81.126 | 81.093 | 81.057 | 25.8 | 25.6 | 596.23 | 44.849 | 44 450 | 8 0.012 |
| | | 0.022 | 81.055 | 81.033 | | 25.8 | 25.6 | 397.82 | 45.967 | 44.458 | |
| | | 0.011 | 81.015 | 81.003 | | 25.8 | 25.6 | 198.41 | 43.640 | | |

Klinkenberg correction

Regarding sample DM2, the Klinkenberg correction was performed using the lowest pressure values, 5 and 25 bar, measured with nitrogen, yielding an absolute permeability of 2.1 mD (Figure 28). Using the same correction, the DM3 sample yielded an absolute permeability value of 44 mD based on all measurements obtained with nitrogen which exhibit a generally linear trend with increasing pressure (Figure 29). This correction was not applied to the data obtained for sample DM1, as it exhibits a strongly non-linear behaviour (Figure 27).

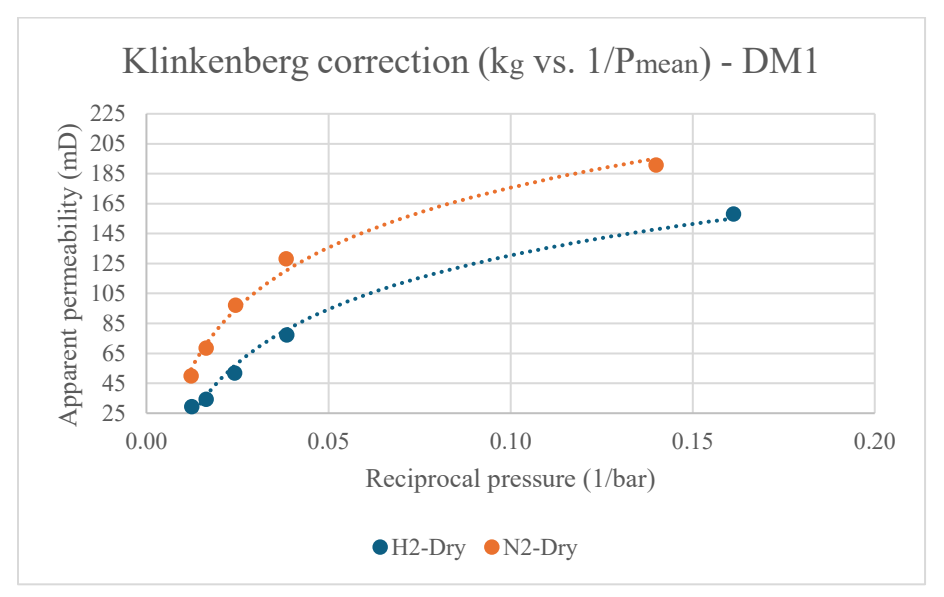


Figure 27. Klinkenberg correction graph for Hydrogen Permeameter results of sample DM1 under dry conditions.

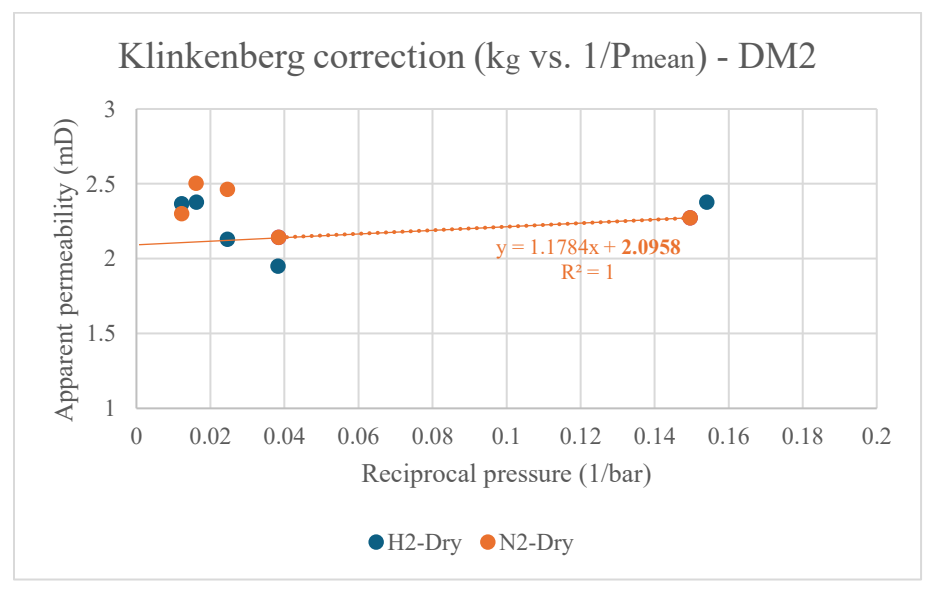


Figure 28. Klinkenberg correction graph for Hydrogen Permeameter results of sample DM2 under dry conditions.

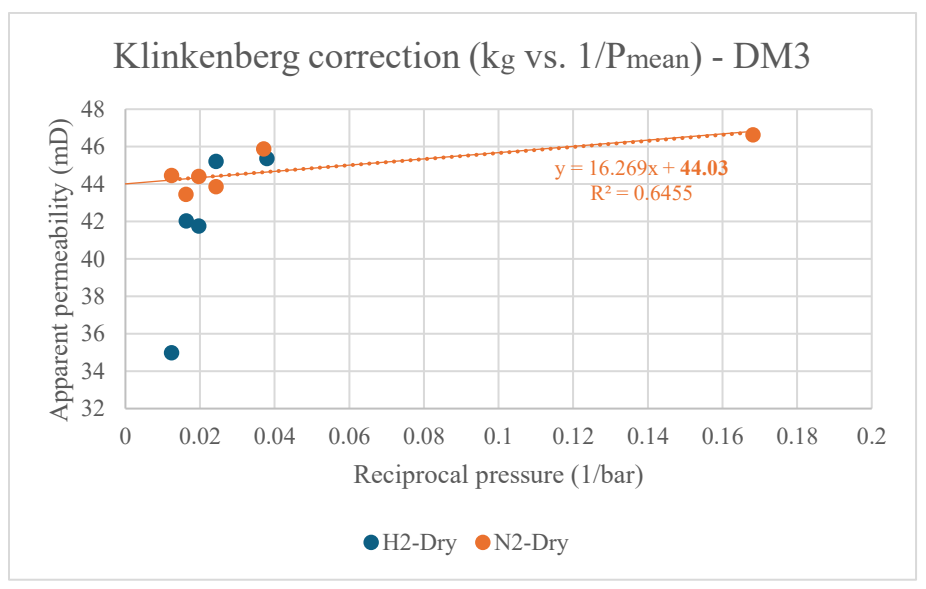


Figure 29. Klinkenberg correction graph for Hydrogen Permeameter results of sample DM3 under dry conditions.

5.3. Irreducible Water Saturation (Swi)

Water saturation measurements across the three rock samples revealed marked differences in water retention. The results indicated that sample DM1 showed S_{wi} value of 0.465, while DM2 recorded 0.366, and DM3 exhibited 0.578. Among the three, DM3 displayed the highest irreducible water saturations, followed by DM1 with intermediate values, and DM2 with the lowest.

Table 16. Irreducible water saturation results.

| | Weight | 98.487 g | 106.526 g | 102.226 g |
|-----|------------|-----------|-----------|-----------------------------|
| DM1 | Saturation | 0.0 | 1.0 | 0.465 (S _{wi}) |
| | Weight | 190.604 g | 201.331 g | 194.529 g |
| DM2 | Saturation | 0.0 | 1.0 | 0.3659 (Swi) |
| | Weight | 164.652 g | 178.611 g | 172.712 g |
| DM3 | Saturation | 0.0 | 1.0 | 0.5775 (Swi) |

5.4. Hydrogen Permeameter Measurements: H₂ vs. N₂ Effective Permeability Under Irreducible Water Saturation

Permeability tests under irreducible water saturation (effective permeability) were performed at a confining pressure of 130 bar and temperature of 25°C, using nitrogen and hydrogen at 5, 25, 40, 60, and 80 bar pressures with backpressure applied (Tables 17, 18 and 19).

For sample DM1, both hydrogen and nitrogen data exhibited a nonlinear decreasing trend of apparent effective permeability with the reciprocal of pressure, converging at higher pressures. Results showed that hydrogen values ranged between 91 and 23 mD, while nitrogen ranged from 114 to 43 mD, with nitrogen consistently exhibiting higher permeability. The difference between the two gases becomes progressively smaller as pressure increases. In the case of sample DM2, hydrogen effective permeability varied from 0.22 to 0.24 mD, and nitrogen from 0.42 to 0.44 mD, both displaying very limited sensitivity to pressure changes. Finally, in sample DM3, hydrogen effective permeability varied from 25.1 to 21.1 mD, showing a nonlinear decrease with pressure above 25 bar. Nitrogen data showed a slightly decreasing linear trend with values between 21.2 and 19.7 mD.

Klinkenberg correction

For sample DM1, the Klinkenberg correction was not applied due to its non-linear behaviour. In contrast, for DM2, the corrected effective permeabilities were 0.21 mD to hydrogen and 0.42 mD to nitrogen. For DM3, the nitrogen measurements yielded an effective permeability of 20 mD after correction (Figures 30, 31 and 32).

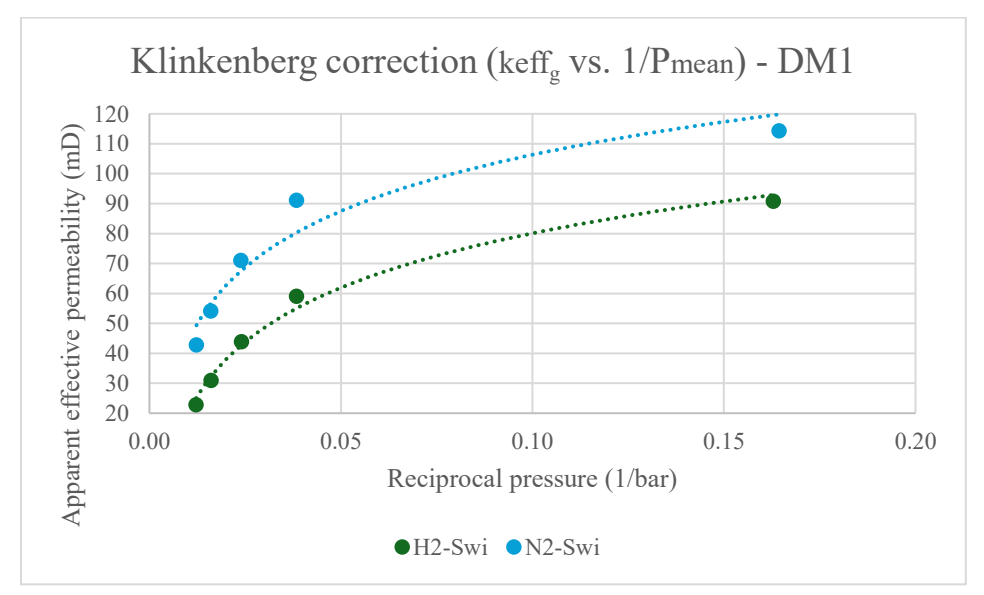


Figure 30. Klinkenberg correction graph for Hydrogen Permeameter results of sample DM1 under irreducible water saturation conditions.

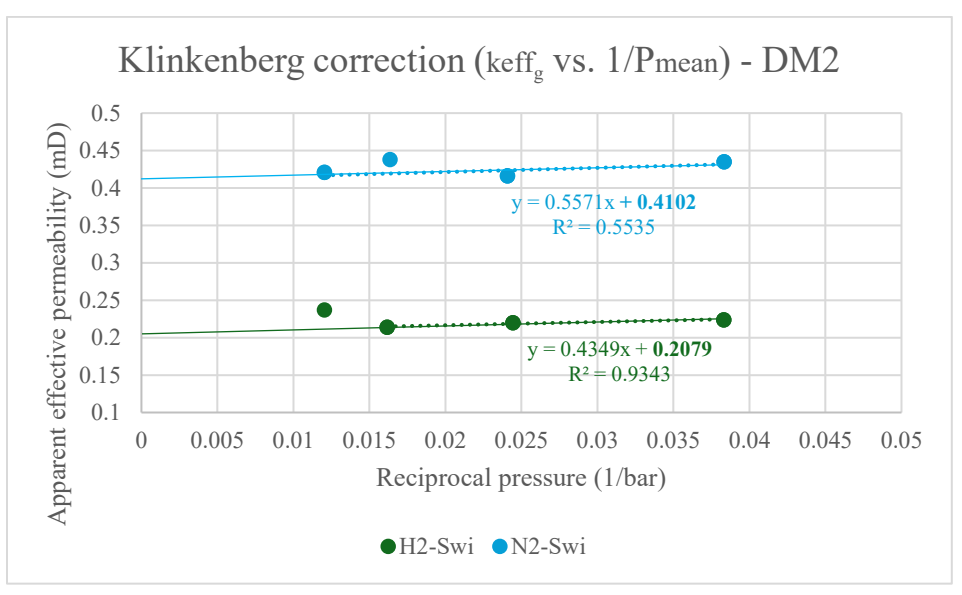


Figure 31. Klinkenberg correction graph for Hydrogen Permeameter results of sample DM2 under irreducible water saturation conditions.

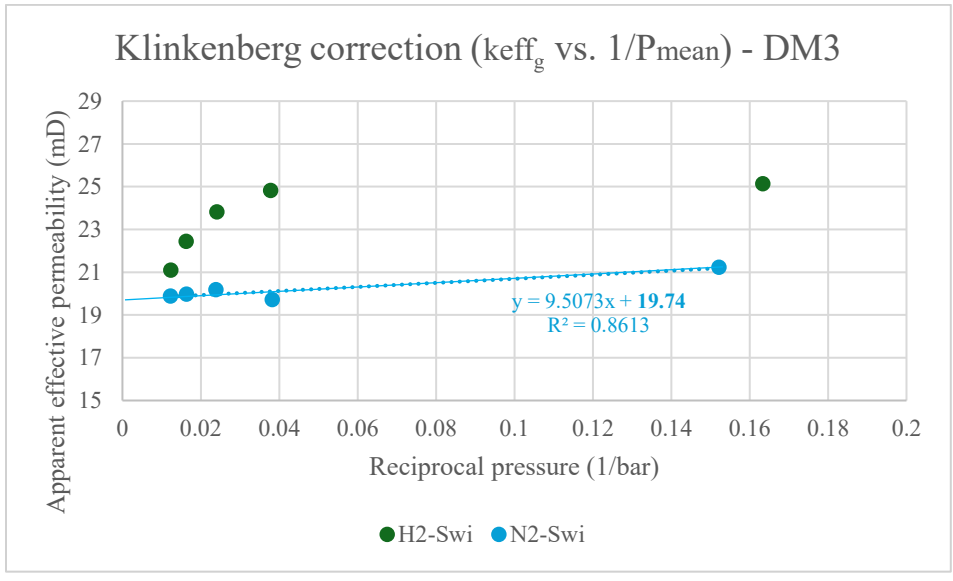


Figure 32. Klinkenberg correction graph for Hydrogen Permeameter results of sample DM3 under irreducible water saturation conditions.

 Table 17. DM1 Hydrogen Permeameter permeability results under irreducible saturation conditions.

| | | ΔP | P _{Inlet} | Poutlet | P _{Mean} | T _{Room} | T _{Sample} | Q | k | $\mathbf{k}_{\mathbf{g}}$ | 1/P _{mean} |
|----------------------------|-------|-------|--------------------|---------|-------------------|-------------------|---------------------|---------|---------|---------------------------|----------------------|
| | | (bar) | (bar) | (bar) | (bar) | (°C) | (°C) | Ncc/min | (mD) | (mD) | (bar ⁻¹) |
| | | 0.076 | 6.219 | 6.143 | | 25.8 | 25.5 | 801.00 | 97.149 | | |
| | | 0.058 | 6.191 | 6.133 | 6.138 | 25.8 | 25.5 | 601.00 | 95.896 | 90.882 | 0.163 |
| | | 0.040 | 6.144 | 6.103 | 0.136 | 25.8 | 25.5 | 400.00 | 92.599 | 90.002 | 0.103 |
| | | 0.022 | 6.095 | 6.073 | | 25.8 | 25.5 | 200.00 | 84.588 | | |
| | | 0.021 | 26.055 | 26.033 | | 25.8 | 25.6 | 801.00 | 82.675 | | |
| | | 0.017 | 26.040 | 26.023 | 26.026 | 25.8 | 25.6 | 601.00 | 77.759 | 59.118 | 0.038 |
| | | 0.014 | 26.037 | 26.023 | 20.020 | 25.8 | 25.6 | 400.00 | 64.223 | 37.110 | 0.036 |
| | | 0.009 | 26.003 | 25.993 | | 25.8 | 25.6 | 200.00 | 46.859 | | |
| | | 0.016 | 41.569 | 41.553 | | 25.8 | 25.5 | 801.00 | 71.378 | | |
| | H_2 | 0.014 | 41.557 | 41.543 | 41.542 | 25.8 | 25.5 | 601.00 | 60.169 | 43.697 | 0.024 |
| | 112 | 0.011 | 41.554 | 41.543 | T1.JT4 | 25.8 | 25.5 | 400.00 | 49.788 | 43.077 | 0.024 |
| | | 0.009 | 41.512 | 41.503 | | 25.8 | 25.5 | 200.00 | 32.541 | | |
| | | 0.014 | 62.117 | 62.103 | | 25.8 | 25.5 | 801.00 | 53.815 | | |
| | | 0.012 | 62.085 | 62.073 | 62.071 | 25.8 | 25.5 | 601.00 | 46.074 | 31.031 | 0.016 |
| | | 0.010 | 62.073 | 62.063 | 02.071 | 25.8 | 25.5 | 400.00 | 36.383 | 31.031 | 0.010 |
| | | 0.009 | 62.032 | 62.023 | | 25.8 | 25.5 | 200.00 | 21.844 | | |
| | | 0.013 | 81.916 | 81.903 | | 25.8 | 25.6 | 801.00 | 43.165 | | 0.012 |
| | | 0.012 | 81.915 | 81.903 | 81.884 | 25.8 | 25.6 | 601.00 | 36.576 | 22.870 | |
| \mathbf{S}_{wi} | | 0.010 | 81.884 | 81.873 | | 25.8 | 25.6 | 400.00 | 27.162 | | 0.012 |
| - 1 | | 0.009 | 81.842 | 81.833 | | 25.8 | 25.6 | 200.00 | 15.701 | | |
| DM1 | | 0.064 | 6.167 | 6.103 | | 25.8 | 25.5 | 396.83 | 115.574 | | 0.164 |
| D | | 0.034 | 6.107 | 6.073 | 6.082 | 25.8 | 25.5 | 198.41 | 111.061 | | |
| | | 0.019 | 6.072 | 6.053 | 0.062 | 25.8 | 25.5 | 99.21 | 100.768 | 114.575 | |
| | | 0.012 | 6.045 | 6.033 | | 25.8 | 25.5 | 49.60 | 79.056 | | |
| | | 0.033 | 26.027 | 25.993 | | 25.8 | 25.5 | 794.64 | 106.592 | | |
| | | 0.026 | 26.019 | 25.993 | 25.999 | 25.8 | 25.5 | 596.23 | 103.552 | 91.172 | 0.038 |
| | | 0.018 | 26.001 | 25.983 | 23.777 | 25.8 | 25.5 | 396.83 | 98.292 | 71.172 | 0.036 |
| | | 0.012 | 25.995 | 25.983 | | 25.8 | 25.5 | 198.41 | 76.694 | | |
| | | 0.023 | 41.846 | 41.823 | | 25.8 | 25.5 | 794.64 | 97.268 | | |
| | N_2 | 0.018 | 41.811 | 41.793 | 41.809 | 25.8 | 25.5 | 596.23 | 92.702 | 71.129 | 0.024 |
| | 1 12 | 0.014 | 41.808 | 41.793 | 41.007 | 25.8 | 25.5 | 396.83 | 78.529 | /1.12/ | 0.024 |
| | | 0.010 | 41.803 | 41.793 | | 25.8 | 25.5 | 198.41 | 57.888 | | |
| | | 0.012 | 62.276 | 62.263 | | 25.8 | 25.5 | 396.83 | 62.690 | | |
| | | 0.009 | 62.253 | 62.243 | 62.245 | 25.8 | 25.5 | 198.41 | 41.470 | 54.165 | 0.016 |
| | | 0.008 | 62.241 | 62.233 | | 25.8 | 25.5 | 99.21 | 24.414 | 34.103 | 0.010 |
| | | 0.007 | 62.230 | 62.223 | | 25.8 | 25.5 | 49.60 | 13.978 | | |
| | | 0.012 | 81.395 | 81.383 | | 25.8 | 25.5 | 396.83 | 50.856 | | 0.012 |
| | | 0.010 | 81.403 | 81.393 | 81 309 | 25.8 | 25.5 | 198.41 | 31.848 | 42.824 | |
| | | 0.008 | 81.412 | 81.403 | → 81.398 ⊢ | 25.8 | 25.5 | 99.21 | 18.007 | 74.047 | |
| | | 0.008 | 81.401 | 81.393 | | 25.8 | 25.5 | 48.99 | 9.578 | | |

 Table 18. DM2 Hydrogen Permeameter permeability results under irreducible saturation conditions.

| | | ΔΡ | P_{Inlet} | Poutlet | P_{Mean} | T_{Room} | T _{Sample} | Q | k | $\mathbf{k_{g}}$ | 1/P _{mean} |
|----------|--------------|-------|-------------|---------|------------|------------|---------------------|---------|-------|------------------|----------------------|
| | | (bar) | (bar) | (bar) | (bar) | (°C) | (°C) | Ncc/min | (mD) | (mD) | (bar ⁻¹) |
| | | 0.365 | 26.349 | 25.983 | | 25.8 | 25.6 | 20.00 | 0.210 | | |
| | | 0.236 | 26.209 | 25.973 | 26.103 | 25.8 | 25.6 | 15.00 | 0.244 | 0.224 | 0.038 |
| | | 0.159 | 26.133 | 25.973 | | 25.8 | 25.6 | 10.00 | 0.241 | | |
| | | 0.219 | 41.033 | 40.813 | | 25.8 | 25.6 | 20.00 | 0.224 | | |
| | | 0.170 | 40.973 | 40.803 | 40.892 | 25.8 | 25.6 | 15.00 | 0.217 | 0.220 | 0.024 |
| | H_2 | 0.124 | 40.927 | 40.803 | | 25.8 | 25.6 | 10.00 | 0.198 | | |
| | П2 | 0.150 | 61.963 | 61.813 | | 25.8 | 25.6 | 20.00 | 0.218 | | |
| | | 0.118 | 61.901 | 61.783 | 61.852 | 25.8 | 25.6 | 15.00 | 0.208 | 0.214 | 0.016 |
| | | 0.085 | 61.868 | 61.783 | | 25.8 | 25.6 | 10.00 | 0.192 | | |
| | | 0.103 | 83.126 | 83.023 | | 25.8 | 25.5 | 20.00 | 0.237 | | |
| S_{wi} | | 0.081 | 83.094 | 83.013 | 83.050 | 25.8 | 25.5 | 15.00 | 0.227 | 0.237 | 0.012 |
| 1 | | 0.057 | 83.050 | 82.993 | | 25.8 | 25.5 | 10.00 | 0.216 | | |
| DM2 | | 0.343 | 26.307 | 25.963 | | 25.8 | 25.5 | 19.84 | 0.451 | | |
| Ω | | 0.273 | 26.236 | 25.963 | 26.090 | 25.8 | 25.5 | 14.88 | 0.427 | 0.435 | 0.038 |
| | | 0.185 | 26.128 | 25.943 | | 25.8 | 25.5 | 9.92 | 0.420 | | |
| | | 0.229 | 41.672 | 41.443 | | 25.8 | 25.5 | 19.84 | 0.432 | | |
| | | 0.180 | 41.603 | 41.423 | 41.515 | 25.8 | 25.5 | 14.88 | 0.413 | 0.416 | 0.024 |
| | N_2 | 0.123 | 41.536 | 41.413 | | 25.8 | 25.5 | 9.92 | 0.403 | | |
| | 1 N 2 | 0.147 | 61.270 | 61.123 | | 25.8 | 25.5 | 19.84 | 0.467 | | |
| | | 0.120 | 61.173 | 61.053 | 61.119 | 25.8 | 25.5 | 14.88 | 0.431 | 0.438 | 0.016 |
| | | 0.085 | 61.088 | 61.003 | | 25.8 | 25.5 | 9.92 | 0.405 | | |
| | | 0.118 | 83.101 | 82.983 | | 25.8 | 25.6 | 19.84 | 0.442 | | |
| | | 0.092 | 83.025 | 82.933 | 82.959 | 25.8 | 25.6 | 14.88 | 0.423 | 0.421 | 0.012 |
| | | 0.067 | 82.890 | 82.823 | | 25.8 | 25.6 | 9.92 | 0.391 | | |

 Table 19. DM3 Hydrogen Permeameter permeability results under irreducible saturation conditions.

| | | ΔΡ | P _{Inlet} | Poutlet | P _{Mean} | T_{Room} | T _{Sample} | Q | k | $\mathbf{k}_{\mathbf{g}}$ | 1/P _{mean} |
|----------------------------|-------|-------|--------------------|---------|-------------------|-------------------|---------------------|---------|--------|---------------------------|----------------------|
| | | (bar) | (bar) | (bar) | (bar) | (°C) | (°C) | Ncc/min | (mD) | (mD) | (bar ⁻¹) |
| | | 0.234 | 6.327 | 6.093 | | 25.8 | 25.5 | 400.00 | 25.504 | | |
| | | 0.125 | 6.198 | 6.073 | 6.121 | 25.8 | 25.5 | 200.00 | 24.211 | 25.136 | 0.163 |
| | | 0.066 | 6.119 | 6.053 | 0.121 | 25.8 | 25.5 | 100.00 | 23.041 | 25.130 | 0.103 |
| | | 0.036 | 6.069 | 6.033 | | 25.8 | 25.5 | 50.00 | 21.158 | | |
| | | 0.113 | 26.526 | 26.413 | | 25.8 | 25.5 | 801.00 | 24.910 | | |
| | | 0.086 | 26.489 | 26.403 | 26.440 | 25.8 | 25.5 | 601.00 | 24.616 | 24.833 | 0.038 |
| | | 0.059 | 26.472 | 26.413 | 20.440 | 25.8 | 25.5 | 400.00 | 23.748 | 24.633 | 0.038 |
| | | 0.033 | 26.416 | 26.383 | | 25.8 | 25.5 | 200.00 | 21.664 | | |
| | | 0.075 | 41.508 | 41.433 | | 25.8 | 25.5 | 801.00 | 23.988 | | |
| | H_2 | 0.058 | 41.481 | 41.423 | 41.440 | 25.8 | 25.5 | 601.00 | 23.405 | 23.825 | 0.024 |
| | 112 | 0.041 | 41.454 | 41.413 | 41.440 | 25.8 | 25.5 | 400.00 | 22.203 | 23.623 | 0.024 |
| | | 0.023 | 41.417 | 41.393 | | 25.8 | 25.5 | 200.00 | 19.228 | | |
| | | 0.054 | 61.477 | 61.423 | | 25.8 | 25.5 | 801.00 | 22.774 | | |
| | | 0.042 | 61.435 | 61.393 | 61.399 | 25.8 | 25.5 | 601.00 | 21.675 | 22.442 | 0.016 |
| | | 0.030 | 61.403 | 61.373 | 01.399 | 25.8 | 25.5 | 400.00 | 20.234 | 22.442 | 0.010 |
| | | 0.019 | 61.353 | 61.333 | | 25.8 | 25.5 | 200.00 | 15.709 | | |
| | | 0.043 | 81.137 | 81.093 | | 25.8 | 25.5 | 801.00 | 21.405 | | |
| | | 0.034 | 81.097 | 81.063 | 81.061 | 25.8 | 25.5 | 601.00 | 20.342 | 21.095 | 0.012 |
| \mathbf{S}_{wi} | | 0.025 | 81.059 | 81.033 | 81.061 | 25.8 | 25.5 | 400.00 | 18.310 | | 0.012 |
| S | | 0.017 | 81.010 | 80.993 | | 25.8 | 25.5 | 200.00 | 14.045 | | |
| DM3 - | | 0.514 | 6.997 | 6.483 | | 25.8 | 25.5 | 396.83 | 21.288 | | |
| | | 0.262 | 6.715 | 6.453 | 6.569 | 25.8 | 25.5 | 198.41 | 21.418 | 21.237 | 0.152 |
| | | 0.137 | 6.560 | 6.423 | 0.309 | 25.8 | 25.5 | 99.21 | 20.701 | 21.237 | 0.132 |
| | | 0.075 | 6.498 | 6.423 | | 25.8 | 25.5 | 49.60 | 19.077 | | |
| | | 0.292 | 26.385 | 26.093 | | 25.8 | 25.6 | 794.64 | 19.631 | | |
| | | 0.213 | 26.297 | 26.083 | 26.178 | 25.8 | 25.6 | 596.23 | 20.165 | 19.726 | 0.038 |
| | | 0.140 | 26.233 | 26.093 | 20.176 | 25.8 | 25.6 | 396.83 | 20.508 | 19.720 | 0.038 |
| | | 0.072 | 26.156 | 26.083 | | 25.8 | 25.6 | 198.41 | 19.833 | | |
| | | 0.179 | 42.092 | 41.913 | | 25.8 | 25.6 | 794.64 | 20.302 | | |
| | N_2 | 0.132 | 42.026 | 41.893 | 41.952 | 25.8 | 25.6 | 596.23 | 20.608 | 20.189 | 0.024 |
| | 1\12 | 0.088 | 41.981 | 41.893 | 41.932 | 25.8 | 25.6 | 396.83 | 20.655 | 20.109 | 0.024 |
| | | 0.047 | 41.930 | 41.883 | | 25.8 | 25.6 | 198.41 | 19.329 | | |
| | | 0.127 | 61.140 | 61.013 | | 25.8 | 25.6 | 794.64 | 20.170 | | |
| | | 0.094 | 61.077 | 60.983 | 61.028 | 25.8 | 25.6 | 596.23 | 20.463 | 19.974 | 0.016 |
| | | 0.063 | 61.046 | 60.983 | 01.028 | 25.8 | 25.6 | 396.83 | 20.261 | 19.974 | 0.010 |
| | | 0.034 | 61.008 | 60.973 | | 25.8 | 25.6 | 198.41 | 18.561 | | |
| | | 0.098 | 81.321 | 81.223 | | 25.8 | 25.6 | 794.64 | 20.149 | | |
| | | 0.073 | 81.266 | 81.193 | Q1 227 | 25.8 | 25.6 | 596.23 | 20.300 | 19.886 | 0.012 |
| | | 0.049 | 81.242 | 81.193 | 81.227 | 25.8 | 25.6 | 396.83 | 20.035 | 17.000 | 0.012 |
| | | 0.027 | 81.201 | 81.173 | | 25.8 | 25.6 | 198.41 | 18.024 | | |

5.5. Knudsen Number (Kn): Continuum Flow vs. Slip Flow

The Knudsen number (Kn) results (Table 20) show that, for sample DM1, under dry conditions there is clear evidence of gas slippage when measured with hydrogen at pressures between 5 and 25 bar, while for nitrogen, slippage is only observed at 5 bar. Under irreducible water saturation, slip flow is detected only at 5 bar with nitrogen, whereas with hydrogen, the slippage effect extends up to 40 bar. For sample DM2, the Kn results indicate slip-flow behaviour under all measurement conditions, both in the dry state and under irreducible water saturation, with higher Kn values recorded in the latter. Across all tested pressures, Kn decreases consistently as pressure increases, although the transition to continuum flow is not reached. In the case of sample DM3, the results show that, under dry conditions, slip flow occurs only at 5 bar when measured with both nitrogen and hydrogen. Under irreducible water saturation, slip flow is observed at 5, 25, and 40 bar when measured with hydrogen, whereas for nitrogen, it is limited to 5 and 25 bar. Overall, for all samples, higher Kn values are obtained when measurements are performed with hydrogen compared to nitrogen. In all cases, Knudsen number decreases with increasing pressure and permeability (Figures 33, 34, and 35).

Table 20. Knudsen number calculation for all samples (Blue=continuum flow, Green=slip flow).

| Sample | Gas type | Pressure (bar) | k _g (mD) | k _g (m ²) | φ | d (µm) | λ (μm) | Kn |
|--------|-------------|----------------|------------------------|----------------------------------|--------|-----------|-----------|--------|
| | | 5 | 158.15 | 1.561E-13 | 0.2192 | 4.773 | 0.02219 | 0.0046 |
| | | 25 | 77.293 | 7.628E-14 | 0.2192 | 3.337 | 0.00444 | 0.0013 |
| | H_2 | 40 | 51.841 | 5.116E-14 | 0.2192 | 2.733 | 0.00277 | 0.0010 |
| | | 60 | 34.32 | 3.387E-14 | 0.2192 | 2.224 | 0.00185 | 0.0008 |
| DM1 | | 80 | 29.370 | 2.899E-14 | 0.2192 | 2.057 | 0.00139 | 0.0007 |
| Dry | | 5 | 190.74 | 1.882E-13 | 0.2192 | 5.242 | 0.01399 | 0.0027 |
| | | 25 | 128.25 | 1.266E-13 | 0.2192 | 4.299 | 0.00280 | 0.0007 |
| | N_2 | 40 | 97.133 | 9.586E-14 | 0.2192 | 3.741 | 0.00175 | 0.0005 |
| | | 60 | 68.599 | 6.770E-14 | 0.2192 | 3.144 | 0.00117 | 0.0004 |
| | | 80 | 49.882 | 4.923E-14 | 0.2192 | 2.681 | 0.00087 | 0.0003 |
| | | 5 | 2.376 | 2.345E-15 | 0.1454 | 0.718 | 0.02219 | 0.0309 |
| | | 25 | 1.949 | 1.924E-15 | 0.1454 | 0.651 | 0.00444 | 0.0068 |
| | H_2 | 40 | 2.130 | 2.102E-15 | 0.1454 | 0.680 | 0.00277 | 0.0041 |
| | | 60 | 2.378 | 2.347E-15 | 0.1454 | 0.719 | 0.00185 | 0.0026 |
| DM2 | | 80 | 2.367 | 2.336E-15 | 0.1454 | 0.717 | 0.00139 | 0.0019 |
| Dry | | 5 | 2.272 | 2.242E-15 | 0.1454 | 0.702 | 0.01399 | 0.0199 |
| | | 25 | 2.141 | 2.113E-15 | 0.1454 | 0.682 | 0.00280 | 0.0041 |
| | N_2 | 40 | 2.462 | 2.430E-15 | 0.1454 | 0.731 | 0.00175 | 0.0024 |
| | | 60 | 2.504 | 2.471E-15 | 0.1454 | 0.737 | 0.00117 | 0.0016 |
| | | 80 | 2.301 | 2.271E-15 | 0.1454 | 0.707 | 0.00087 | 0.0012 |

| | | | ı | I | 1 | 1 | | |
|----------|-------|----|--------|-----------|--------|-------|---------|--------|
| | | 25 | 45.371 | 4.478E-14 | 0.1774 | 2.842 | 0.00444 | 0.0016 |
| | H_2 | 40 | 45.210 | 4.462E-14 | 0.1774 | 2.837 | 0.00277 | 0.0010 |
| | 112 | 60 | 42.039 | 4.149E-14 | 0.1774 | 2.736 | 0.00185 | 0.0007 |
| DM3 | | 80 | 34.987 | 3.453E-14 | 0.1774 | 2.496 | 0.00139 | 0.0006 |
| Dry | | 5 | 46.629 | 4.602E-14 | 0.1774 | 2.881 | 0.01399 | 0.0049 |
| | | 25 | 45.881 | 4.528E-14 | 0.1774 | 2.858 | 0.00280 | 0.0010 |
| | N_2 | 40 | 43.873 | 4.330E-14 | 0.1774 | 2.795 | 0.00175 | 0.0006 |
| | | 60 | 43.453 | 4.289E-14 | 0.1774 | 2.781 | 0.00117 | 0.0004 |
| | | 80 | 44.458 | 4.388E-14 | 0.1774 | 2.813 | 0.00087 | 0.0003 |
| | | 5 | 90.882 | 8.969E-14 | 0.2192 | 3.619 | 0.02219 | 0.0061 |
| | | 25 | 59.118 | 5.834E-14 | 0.2192 | 2.918 | 0.00444 | 0.0015 |
| | H2 | 40 | 43.967 | 4.339E-14 | 0.2192 | 2.517 | 0.00277 | 0.0011 |
| | | 60 | 31.031 | 3.063E-14 | 0.2192 | 2.114 | 0.00185 | 0.0009 |
| DM1 | | 80 | 22.870 | 2.257E-14 | 0.2192 | 1.815 | 0.00139 | 0.0008 |
| S_{wi} | | 5 | 114.38 | 1.129E-13 | 0.2192 | 4.059 | 0.01399 | 0.0034 |
| | | 25 | 91.172 | 8.998E-14 | 0.2192 | 3.624 | 0.00280 | 0.0008 |
| | N2 | 40 | 71.129 | 7.020E-14 | 0.2192 | 3.201 | 0.00175 | 0.0005 |
| | | 60 | 54.165 | 5.346E-14 | 0.2192 | 2.794 | 0.00117 | 0.0004 |
| | | 80 | 42.824 | 4.226E-14 | 0.2192 | 2.484 | 0.00087 | 0.0004 |
| | | 25 | 0.224 | 2.211E-16 | 0.1454 | 0.221 | 0.00444 | 0.0201 |
| | H2 | 40 | 0.220 | 2.171E-16 | 0.1454 | 0.219 | 0.00277 | 0.0127 |
| | 112 | 60 | 0.214 | 2.112E-16 | 0.1454 | 0.216 | 0.00185 | 0.0086 |
| DM2 | | 80 | 0.237 | 2.339E-16 | 0.1454 | 0.227 | 0.00139 | 0.0061 |
| S_{wi} | | 25 | 0.435 | 4.293E-16 | 0.1454 | 0.307 | 0.00280 | 0.0091 |
| | N2 | 40 | 0.416 | 4.106E-16 | 0.1454 | 0.301 | 0.00175 | 0.0058 |
| | 112 | 60 | 0.438 | 4.323E-16 | 0.1454 | 0.308 | 0.00117 | 0.0038 |
| | | 80 | 0.421 | 4.155E-16 | 0.1454 | 0.302 | 0.00087 | 0.0029 |
| | | 5 | 25.136 | 2.481E-14 | 0.1774 | 2.115 | 0.02219 | 0.0105 |
| | | 25 | 24.833 | 2.451E-14 | 0.1774 | 2.103 | 0.00444 | 0.0021 |
| | H2 | 40 | 23.825 | 2.351E-14 | 0.1774 | 2.059 | 0.00277 | 0.0013 |
| | | 60 | 22.442 | 2.215E-14 | 0.1774 | 1.999 | 0.00185 | 0.0009 |
| DM3 | | 80 | 21.095 | 2.082E-14 | 0.1774 | 1.938 | 0.00139 | 0.0007 |
| S_{wi} | | 5 | 21.237 | 2.096E-14 | 0.1774 | 1.944 | 0.01399 | 0.0072 |
| | | 25 | 19.726 | 1.947E-14 | 0.1774 | 1.874 | 0.00280 | 0.0015 |
| | N2 | 40 | 20.189 | 1.992E-14 | 0.1774 | 1.896 | 0.00175 | 0.0009 |
| | | 60 | 19.974 | 1.971E-14 | 0.1774 | 1.886 | 0.00173 | 0.0006 |
| | | | | | | | | |
| | | 80 | 19.886 | 1.963E-14 | 0.1774 | 1.882 | 0.00087 | 0.0005 |

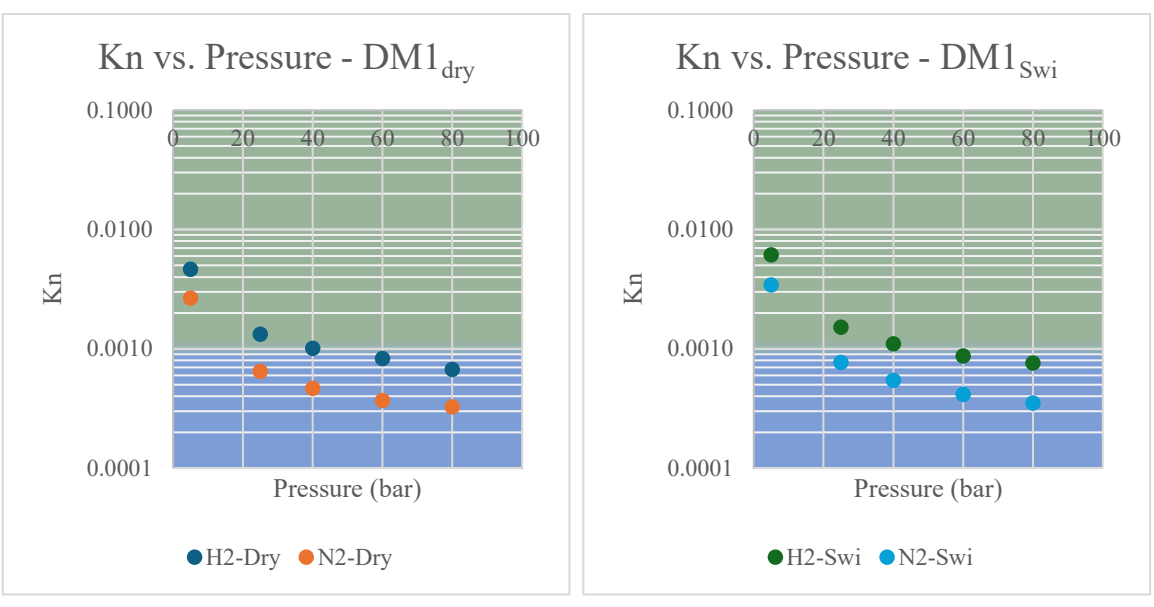


Figure 33. Knudsen number vs. Pressure under dry and irreducible water saturation conditions for sample DM1 (Blue=Continuum flow, Green=Slip flow).

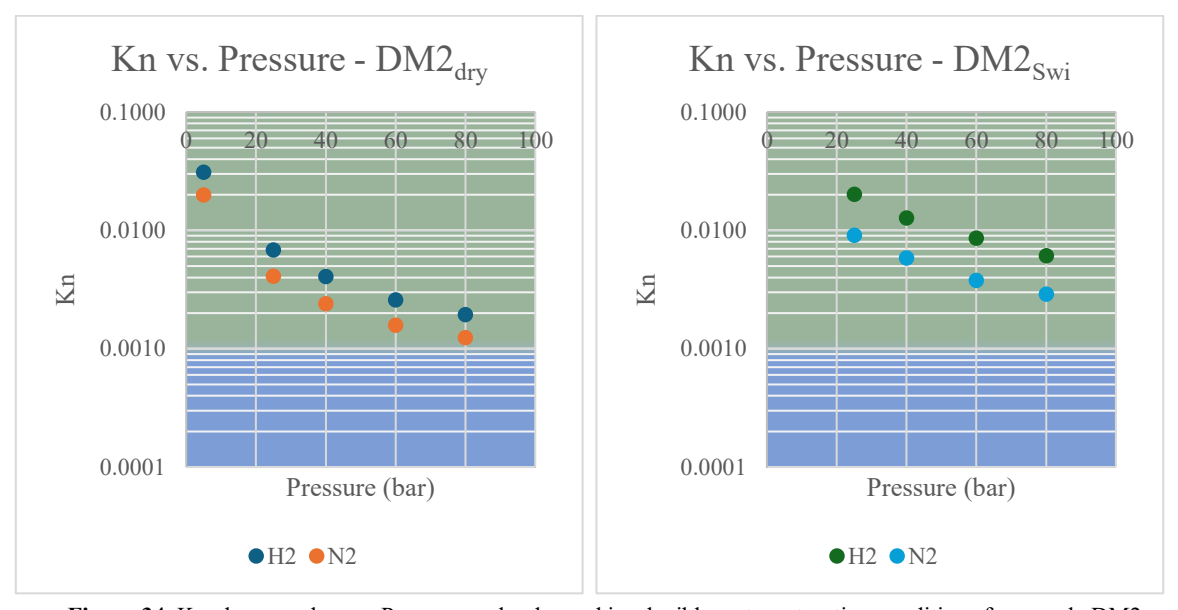
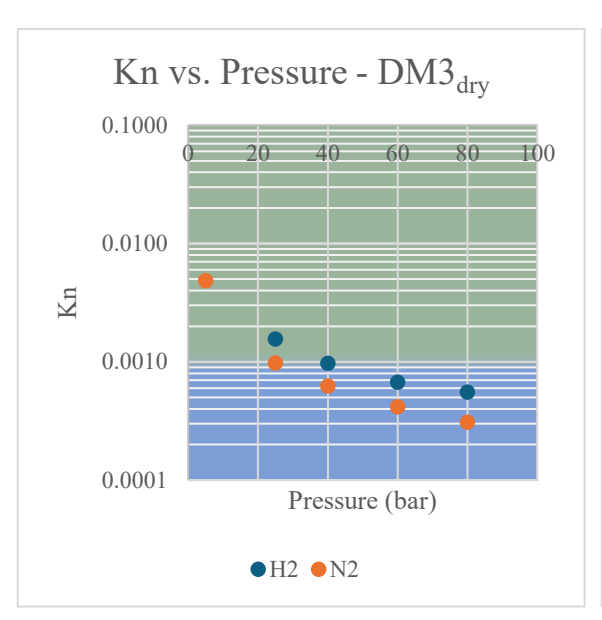


Figure 34. Knudsen number vs. Pressure under dry and irreducible water saturation conditions for sample DM2 (Blue=Continuum flow, Green=Slip flow).



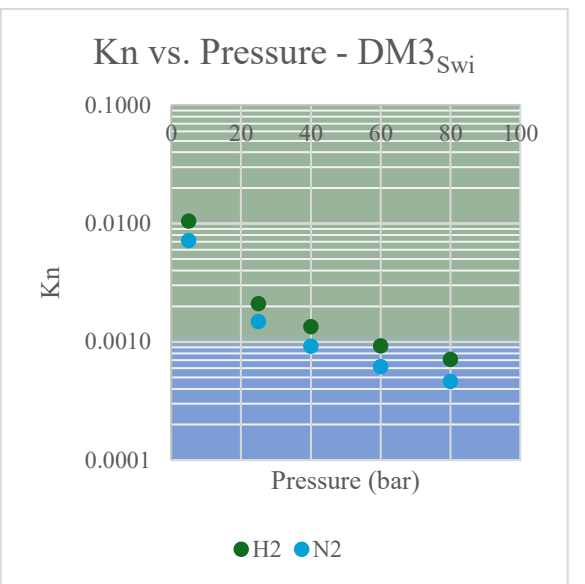


Figure 35. Knudsen number vs. Pressure under dry and irreducible water saturation conditions for sample DM3 (Blue=Continuum flow, Green=Slip flow).

6. Discussion

6.1. PoroPerm: Nitrogen Permeability to Absolute Permeability Under Dry Conditions

Based on the absolute permeability values obtained after applying the Klinkenberg correction to nitrogen measurements at low pressures, sample DM1 can be classified as a high-permeability rock (>100 mD), sample DM2 as a tight rock (<5 mD), and sample DM3 as a medium-permeability rock (between 5 and 100 mD). All samples exhibit a noticeable decrease in permeability as the measurement pressure increases.

On the whole, the Klinkenberg correction becomes increasingly important across all samples, as the difference between apparent and absolute permeability can be significant. In this study, the apparent permeability decreased from 200–194 mD to 123 mD for the high-permeability sample, from 50–45 mD to 39 mD for the medium-permeability rock, and from 4–6 mD to 3.3 mD for the low-permeability rock. Neglecting this correction can result in an overestimation of absolute permeability by approximately 18–38%, particularly in rocks with very high or very low permeability (Table 21).

| Sample | Apparent permeability to nitrogen (PoroPerm) | Absolute permeability (Klinkenberg correction) | Difference | Classification | | | | | | | |
|--------|--|--|------------|------------------------|--|--|--|--|--|--|--|
| DM1 | 200-194 mD Mean: 197mD | 123 mD | 38% | High permeability | | | | | | | |
| DM2 | 4-6 mD Mean: 5 mD | 3.3 mD | 34% | Low permeability | | | | | | | |
| DM3 | 50-45 mD Mean: 47.5 mD | 39 mD | 18% | Medium permeability | | | | | | | |

Table 21. Apparent permeability to nitrogen vs. Absolute permeability for PoroPerm results.

6.2. Hydrogen Permeameter: Nitrogen Permeability to Absolute Permeability Under Dry Conditions

Hydrogen Permeameter results, measured with applied backpressure and nitrogen, show only a minor or nearly negligible decrease in permeability as the measurement pressure increased (Figures 27 and 28), except for sample DM1, which shows a distinct behaviour that will be addressed later. This pattern confirms that gas slippage is effectively suppressed at higher pressures (Li *et al.*, 2009). Under these conditions, the measured permeability is very similar to the absolute permeability obtained after applying the Klinkenberg correction.

For sample DM2, the difference between the apparent and corrected permeability was approximately 7%. Despite the low permeability and its consistent slip-flow regime, as indicated by the Knudsen number, the Klinkenberg-corrected values closely match the

experimental measurements. In the case of sample DM3, the difference was less than 2%, considering the mean of the measured data (Table 22).

Overall, these results indicate that permeability measured with this permeameter under controlled backpressure conditions is highly representative of the true rock permeability and demonstrate that backpressure-controlled nitrogen measurements can effectively minimize the influence of gas slippage, providing permeability values that closely represent absolute permeability, even in low-permeability samples.

| Table 22 . Apparent permeability to nitrog | gen vs. Absolute permeabili | ity for Hydrogen Perme | eameter results. |
|---|-----------------------------|------------------------|------------------|
|---|-----------------------------|------------------------|------------------|

| Sample | Apparent permeability to nitrogen (H2Perm) | Absolute permeability (Klinkenberg correction) | Difference | Classification |
|--------|--|--|------------|------------------------|
| DM2 | 2.5-2.0 mD Mean:2.25 mD | 2.1 mD | 7% | Low permeability |
| DM3 | 46-43 mD Mean: 44.5 mD | 44 mD | 1% | Medium permeability |

6.3. PoroPerm vs. Hydrogen Permeameter

The primary distinction between both instruments lies in their operating conditions. The Hydrogen Permeameter functions under backpressure, elevated confining stress, and temperature control, whereas the PoroPerm operates at lower pressures and without backpressure regulation. Consequently, the apparent permeability values obtained with the PoroPerm are typically higher, mainly due to the gas slippage phenomenon described by Klinkenberg (1941), which can be mitigated by increasing mean pressure and applying backpressure (Li et al., 2009).

Despite the differences in operation, results from both systems can be related through the Klinkenberg correction. When this correction is applied to the PoroPerm measurements, the resulting values could be comparable to those obtained with the Hydrogen Permeameter, especially at higher pressures where gas slippage becomes negligible.

For sample DM1 (Figure 36), a direct comparison between the absolute permeability obtained from the PoroPerm and that from the Hydrogen Permeameter using nitrogen was not possible, as the latter displayed a markedly non-linear response with no evident correlation at elevated pressures. Nevertheless, the lowest-pressure point measured with the Hydrogen Permeameter (5 bar) yielded a slightly smaller permeability, likely due to its higher confining pressure, and is comparable to the low-pressure PoroPerm measurements, although it does not fit within the correction trend.

In the case of sample DM2 (Figure 37), the permeability obtained with the PoroPerm, which showed a clear linear trend, was marginally higher than that derived from the Hydrogen

Permeameter. This small difference is consistent with the influence of higher confining pressures in the Hydrogen Permeameter, which may compact the rock matrix and close microfractures, slightly decreasing permeability. Thus, both instruments produced comparable results for this rock.

For sample DM3 (Figure 38), a higher degree of data scatter was observed in the PoroPerm results, preventing a similar correlation. Consequently, the absolute permeability appeared lower than that measured with the Hydrogen Permeameter. However, when only the lower-pressure and higher-permeability points from the PoroPerm were used in the Klinkenberg correction, both datasets converged more closely, as seen for the low-permeability case. This behaviour highlights that data dispersion is a key factor affecting the accuracy of PoroPerm measurements and their comparability with Hydrogen Permeameter results, with scatter generally increasing as permeability rises.

On the whole, experimental results obtained from the PoroPerm show that permeability measurements in highly permeable rocks are often more scattered. This increased scatter is mostly due to instrument and operational limitations rather than the rock's intrinsic properties. Low pressure gradients across the core make the measurements sensitive to small fluctuations in flow control, sensor noise, or temperature changes. High flow rates can also prevent steady-state conditions from being reached, while the dynamic response of valves and flow controllers can create transient pressure oscillations. Minor heterogeneities or preferential flow paths further contribute to the scattered values, even though the Klinkenberg correction itself has only a minor effect in these rocks. In contrast, low-permeability rocks tend to produce less scattered and more reproducible results. Larger pressure drops generate stronger signals relative to noise, and lower flow rates allow the system to stabilize more effectively. Gas flow in these samples generally occurs under slip-flow conditions, where the relationship between apparent permeability and the reciprocal of mean pressure is linear and predictable. As a result, although the intrinsic Klinkenberg effect is stronger in lowpermeability rocks, the measured data are less scattered especially due to reduced experimental sensitivity (Klinkenberg, 1941; Jones, 1972; Cui et al., 2009, Li et al., 2009).

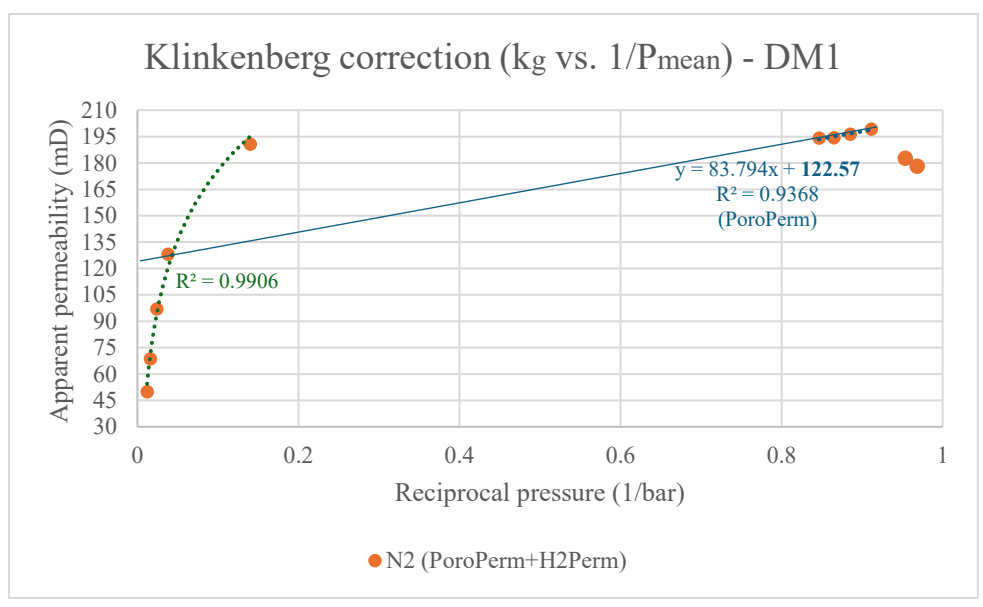


Figure 36. Klinkenberg correction graph for Hydrogen Permeameter vs PoroPerm results of sample DM1 under dry conditions.

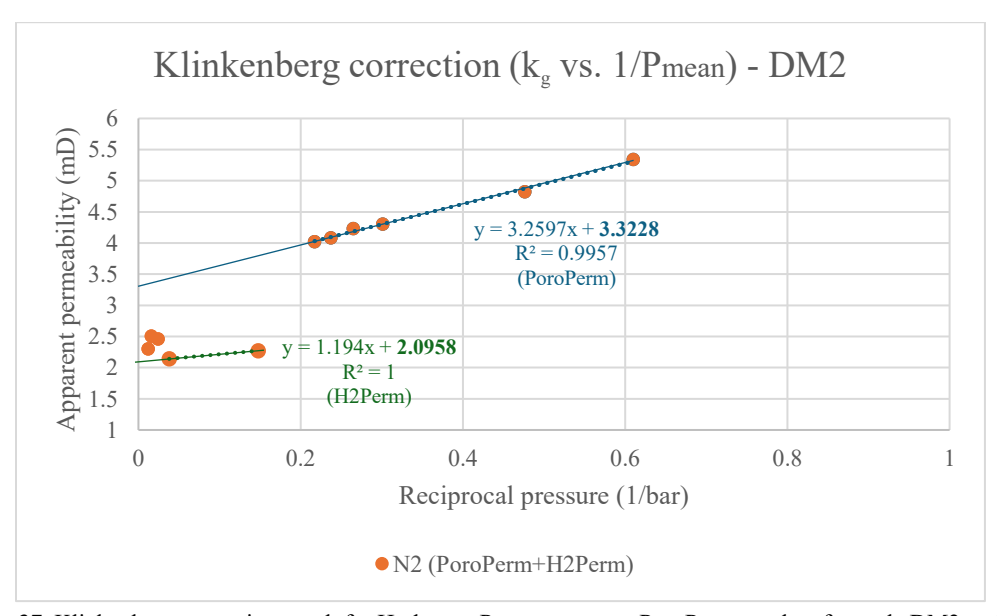


Figure 37. Klinkenberg correction graph for Hydrogen Permeameter vs PoroPerm results of sample DM2 under dry conditions.

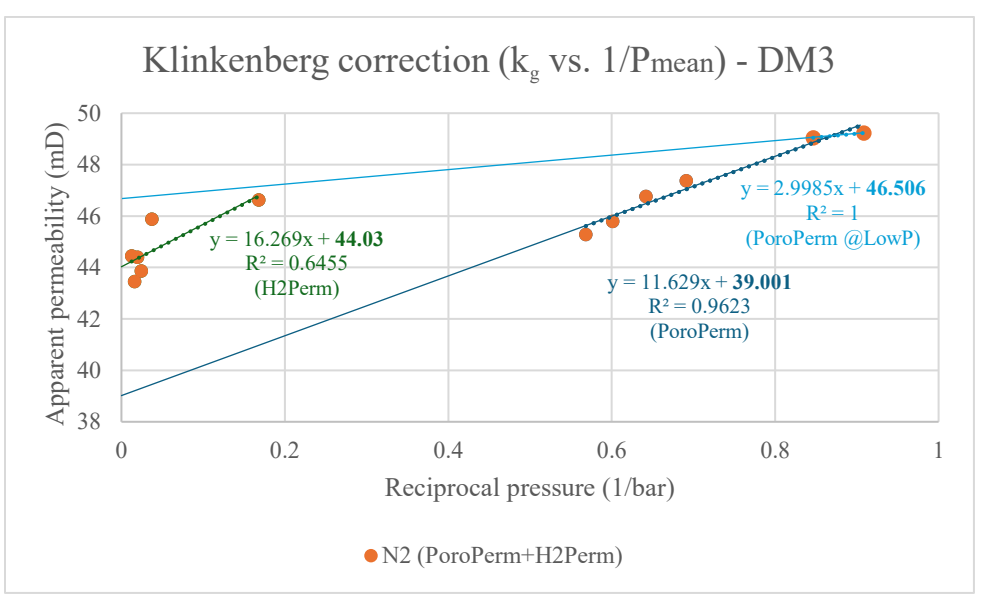


Figure 38. Klinkenberg correction graph for Hydrogen Permeameter vs PoroPerm results of sample DM3 under dry conditions.

6.4. Permeability Under Dry Conditions: H2 vs. N2

When comparing nitrogen (N₂) and hydrogen (H₂) as test gases, the differences are primarily due to their fundamental molecular properties rather than viscosity or density–pressure effects (Klinkenberg, 1941). Hydrogen, with its smaller molecular diameter (0.289 nm) and longer mean free path throughout the analysed pressure range, is more prone to gas slippage than nitrogen (0.364 nm), whose molecules collide more frequently. However, results obtained with the Hydrogen Permeameter show that hydrogen does not consistently lead to a noticeably higher apparent permeability compared to nitrogen. The observed differences between the two gases are generally minor and, in practical terms, negligible. For the low-permeability sample (DM2), these differences are typically below 0.5 mD, while for the medium-permeability (DM3) sample they can reach up to 5 mD (Figure 40 and 41).

Despite these small variations, the overall impact of molecular differences on measured permeability is limited under the experimental conditions used. The application of backpressure reduces slip-flow effects, and the combination of high confining pressures and controlled flow rates in the Hydrogen Permeameter helps stabilize the measurements. As a result, the apparent permeability obtained with both gases closely matches the absolute permeability derived after applying the Klinkenberg correction, with no significant discrepancies observed. These results demonstrate that, under dry conditions and proper testing protocols, both nitrogen and hydrogen provide reliable and comparable estimates of permeability. This consistency has been confirmed across multiple studies, supporting the use of either gas for routine laboratory measurements of core samples (Li et al., 2009).

6.5. Effective Permeability at Irreducible Water Saturation: Role of Irreducible Water

For sample DM1, the comparison between dry and saturated conditions reveals a noticeable reduction in gas permeability at low pressures (around 5 bar), reaching approximately 40% for nitrogen and 43% for hydrogen. As pressure increases, this difference gradually decreases, falling to about 14% for nitrogen and 22% for hydrogen, with nitrogen consistently presenting slightly higher apparent effective permeability values (Figure 39). In the case of DM2, the presence of irreducible water produced a much stronger effect, leading to an 80–90% decline in permeability compared to the dry condition. Despite this marked reduction, nitrogen maintained a higher effective permeability than hydrogen throughout the tests range (Figure 40). For DM3, permeability decreased by roughly 48–54% relative to the dry state. In contrast with the other two samples, hydrogen showed higher effective permeability values than nitrogen (Figure 41).

All samples show a clear decline in gas permeability when irreducible water was present, and the magnitude of this reduction follows a consistent pattern: it was most pronounced in the low-permeability rock (DM2), moderate in the intermediate sample (DM3), and least significant in the high-permeability rock (DM1) (Figures 38, 39 and 40). This response reflects well-established petrophysical behaviour. In tight formations, even small amounts of bound water can occupy a substantial portion of the effective pore volume, restrict the available flow channels, and significantly increase flow resistance. In contrast, rocks with larger and better-connected pores experience less interference from irreducible water, since wider throats diminish capillary forces and maintain more open pathways for gas movement. As a result, gas permeability decreases in proportion to both the level of water saturation and the pore-size distribution of the medium. Overall, the observed pattern confirms the expected response of partially saturated porous media, where residual water limits gas flow by blocking fine pores and enhancing capillary resistance (Li *et al*, 2020).

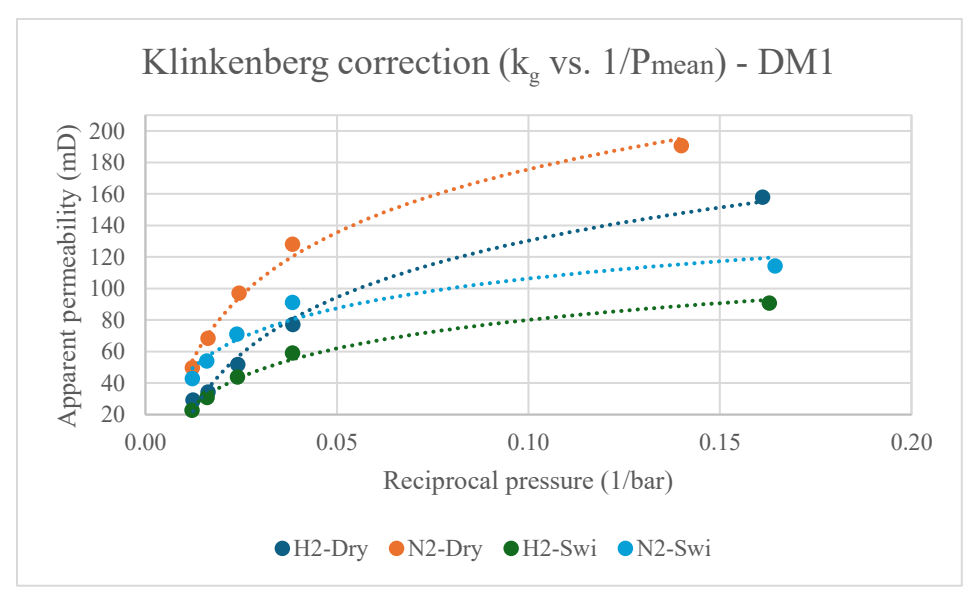


Figure 39. Klinkenberg correction graph for Hydrogen Permeameter results of sample DM1 under dry conditions vs. irreducible water saturation conditions.

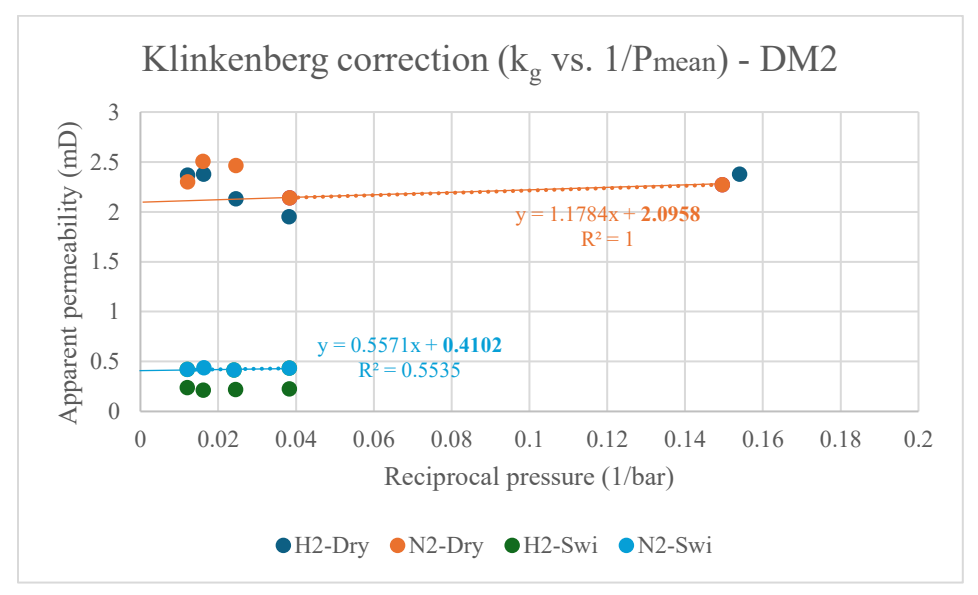


Figure 40. Klinkenberg correction graph for Hydrogen Permeameter results of sample DM2 under dry conditions vs. irreducible water saturation conditions.

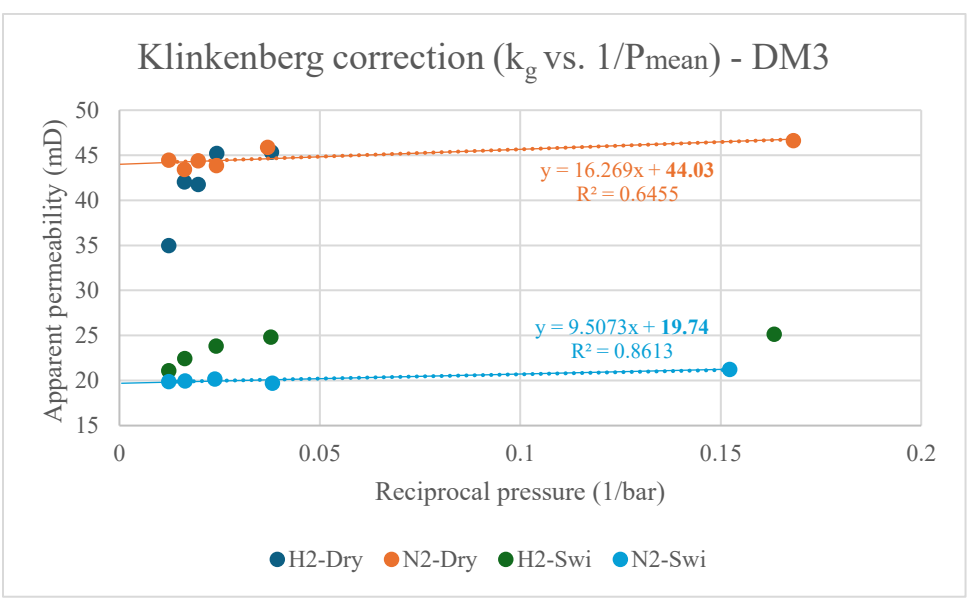


Figure 41. Klinkenberg correction graph for Hydrogen Permeameter results of sample DM3 under dry conditions vs. irreducible water saturation conditions.

6.6. Permeability Under Irreducible Water Saturation Conditions: H2 vs. N2

The comparison between hydrogen (H₂) and nitrogen (N₂) permeability for samples DM1, DM2, and DM3 reveals that apparent gas effective permeability is influenced not only by intrinsic pore structure but also by measurement sequence, gas properties, and preconditioning procedures. These factors collectively affect pore-network connectivity, flow regime (viscous, slip, or Knudsen), and potential hysteresis or "pore-memory" effects during gas-substitution experiments.

For samples DM1 and DM2, tested first with hydrogen and later with nitrogen, showed a lower effective permeability to hydrogen than to nitrogen (Figures 38 and 39). This behaviour suggests surface hysteresis and conditioning effects induced by the initial exposure to hydrogen (Lysyy et al., 2022; Boon & Hajibeygi, 2022). Several studies report that hydrogen can adsorb onto mineral surfaces and that residual water and wettability play a critical role in gas flow (Aslannezhad et al., 2023). Processes such as molecular adsorption, capillary condensation, or slight alterations in wettability may reduce the effective pore radius, restricting gas flow during the first measurement. When nitrogen is introduced afterward, partial hydrogen desorption and re-equilibration of capillary interfaces may occur, leading to a higher measured permeability. This sequence-dependent behaviour exemplifies a pore-memory effect, where the rock may retain characteristics from the previous gas saturation state, influencing subsequent flow responses (Lan et al., 2024).

In contrast, sample DM3, which was tested first with nitrogen and subsequently with hydrogen, a higher effective permeability to hydrogen was observed (Figure 41). This

outcome agrees with studies showing that gases with smaller molecular size, higher diffusivity, and lower viscosity (such as hydrogen) tend to exhibit enhanced apparent permeability due to stronger gas-slippage and reduced molecular drag effects (Klinkenberg, 1941; Civan, 2010). Injecting hydrogen after nitrogen can also increase the measured effective permeability since hydrogen can penetrate smaller pore throats and previously disconnected zones of the network, thus improving flow connectivity. In addition, its higher diffusivity may help displace residual nitrogen or moisture, temporarily enhancing gas mobility. Therefore, the greater hydrogen effective permeability in DM3 likely reflects a transient mobility enhancement rather than a permanent change in pore structure.

An additional contributor to the observed variations may be the use of nitrogen to establish irreducible water saturation prior to gas permeability testing. This pre-conditioning step alters the fluid distribution within the pore space by partially redistributing or removing capillary water and modifying gas—water interfaces. Residual nitrogen could remain adsorbed or trapped in microporous regions (Al-Yaseri *et al.*, 2022), especially in low-permeability samples such as DM2, thereby affecting subsequent hydrogen flow. The contrast in diffusivity and solubility between the two gases, with hydrogen being more diffusive and less soluble in water, may amplifies these effects if complete pore restoration is not achieved. Such phenomena generate a pore-memory effect, in which the rock retains residual features of the prior saturation state that influence the next permeability measurement (Lan *et al.*, 2024).

On the whole, the contrasting behaviour of the samples demonstrates that gas effective permeability at irreducible water saturation is path dependent. The interplay among gas substitution, wettability, slippage, and pore-memory mechanisms indicates that measured effective permeability is a property function of experimental history. For laboratory protocols and hydrogen-storage simulations, this implies that both the sequence of gas exposure and sample pre-conditioning must be standardized, or at least reported explicitly, since they can alter the measurements under irreducible water saturation conditions. Neglecting these effects may lead to either under- or over-estimation of reservoir deliverability and injectivity.

In the context of UHS, where alternating injections of hydrogen, methane, or carbon dioxide are expected, these sequence-related and saturation-history effects become especially relevant for predicting operational performance and assessing formation integrity.

While the proposed mechanisms are physically consistent with current understanding, not all of them were directly measured in the present study (e.g., hydrogen adsorption, residual-water quantification, or post-test pore-structure imaging). Therefore, some interpretations remain hypotheses supported by some literature rather than direct observations. Future work should aim to: 1) reverse the measurement sequence to quantify the permeability difference caused solely by gas order, 2) determine residual-water distribution using complementary

methods such as mercury porosimetry, micro-CT, or NMR imaging, 3) conduct diffusion or single-pore permeability tests with lighter and heavier gases to verify preferential access of hydrogen to micropores, 4) model the combined effects of slippage, Knudsen flow, adsorption, and water saturation to reproduce the observed trends numerically. Such approaches would help distinguish true permeability variations from experimental artefacts caused by pore-memory or hysteresis effects.

6.7. The Non-Linearity: Apparent Permeability vs. Mean Reciprocal Pressure

Sample DM1 (Both under dry and irreducible water saturation conditions

Experimental results demonstrate a pronounced decrease in apparent permeability with increasing mean pressure and decreasing flow rate, displaying a nonlinear, approximately logarithmic trend. This behaviour is observed for both under dry and irreducible water saturation conditions, as well as for measurements performed with different gases.

Under dry conditions, nitrogen permeability drops from about 190 mD at 5 bar to 50 mD at 80 bar, a 74 % decline with increasing pressure. When the same core is tested at irreducible water saturation (Swi), the values fall from 114 mD to 42 mD, a 63 % decrease. Hydrogen shows the same behaviour: 158 mD to 29 mD in the dry case (82 %) and 90 mD to 22 mD under Swi (76 %) (Figure 39). These substantial reductions, ranging from roughly 60% to over 80%, highlight that the observed permeability decline is far more pronounced than what could be attributed solely to gas slippage (Klinkenberg effect). These results illustrate that the reduction in permeability is substantial for all gases and saturation conditions, indicating that it is not caused by residual water or saturation effects. Moreover, the apparent permeability values for dry and Swi-saturated samples converge at high pressures, with differences reducing from 40–45% at low pressure to less than 20% at 80 bar for both gases. This convergence demonstrates that the dominant mechanisms controlling flow are intrinsic gas—rock interactions, rather than the presence of water.

This sample is characterized by high permeability, low compaction, substantial heterogeneity, and the presence of fines. Regarding this, the decrease in apparent permeability could arise from a combination of factors: 1) reduction of gas slip (Klinkenberg effect) with increasing pressure, 2) pore-scale heterogeneity (Cui *et al.*, 2009) including preferential flow channels that are more active at higher flow rates and less active at lower rates, and 3) effects from fines rearrangement or local pore deformation. Notably, the linear relationship between normalized flow rate (Q/A) and the compressibility-corrected pressure term $(p_1^2 - p_2^2)/(LP_1)$ confirms that flow is Darcian and viscous-dominated, with negligible contribution from non-Darcy inertial (Forchheimer) effects. Therefore, the observed rate-dependent variations in permeability may reflect the selective activation of preferential pathways and intrinsic gas-rock interactions, not inertial effects.

Sample DM3 (Under irreducible water saturation conditions)

The slight non-linear decrease in apparent effective permeability with pressure observed during hydrogen testing is most likely related to experimental leakage rather than a genuine change in the material's intrinsic flow properties. When minor leaks occur in the system, through seals, fittings, or valves, part of the hydrogen escapes before passing through the sample. As a result, the upstream pressure and the effective pressure gradient across the specimen are partially lost, which leads to a lower measured gas flow rate. Consequently, the calculated permeability appears to decrease even though the actual permeability of the porous medium remains constant.

This phenomenon is particularly relevant for hydrogen because of its exceptionally low molecular weight and small kinetic diameter (0.289 nm). These characteristics allow the gas to diffuse through microdefects and materials that are completely impermeable to larger molecules such as nitrogen. The effect becomes more noticeable at higher pressures, where leakage paths are more active and the total pressure loss across the sample increases.

Therefore, the apparent reduction in permeability with pressure should be interpreted as an experimental artifact rather than a true physical effect. Ensuring perfect system tightness is essential to avoid such deviations. The use of metallic gaskets, helium pre-tests, and continuous monitoring of line integrity are recommended to minimize leakage and to obtain reliable and reproducible permeability measurements, especially when working with hydrogen.

6.8. Critical Considerations in Measuring Hydrogen Permeability

When measuring hydrogen permeability in rock samples, several critical factors must be addressed to ensure accurate and reliable results. One of the most significant issues is leakage. Hydrogen is an extremely small and diffusive molecule, capable of escaping through microcracks, imperfect seals, or fittings in the experimental setup. Even minor leaks can lead to substantial overestimation of permeability because part of the measured flow bypasses the sample.

Another important aspect to consider is the stabilization time required for the system to reach steady-state flow. In high-permeability samples, hydrogen tends to stabilize quickly, whereas samples with lower permeability may require significantly longer periods to equilibrate. If data are collected before steady-state conditions are fully achieved, the resulting permeability values can be either underestimated or overestimated. For this reason, it is essential to monitor both pressure and flow rate over time and only record data once a stable regime is consistently observed.

Residual water within the rock matrix can also have a notable influence on the results. Even small amounts of water occupying the pore spaces can reduce the effective permeability to hydrogen and introduce hysteresis effects. This is particularly relevant for low-permeability samples, where partial saturation can severely restrict gas movement.

Additional factors, such as temperature control and rock heterogeneity, must also be considered. Temperature fluctuations can alter gas viscosity and density, while heterogeneities within the sample can lead to localized variations in the measured permeability, affecting the overall reliability of the results. In some cases, microfractures, vugs, or anisotropy in the sample can dominate flow, making single-point measurements unrepresentative of bulk behaviour. Careful sample preparation, repeated measurements, and the use of multiple samples or directions are therefore recommended.

Recognizing and mitigating these criticalities is essential for reliable experimental data and meaningful interpretation in the context of underground hydrogen storage.

7. Conclusions

This study assessed hydrogen and nitrogen permeability for three sandstone samples under dry and irreducible-water conditions, employing two steady-state systems: a low-pressure PoroPerm and a high-pressure Hydrogen Permeameter. The results collectively explain how pressure regime, gas type, saturation, and testing sequence govern gas flow in formations relevant to underground hydrogen storage (UHS).

PoroPerm tests at low mean pressure revealed a strong pressure dependence of permeability due to gas slippage. After correcting the nitrogen data using the Klinkenberg method, the samples exhibited these absolute permeability levels: DM1 was highly permeable, DM3 had moderate permeability, and DM2 was classified as tight. Ignoring this correction would lead to an overestimation of absolute permeability by as much as 40%. In contrast, the Hydrogen Permeameter, operating under backpressure, confining stress, and temperature control, effectively minimised slippage; corrected and apparent permeabilities differed by less than 10%, even for the tight sample. Thus, backpressure regulation yields permeability values close to the intrinsic rock property.

Comparison between the instruments confirmed that discrepancies arise from measurement conditions, not from the rock characteristics. PoroPerm data tend to be more scattered in highly permeable rocks due to low pressure gradients, transient valve responses, and thermal fluctuations, whereas low-permeability samples produce smoother and more linear Klinkenberg trends. This operational sensitivity explains why the Hydrogen Permeameter provides more stable, reproducible data, suitable for reservoir-representative permeability.

Under dry conditions, measurements obtained with the Hydrogen Permeameter indicated that hydrogen and nitrogen permeabilities were essentially equivalent. Hydrogen's smaller molecular diameter, longer mean free path, and higher diffusivity only increased apparent permeability at the lowest pressures. At irreducible water saturation, all rocks exhibited substantial permeability reductions: around 40% for the most permeable sample (DM1), roughly 50% for DM3, and up to 90% for DM2. The trend confirms that residual water preferentially occupies the smallest throats due to capillary forces thus reducing the gas-filled pore volume.

Knudsen-number analysis clarified the flow regimes. DM2 remained in slip flow throughout the entire pressure range, even under backpressure, indicating consistently fine effective pores. DM1 and DM3 progressively shifted from slip to continuum flow with increasing pressure, above 5 bar for DM3 and 25 bar for DM1. Under irreducible-water saturation, slip flow persisted to higher pressures (40 bar) since the presence of water restricts gas pathways, effectively decreasing the characteristic pore diameter. This reduction of this parameter

increased the Knudsen number, allowing slippage effects to remain significant even at higher pressures compared to dry conditions results.

Flow experiments at S_{wi} revealed a behaviour which depends of the sequence of gas used to flow the plugs. When hydrogen measurements preceded nitrogen (DM1, DM2), its effective permeability was lower, likely reflecting transient adsorption, capillary condensation, or wettability changes narrowing the flow paths. When the order was reversed (DM3), hydrogen showed higher permeability, probably due to its smaller size and ability to re-open previously disconnected pores. These outcomes demonstrate a pore-memory effect, meaning that permeability at partial saturation depends on the testing history. Thus, the test sequence must be explicitly accounted for when designing laboratory protocols, interpreting lab test results and forecasting alternating gas-injection cycles in UHS operations.

The non-linear reduction of apparent permeability with pressure observed in DM1 under both dry and saturated states highlights that such reduction exceeds the expected Klinkenberg effect. The behaviour likely results from heterogeneity, selective activation of flow channels, and fines rearrangement rather than inertial (Forchheimer) effects, as confirmed by Darcyflow diagnostics. In DM3, a small apparent drop in hydrogen permeability with pressure was attributed to leakage through seals or fittings, an artefact accentuated by hydrogen's high diffusivity and ability to permeate even through the joint threads. Preventing leaks and confirming system tightness are therefore indispensable for accurate hydrogen testing.

This study demonstrates that reliable hydrogen permeability assessment requires strict control of pressure, temperature, and saturation, complemented by adequate stabilization time and airtight operations. Under controlled conditions, nitrogen can serve as a dependable proxy for hydrogen, as both gases yield comparable intrinsic permeability once slippage and gas (or water) saturation are considered.

8. References

- Al-Yaseri, A., Esteban, L., Giwelli, A., Sarout, J., Lebedev, M., & Sarmadivaleh, M. (2022). Initial and residual trapping of hydrogen and nitrogen in Fontainebleau sandstone using nuclear magnetic resonance core flooding. *International Journal of Hydrogen Energy*, 47(53), 22482–22494. https://doi.org/10.1016/j.ijhydene.2022.05.059
- American Petroleum Institute. (1998, February). Recommended practice for core analysis (API Recommended Practice 40, 2nd ed.). American Petroleum Institute.
- Amid, A., Mignard, D. & Wilkinson, M. (2016). Seasonal storage of hydrogen in a depleted natural gas reservoir. International Journal of Hydrogen Energy, 41(12), 5549–5560. https://doi.org/10.1016/j.ijhydene.2016.02.036
- Aslannezhad, M., Ali, M., Kalantariasl, A., Sayyafzadeh, M., You, Z., Iglauer, S., & Keshavarz, A. (2023). A review of hydrogen/rock/brine interaction: Implications for hydrogen geo-storage. *Progress in Energy and Combustion Science*, *95*, 101066. https://doi.org/10.1016/j.pecs.2022.101066
- Boon, M., & Hajibeygi, H. (2022). Experimental characterization of H₂/water multiphase flow in heterogeneous sandstone rock at the core scale relevant for underground hydrogen storage (UHS). *Scientific Reports*, 12, 14604. https://doi.org/10.1038/s41598-022-18759-8
- Civan, F. (2010). Effective correlation of apparent gas permeability in tight porous media. *Transport in Porous Media*, 82(2), 375–384. https://doi.org/10.1007/s11242-009-9432-z
- Collins, R. E., & Crawford, P. B. (1953). Calculations of unsteady-state gas flow through porous media, corrected for Klinkenberg effects. *AIME Transactions*, 198, 339–340.
- Cui, X., Bustin, A. M. M., & Bustin, R. M. (2009). Measurements of gas permeability and diffusivity of tight reservoir rocks: Different approaches and their applications. *Geofluids*, 9(3), 208–223. https://doi.org/10.1111/j.1468-8123.2009.00244.x
- Cussler, E. L. (2009). *Diffusion: Mass transfer in fluid systems* (3rd ed.). Cambridge University Press.
- Dehury, R., Chowdhury, S., & Sangwai, J. S. (2024). Dynamics of hydrogen storage in subsurface saline aquifers: A computational and experimental pore-scale displacement study. *International Journal of Hydrogen Energy, 69*(11), 817–836. https://doi.org/10.1016/j.ijhydene.2024.05.009
- Fancher, G. H., & Lewis, J. A. (1933). Flow of simple fluids through porous materials. *Industrial & Engineering Chemistry*, 25(10), 1139–1147.
- Firoozabadi, A., & Katz, D. L. (1979). An analysis of high-velocity gas flow through porous media. *Journal of Petroleum Technology*, 31(2), 211–216.
- Graham, T. (1833). On the law of the diffusion of gases. *Philosophical Magazine, Series* 2, 2, 175–190.

- Green, L., Jr., & Duwez, P. (1951). Fluid flow through porous metals. *Journal of Applied Mechanics*, 18(1), 39–45.
- Guria, C. (2023). Pressure- and temperature-dependent Klinkenberg slippage effect in porous media to non-ideal gases. *Geoenergy Science and Engineering*. Advance online publication. https://doi.org/10.1016/j.geoen.2023.211629
- Hubbert, M. K. (1956). Darcy's law and the field equations of the flow of underground fluids. *Transactions of the AIME*, 207(1), 222–239. https://doi.org/10.2118/749-G
- Jones, F. O. (1972). A laboratory study of the effects of confining pressure on fracture flow and storage capacity in carbonate rocks. *Journal of Petroleum Technology*, 24(1), 21–29. https://doi.org/10.2118/3523-PA
- Jones, S. C. (1972). A rapid accurate unsteady-state Klinkenberg permeameter. Scandinavian Petroleum Engineering Journal, 12(5), 383–397.
- Jones, S. C., & Roszelle, W. O. (1978). Graphical techniques for determining relative permeability from displacement experiments. *Journal of Petroleum Technology*, 30(5), 807–817. https://doi.org/10.2118/6045-PA
- Kandlikar, S. G., Garimella, S., Li, D., Colin, S., & King, M. R. (2014). *Heat transfer and fluid flow in minichannels and microchannels* (2nd ed.). Butterworth-Heinemann. Kennedy, M. (2024). *Practical petrophysics* (2nd ed.). Elsevier.
- Klinkenberg, L. J. (1941). The permeability of porous media to liquids and gases. In *Drilling and Production Practice 1941* (pp. 200–213). American Petroleum Institute.
- Kozhevnikov, E. V., Turbakov, M. S., Riabokon, E. P., Gladkikh, E. V., Guzev, M. V., Qi, C., & Li, X. (2024). The mechanism of porous reservoir permeability deterioration due to pore pressure decrease. *Advances in Geo-Energy Research*, *13*(2), 96–105. https://doi.org/10.46690/ager.2024.08.04
- Lan, Y., Guo, P., Liu, Y., Wang, S., Cao, S., Zhang, J., Sun, W., Qi, D., & Ji, Q. (2024). State of the art on relative-permeability hysteresis in porous media: Petroleum engineering application. *Applied Sciences*, 14(11), 4639. https://doi.org/10.3390/app14114639
- Leverett, M. C. (1941). Capillary behavior in porous solids. *Transactions of the American Institute of Mining, Metallurgical, and Petroleum Engineers, 142*(1), 152–169. https://doi.org/10.2118/941152-G
- Li, S., Dong, M., & Li, Z. (2009). Measurement and revised interpretation of gas flow behavior in tight reservoir cores. *Journal of Petroleum Science and Engineering*, 65(1–2), 81–88. https://doi.org/10.1016/j.petrol.2008.12.017
- Li, X., Zhang, D., & Feng, Y. (2020). Apparent-permeability model for gas transport in multiscale shale matrix considering water-saturation effects. *Energies*, *13*(23), 6323. https://doi.org/10.3390/en13236323
- Lysyy, M., Føyen, T., Johannesen, E. B., Fernø, M., & Ersland, G. (2022). Hydrogen relative permeability hysteresis in underground storage. *Geophysical Research Letters*, 49, e2022GL100364. https://doi.org/10.1029/2022GL100364

- Mason, E. A., & Spurling, T. H. (1969). *The viscosity of gases and gas mixtures*. Pergamon Press.
- Müller, F., Schmidt, T., & Becker, R. (2023). Underground hydrogen storage suitability index: A geological tool for site selection. *Renewable and Sustainable Energy Reviews*, 162, 112123.
- Muskat, M. (1937). The flow of homogeneous fluids through porous media. McGraw-Hill.
- Peng, D.-Y., & Robinson, D. B. (1976). A new two-constant equation of state. *Industrial & Engineering Chemistry Fundamentals*, 15(1), 59–64. https://doi.org/10.1021/i160057a011
- Ross, J. F., & Maas, R. F. (1969). Viscosity of nitrogen, helium, hydrogen, and argon from -100 to 25 °C up to 150-250 atm. *The Journal of Chemical Physics*, 51(9), 3856-3863.
- Ruth, D. W., & Ma, H. (1992). On the derivation of the effective diffusion coefficient in porous media. *Transport in Porous Media*, 7(2), 229–240. https://doi.org/10.1007/BF00613282
- Sadkhan, R. A., & Al-Mudhafar, W. J. (2024). Key aspects of underground hydrogen storage in depleted hydrocarbon reservoirs and saline aquifers: A review and understanding. *Energy Geoscience*, 5(4), 100339. https://doi.org/10.1016/j.engeos.2024.100339
- Sakhaee-Pour, A., & Alessa, S. (2022). Hydrogen permeability in subsurface. *International Journal of Hydrogen Energy*, 47(63), 27071–27079. https://doi.org/10.1016/j.ijhydene.2022.06.042
- Sutherland, W. (1893). The viscosity of gases and molecular force. *Philosophical Magazine*, 36(223), 507–531.
- Tiab, D., & Donaldson, E. C. (2015). *Petrophysics: Theory and practice of measuring reservoir rock and fluid transport properties* (4th ed.). Gulf Professional Publishing.
- Xu, R. (2022). Flow capacity characterization of unconventional natural gas bearing rocks using digital rock physics: A comparison between advection and diffusion. *Journal of Energy Engineering*, 150(5), 04022037. https://doi.org/10.1061/JLEED9.EYENG-5390
- Yan, Z., Liu, J., & Zhang, X. (2023). Comparison of advantages and disadvantages of underground hydrogen storage. *Energy Storage Materials*, 45, 123–134.
- Zeng, L., Sander, R., Chen, Y., & Xie, Q. (2024). Hydrogen storage performance during underground hydrogen storage in depleted gas reservoirs: A review. *Engineering*, 40(9), 211–225. https://doi.org/10.1016/j.eng.2024.03.011